

ADA042147

AFML-TR-77-22

12

J

DEVELOPMENT OF LOW-COST HARDENED ZINC SELENIDE FOR IR WINDOWS

Raytheon Company
Research Division
Waltham, MA 02154

COPY AVAILABLE TO DDC DOES NOT
PERMIT FULLY LEGIBLE PRODUCTION

April 1977

Final Report 15 May 1975 to 15 December 1976

Approved for public release; distribution unlimited

REPRODUCED FROM
BEST AVAILABLE COPY

Prepared for

AIR FORCE MATERIALS LABORATORY
AIR FORCE WRIGHT AERONAUTICAL LABORATORIES
AIR FORCE SYSTEMS COMMAND
WRIGHT-PATTERSON AIR FORCE BASE, OHIO 45433

U NO.

DC FILE COPY

DDC

JUL 27 1977

NOTICE

When Government drawings, specifications, or other data are used for any purpose other than in connection with a definitely related Government procurement operation, the United States Government thereby incurs no responsibility nor any obligation whatsoever; and the fact that the government may have formulated, furnished, or in any way supplied the said drawings, specifications, or other data, is not to be regarded by implication or otherwise as in any manner licensing the holder or any other person or corporation, or conveying any rights or permission to manufacture, use, or sell any patented invention that may in any way be related thereto.


This report has been reviewed by the Information Office (OI) and is releasable to the National Technical Information Service (NTIS). At NTIS, it will be available to the general public, including foreign nations.

This technical report has been reviewed and is approved for publication.



David W. Fischer
Project Engineer / Scientist

FOR THE COMMANDER



William G. D. Frederick, Chief
Laser & Optical Materials Branch
Electromagnetic Materials Division
Air Force Materials Laboratory

Copies of this report should not be returned unless return is required by security considerations, contractual obligations, or notice on a specific document.

UNCLASSIFIED

SECURITY CLASSIFICATION OF THIS PAGE (When Data Entered)

REPORT DOCUMENTATION PAGE		READ INSTRUCTIONS BEFORE COMPLETING FORM	
1. REPORT NUMBER AFML TR-77-22	2. GOVT ACCESSION NO.	3. RECIPIENT'S CATALOG NUMBER	
4. TITLE (and Subtitle) DEVELOPMENT OF LOW-COST HARDENED ZINC SELENIDE FOR IR WINDOWS.		5. TYPE OF REPORT & PERIOD COVERED Final Technical Report 15 May 1975-15 Dec 1976	
6. AUTHOR(s) A./Swanson, R./Donadio J./Pappis		7. PERFORMING ORG. REPORT NUMBER S-2140	
8. PERFORMING ORGANIZATION NAME AND ADDRESS Raytheon Company Research Division Waltham, MA 02154		9. CONTRACT OR GRANT NUMBER(s) F33615-75-C-5131 new	
10. CONTROLLING OFFICE NAME AND ADDRESS Air Force Materials Laboratory (LPO) Air Force Systems Command Wright-Patterson AFB, Ohio 45433		11. PROGRAM ELEMENT, PROJECT, TASK AREA & WORK UNIT NUMBERS Project No. 7360 Task No. 736001 Work Unit No. 73600140	
12. MONITORING AGENCY NAME & ADDRESS (if different from Controlling Office)		13. REPORT DATE April 1977	
		14. NUMBER OF PAGES 88 (1298 p.)	
		15. SECURITY CLASS. (of this report) UNCLASSIFIED	
		16a. DECLASSIFICATION/DOWNGRADING SCHEDULE	
17. DISTRIBUTION STATEMENT (of this Report) Approved for public release; distribution unlimited			
18. DISTRIBUTION STATEMENT (of the abstract entered in Block 20, if different from Report)			
19. SUPPLEMENTARY NOTES			
20. KEY WORDS (Continue on reverse side if necessary and identify by block number) Chemical Vapor Deposition Low-Cost FLIR Multispectral Reconnaissance Rain Erosion Resistant Hardened Selenide Composite Window			
21. ABSTRACT (Continue on reverse side if necessary and identify by block number) This development program has established the feasibility of fabricating large-size (13 x 20 in.) durable multispectral FLIR windows by a chemical vapor deposition process at a cost consistent with the program goals. The window is a composite that consists of two layers; a relatively thick (~0.6 in.) zinc selenide substrate and a thin (~0.5 in.) zinc sulfide overcoat. The overcoat is grown on a polished surface of the selenide by a CVD technique. The purpose of the overcoat is to protect the zinc selenide from damage by			

DD FORM 1 JAN 73 1473

EDITION OF 1 NOV 68 IS OBSOLETE

UNCLASSIFIED

SECURITY CLASSIFICATION OF THIS PAGE (When Data Entered)

298320

over

APPROXIMATE
-LY EQUAL
TO

UNCLASSIFIED

SECURITY CLASSIFICATION OF THIS PAGE(When Data Entered)

the impingement of rain drops and other particles at high speeds. Optical evaluation of the composite window indicates that it is capable of meeting specifications of high resolution FLIR systems.

To achieve the above results and to lower the cost of the window the chemical vapor deposition process for depositing zinc selenide was made more economical by improving yield and by using less expensive reactants. Chemical vapor deposition techniques were also developed for growing a thin zinc sulfide layer directly onto a polished zinc selenide substrate. This process is, in principle, less expensive than bonding a thin layer to the surface since it eliminates the use of antireflection coatings on the surface. Furthermore, final figuring of the surfaces, because of optical path changes due to nonuniformity of the interface, is not necessary.

UNCLASSIFIED

SECURITY CLASSIFICATION OF THIS PAGE(When Data Entered)

FOREWORD

This report was prepared by Raytheon Company, Research Division, Waltham, Mass. under Contract No. F33615-75-C-5131, Project No. 7360, Ammendments No. 1 and 2. The work was administered under the direction of the Air Force Materials Laboratory, Wright-Patterson Air Force Base, Ohio. Dr. D. Fischer, AFML/LPO, was the project engineer.

At Raytheon, the investigation was carried out in the Advanced Materials Department. Dr. J. Pappis, the department manager, and Mr. R. Donadio and Dr. A. Swanson were the principal investigators. Contributions to this investigation were also made by Dr. T. Kohane and Mr. J. Connolly.

This is the Final Technical Report for Contract No. F33615-75-C-5131. It covers the period 15 May 1975 to 15 December 1976. The report was given the Raytheon internal number S-2140.

The report was submitted by the authors January 1977.

ACCESSION for		
NTIS	W. & S. Section	<input checked="checked" type="checkbox"/>
DDC	B. & F. Section	<input type="checkbox"/>
UNANNOUNCED		<input type="checkbox"/>
JUSTIFICATION		
BY		
DISTRIBUTION/AVAILABILITY CODES		
Dist.	AVAIL.	and SP. CIAL
A	23	

KYR

TABLE OF CONTENTS

<u>Section</u>		<u>Page</u>
I.	INTRODUCTION	1
II.	FABRICATION TECHNIQUES FOR LOW-COST ZINC SELENIDE	3
	a. Conventional Chemical Vapor Deposition	3
	b. Elemental Process	6
	c. Physical Vapor Deposition	6
III.	EXPERIMENTAL	8
	a. Introduction	8
	b. Elemental Process	8
	c. Physical Vapor Deposition	28
	d. Low-Cost Chemical Vapor Deposition for Zinc Selenide	50
	e. Composite Window Fabrication	56
	f. Rain Erosion Testing	74
IV.	SUMMARY AND CONCLUSIONS	77
	APPENDIX - IMAGE SPOILING MEASUREMENTS	79

LIST OF ILLUSTRATIONS

<u>Figure</u>		<u>Page</u>
1	Photograph of Flow Panel, Furnace, and Reaction Chamber for Deposition of Elemental ZnSe	9
2	Schematic of CVD System for Elemental Zinc Selenide	10
3	Internal Schematic of CVD System for Fabrication Elemental ZnSe	14
4	Spectral Transmittance, Run ZnSe-EE-4, $t = 0.059$ in.	15
5	Deposition Profile in Inches, ZnSe-EE-7	17
6	Spectral Transmittance of Run ZnSe-EE-7, $t = 0.065$ in.	18
7	Schematic of CVD Zinc Selenide Apparatus	19
8	Deposition Profile in Inches ZnSe-EE-9	20
9	Spectral Transmittance, ZnSe-EE-9, $t = 0.119$ in.	21
10	Infrared Transmittance, ZnSe-EE-12, $t = 0.120$ in.	23
11	Details of Selenium Nozzle in Assembly	25
12	Microstructure of Elemental ZnSe, Edge View, Se/Zn Molar ratio = 1.34	29
13	Microstructure of CVD ZnSe, Edge View, H_2Se/Zn Molar ratio 1.25	29
14	Visible Transparency of Physical Vapor Deposited ZnSe	30
15	Typical Infrared Transmittance of 1.5 cm thick PVD ZnSe	31
16	Schematic of Physical Vapor Deposition Apparatus	32
17	Visible Transmittances of 1.27 cm Thick PVD-39 ZnSe and Standard CVD ZnSe	35
18	Infrared Transmittance of Run PVD-39, 1.27 cm thick	36
19	Infrared Transmittance of Run PVD-40, 0.49 cm thick	36
20	Visible Transmittance of Run PVD-40, 1.43 cm thick	38
21	Infrared Transmittance of Run PVD-41, 1.43 cm thick	39
22	Infrared Transmittance of Area Near Center of 15 Inch Dia. Disc, PVD-49, 0.50 cm thick	42

LIST OF ILLUSTRATIONS (Cont'd)

<u>Figure</u>		<u>Page</u>
23	Infrared Transmittance of Area Located 7 in. From Center of 15 in. Dia. Disc, PVD-49, 0.73 cm thick	43
24	Infrared Transmittance of Area Located 14 in. From Center of 15 in. Dia. Disc, PVD-49, 0.73 cm thick	43
25	In-Line Transmittance, PVD-51, $t = 1.5$ cm	44
26	Infrared Transmittance, PVD-52, $t = 0.5$ cm	45
27	Run PVD-53 "As Deposited" Disc	46
28	PVD-53 Edge Polished Specimen Showing Thickness and Optical Clarity at Visible Wavelengths	47
29	Infrared Transmittance, PVD-53, 0.265 in. thick, Edge View	48
30	PVD-53 Under Transmitted Light	49
31	Infrared Transmittance of CVD ZnSe Produced With Low-Cost Materials	52
32	Schematic of Apparatus Used for CVD ZnSe Production Run	53
33	Low Cost ZnSe "As Deposited" Thickness Profile	54
34	Spectral Transmittance of Low-Cost ZnSe, $t = 1.27$ cm	55
35	Infrared Transmittance of Zinc Sulfide Coating Run, ZnSC-1; 0.1 cm Substrate and 0.12 cm Deposition Thickness	59
36	Infrared Transmittance of Zinc Sulfide Coating Run, ZnSC-2, 0.07 cm Substrate and 0.05 cm Deposition Thickness	60
37	Infrared Transmittance of Zinc Sulfide Coating Run, ZnSC-4; 0.07 cm Thick ZnS Deposition on 0.5 cm Thick CVD ZnSe	60
38	Infrared Transmittance of Zinc Sulfide Coating Run ZnSC-5; 0.04 cm Thick ZnS Deposited on 0.69 cm Thick CVD ZnSe	62
39	Infrared Transmittance of Zinc Sulfide Coating Run ZnSC-6; 0.1 cm Thick ZnS Deposited on 0.65 cm Thick CVD ZnSe	62
40	Infrared Transmittance of Zinc Sulfide Coating Run ZnSC-7; 0.18 cm Thick ZnS Deposited on 0.71 cm Thick PVD ZnSe	63
41	Infrared Transmittance of 0.16 cm Thick Zinc Sulfide Layer Deposited During Run ZnSC-7.	63

LIST OF ILLUSTRATIONS (Cont'd)

<u>Figure</u>		<u>Page</u>
42	PVD Zinc Selenide Coated with Zinc Sulfide - Run ZnSC-9 Viewed Through Transmitted Light. (Dimensions 3 in. X 3 in.)	64
43	Infrared Transmittance of Zinc Sulfide Coating Run ZnSC-9; 0.08 cm Thick ZnS Deposited on 0.34 cm Thick PVD ZnSe	65
44	Infrared Transmittance of Zinc Sulfide Coating Run, ZnSC-10; 0.17 cm Thick ZnS Deposited on 0.64 cm Thick PVD ZnSe	65
45	Infrared Transmittance of Zinc Sulfide Coating Run ZnSC-10; 0.06 cm Thick ZnS Deposited on 0.37 cm Thick CVD ZnSe	68
46	Infrared Transmittance of Zinc Sulfide Coating Run ZnSC-11 (Sample B); 0.11 cm ZnS and 0.40 cm CVD ZnSe Thickness	70
47	Infrared Transmittance of Zinc Sulfide Coating Run ZnSC-11 (Sample C); 0.25 cm ZnS and 0.26 cm CVD ZnSe Thickness	70
48	Infrared Transmittance of Zinc Sulfide Coating Run ZnSC-6 (Sample A); 0.1 cm ZnS and 0.4 cm CVD ZnSe Thickness	71
49	Infrared Transmittance of Zinc Sulfide Coating Run ZnSC-6 (Sample B); 0.16 cm ZnS and 0.38 cm CVD ZnSe Thickness	71
50	Infrared Transmittance of Zinc Sulfide Coating Run ZnSC-12; 0.04 cm ZnS and 0.72 cm CVD ZnSe Thickness	72
51	Infrared Transmittance of 0.4 cm Thick Zinc Sulfide Layer Deposited During Run ZnSC-12	72
52	Infrared Transmittance of Zinc Sulfide Coating Run ZnSC-13 0.11 cm ZnS and 0.65 cm PVD ZnSe Thickness	73
A. 1	Image Spoiling Apparatus	84
A. 2	Long Wave Pass Filter Characteristic	85
A. 3	Detector Response with 1000 K Black Body Source	86
A. 4	Typical Image Spoiling Scan	87
A. 5	CAT Output Curves	88

LIST OF TABLES

<u>Table</u>		<u>Page</u>
1	Properties of CVD Zinc Selenide	4
2	Deposition Conditions For Elemental Zinc Selenide	12
3	Properties of Zinc Selenide Deposited at 750° C	27
4	Deposition Conditions for PVD Zinc Selenide	34
5	Image Spoiling Characteristics of Infrared Materials	40
6	Deposition Conditions for Zinc Sulfide Overcoat Experiments	57
7	Thermal Expansion of PVD and CVD Zinc Selenide and CVD Zinc Sulfide	66
8	Rain Erosion Results	75
A1	Results of Image Spoiling Measurements	83

I. INTRODUCTION

The application of FLIR systems to several high performance aircraft such as the B-1, F-4 and F-111, requires that large-size infrared windows capable of transmitting energy between 0.5 and 13 micrometers be available. Furthermore, to withstand the thermal stresses and the hostile environment encountered by such aircraft the window material must also exhibit good thermal stress and resistance to rain erosion. Finally, it is important that the cost of the optical components (such as windows) for these systems be procurable at a reasonable cost.

In earlier forms of airborne electrooptical and FLIR systems used in subsonic aircraft, the conventional material for windows in the 8 to 12 micrometer region was germanium, with oxide-glasses serving the visible and near infrared region including 1.06 micrometers. Both of these materials are strong and durable, but germanium has a major disadvantage for use in high-speed flight where aerodynamic heating results in a substantial increase in absorption of the window at infrared wavelengths that at the same time introduces optical distortion. Both absorptions and distortions can be reduced to acceptable levels by replacing the germanium with zinc selenide. A further advantage of this replacement is the possibility of using the same window at all the required wavelengths - visible for ocular or TV systems, LLLTV for wavelengths beyond 0.75 μm , 1.06 μm for laser designation, 3 to 5 μm for pulse seekers and 8 to 13 μm for FLIR's.

The major drawbacks to the use of state-of-the-art zinc selenide over this wide bandwidth are its durability and cost. The durability (i.e., its rain erosion resistance) of zinc selenide can be significantly increased by the use of dopants such as silicon and/or aluminum. Unfortunately the addition of these dopants even in small concentrations significantly increases the short wavelength scatter and yields a material that is not satisfactory for use at these latter wavelengths.

An alternate approach to the problem and the one evaluated in this program is to fabricate a composite window. The composite consists of a primary element which is zinc selenide of sufficient thickness to resist both mechanical fracture and optical distortion under the expected aerodynamic and mechanical loads. The zinc selenide, in turn, is covered by a layer of a high durability material, namely, CVD zinc sulfide. This material is grown on an optically polished zinc selenide surface by chemical vapor deposition techniques. This technique eliminates the need of anti-reflection coatings at this interface and the need for optically figuring the external surfaces after fabrication since optical path variations are minimal. The thickness of the zinc sulfide layer needed to increase durability to an acceptable level is less than one-tenth of an inch. Under these conditions, the transmittance of the composite will essentially be equal to the transmittance of the zinc selenide.

To reduce the cost of the zinc selenide substrate, three alternate vapor deposition processes were experimentally evaluated during this program. These were an elemental vapor deposition process, a physical vapor deposition process, and a modified chemical vapor deposition process. The results of the experimental work indicated that the modified CVD process is capable of yielding a high quality optical material at a reasonable cost level.

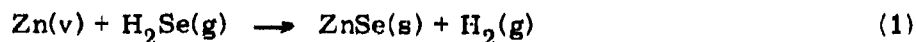
II. FABRICATION TECHNIQUES FOR LOW-COST ZINC SELENIDE

a. Conventional Chemical Vapor Deposition

The Raytheon Research Division has been actively engaged in the fabrication of optical materials by the chemical vapor deposition process (CVD) for a number of years. In this process a material is formed as the product of a high-temperature chemical reaction involving one or more gases. Each gas is an element (or a compound containing the element) of the material to be deposited. The gases flow into the deposition chamber of the furnace where they mix and react to form a dense solid on an appropriate substrate.

CVD processes generally yield a high-purity material because the vapors tend to be self-distilled during transport to the reaction zone. Under correct thermodynamic, kinetic and gas dynamic conditions coherent and dense polycrystalline material will deposit. The mode of deposition can be visualized as a molecule by molecule buildup of material which creates a theoretically dense deposit.

Zinc selenide is deposited by CVD techniques according to the following chemical reaction:



The zinc vapor is generated by heating the metal under a reduced pressure and introducing it into the reaction zone as a vapor by means of a carrier gas. The hydrogen selenide gas which is stored external to the furnace is passed directly into the reaction zone. In the reaction zone the two gases react to deposit the material. The byproducts of the reaction are pumped away and disposed of by suitable methods. For laser quality material the deposition process is carried out at 750° C at a deposition rate of approximately 0.005 in/hr. A typical set of properties of this material are listed in Table 1.

TABLE 1

PROPERTIES OF CVD ZINC SELENIDE

Density (gm/ cc)	5.27
Refractive index, 8-13 μm	2.42 to 2.38
Temperature Coefficient dn/dT (/° C) at 10.6 μm	6×10^{-5}
Transmission, 8-13 μm	> 70 percent
Transmission limits	0.5 to 22 μm
10.6 micrometer absorption (cm^{-1})	4×10^{-4}
Pulse damage threshold (W/cm^2)	$> 3 \times 10^8$
Grain size (microns)	70
Hardness (Knoop 50 gm)	100
Flexural strength (psi, 4 point loading)	7500 ± 1000
Young's modulus (psi)	9.75×10^6
Thermal expansion (/° C, range RT-170° C)	7.57×10^{-6}
Thermal conductivity (25° C, cgs)	0.043
Specific heat (cal/ gm °C)	0.082
Resistivity (ohm-cm)	$\sim 10^{12}$

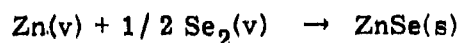
The costs of CVD zinc selenide are primarily governed by the number of usable square inches yielded per run and the cost of hydrogen selenide gas. During the course of this program a mandrel geometry was designed and process conditions were optimized to maximize the number of window blanks yielded per furnace run. In addition, a less expensive grade of hydrogen selenide gas was evaluated, and proved to be useful. Both of these facts allow the material to be produced at a lower cost.

As previously noted, zinc selenide does not perform adequately in a rain environment. After 10 minutes at speeds of 470 miles/hr in one inch/hr simulated rainfall, for example, internal fractures cause the material to become almost opaque. To improve this characteristic without significantly altering its optical properties, thin (< 0.100 in.) overcoat layers of CVD zinc sulfide can be applied to one surface. This material can be attached by one of two techniques. In the first technique one can adhesively bond or use a glass to attach the material. In this case the index of refraction and thickness uniformity of the adhesive or glass must be accurately controlled.

In the second technique zinc sulfide is directly grown by a chemical vapor deposition technique onto the polished surface of the zinc selenide. This latter technique was evaluated in this program and proved to be successful. Structurally this technique is successful since the thermal expansions of the two materials are quite similar. From an optical point of view the technique is successful because of the closeness of the index of refraction of the two materials. Using values of 2.40 and 2.20 for the refractive indices of zinc selenide and zinc sulfide respectively, the reflectivity of the interface is calculated as less than 0.2 percent provided there is intimate contact between the materials. Although zinc sulfide has a much greater absorption coefficient than the zinc selenide, a layer of zinc sulfide ~ 0.050 in. thick will reduce the transmittance by only a small fraction of a percent.

b. Elemental Process

The most direct method by which the cost of zinc selenide can be reduced is to react zinc and selenium vapors directly:



As in the standard chemical vapor deposition process zinc vapor is generated by heating the metal under a reduced pressure and passing it, by use of a carrier gas, into the reaction chamber of the furnace. Selenium vapor is generated in a similar manner and it is also passed into the reaction zone by a carrier gas. The process is cost effective since it does not entail the use of the relatively expensive reactant, hydrogen selenide gas. Under the appropriate processing conditions the free energy change for this reaction can be made similar to that of the more conventional CVD process. Details of the experimental procedures used to deposit material by this process are discussed in another section of this report.

c. Physical Vapor Deposition

Another attractive means of reducing the cost of zinc selenide is by use of a physical vapor deposition process. This process is in reality a vaporization-condensation process. To fabricate zinc selenide as an optical component, zinc selenide powder is heated at a reduced pressure to its evaporation temperature. By placing the mandrel surface, on which deposition occurs, in a cooler section of the furnace (usually 150° to 250° C) the vapors are recondensed and the material is deposited. Physical vapor deposition can be carried out in any type of furnace in which a temperature gradient can be established. In this program a graphite resistance heated vacuum furnace capable of being pumped to ~ 0.2 torr was used. A mandrel assembly consisting of a crucible containing the zinc selenide powder, a graphite pipe and the mandrel, are placed in the furnace so that a temperature gradient is established between the source material and the final mandrel surface. The process can be carried out with or without the use of an auxiliary carrier

gas. Typically, the deposition temperature is between 900° and 1000° C at a system pressure between 0.5 and 1.0 torr. The experimental work done with this process is discussed in a following section of this report.

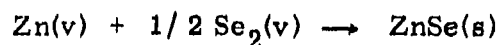
III. EXPERIMENTAL

a. Introduction

As noted in the previous section, three processes were evaluated in an attempt to decrease the costs of zinc selenide. In addition, CVD zinc sulfide was grown on these substrates to improve their resistance to rain erosion. In this section of the report the experimental work done in each of these areas is discussed.

b. Elemental Process

Under a previous program (F33615-74-C-5145) polycrystalline zinc selenide was prepared using elemental zinc and selenide vapors as the reactants, according to the reaction:



Using the appropriate process conditions, the free energy change of this reaction (-23.2 Kcal/ mole) can be made similar to the standard chemical vapor deposition process. A typical set of conditions are: deposition temperature 750° C, system pressure 40 torr, and reactant concentrations of 2.5 moles of each reactant per hour. Using these conditions, specimens 1 × 2 × 0.1 inch were deposited with close to theoretical transmittance in the far infrared. Scatter at visible wavelengths, however, was a problem. The goals of this task of the program therefore were to reduce this scatter, deposit larger size samples, and determine whether the process could be scaled to produce large-size window blanks economically.

The equipment needed to carry out the experimental work on this process is shown in Figures 1 and 2 respectively. The flow panel for the system is pictured on the left. Flowmeters are used to control the carrier gas flow over the liquid zinc and selenium metal retorts. Pressure gauges for the system are also located on this flow panel. The furnace and reaction

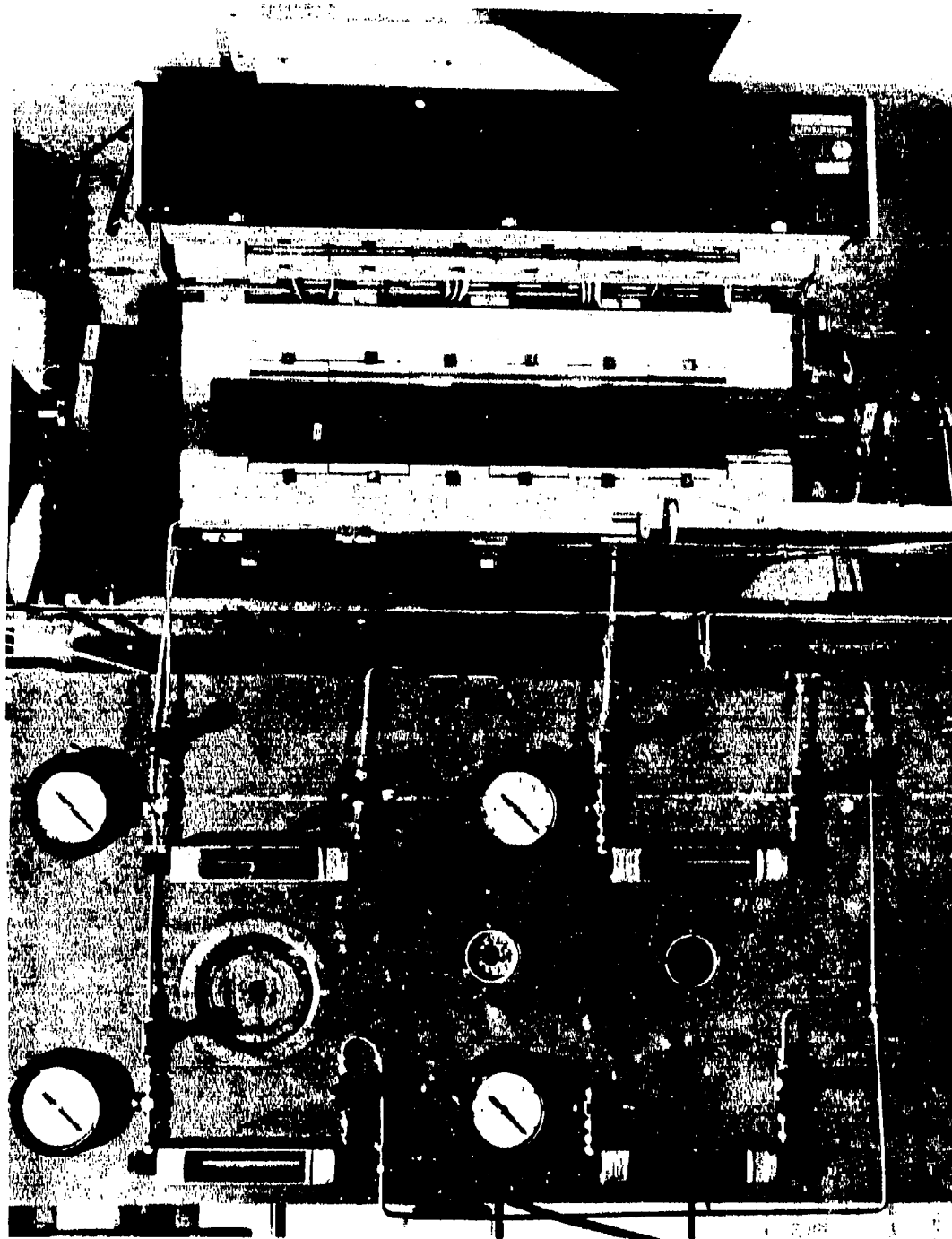


Figure 1. Photograph of Flow Panel, Furnace, and Reaction Chamber for Deposition of Cadmium Telluride

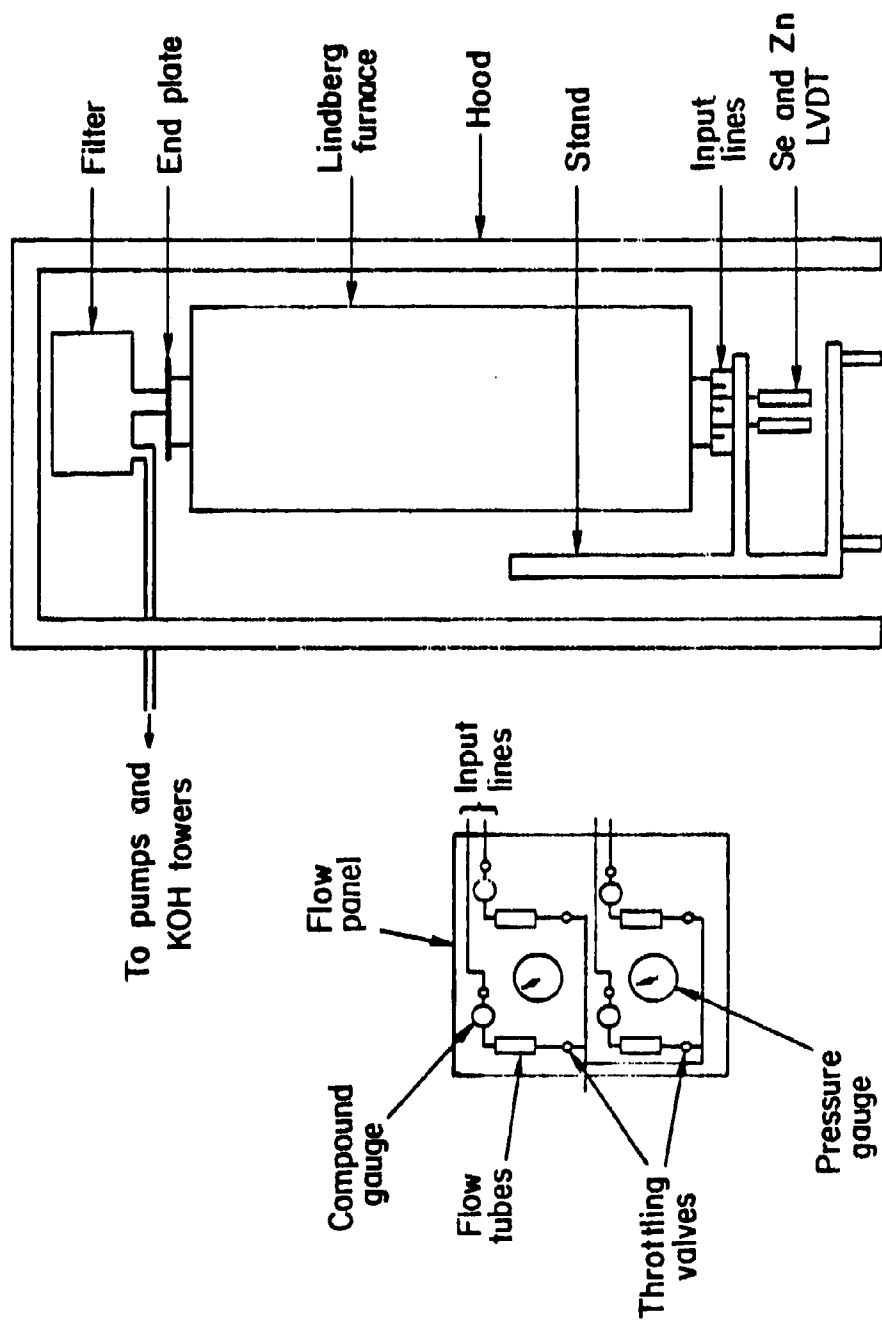


Figure 2. Schematic of CVD System for Elemental Zinc Selenide

chamber are pictured on the righthand side of Figure 1. The reaction chamber consists of two graphite retorts, a mixing chamber, and a mandrel. A schematic of the setup is shown in Figure 3. Each retort contains a graphite float system which is used to monitor the selenium and zinc usage during a deposition run. The excess reactive gases leave the top of the reaction chamber and pass through a dust filter, throttling valve, and a vacuum pump. The exhaust from the pump is then passed through KOH bubblers to neutralize any harmful vapors.

The reaction chamber is heated by a vertical Lindberg 6-zone furnace which is 7 inches in diameter. Each 6-inch zone has an individual controller so that temperature gradients along each zone can be controlled to within $\pm 0.5^{\circ}\text{C}$. The furnace and reaction chamber are housed in a walk-in hood for safety purposes.

During this task of the program twenty-five (25) experimental runs were made. The starting reactants for all runs were zinc and selenium, and the deposition conditions used are listed in Table 2.

The first four runs were made to check out the above described system (Figure 3). The first run in which close-to-theoretically dense material was deposited was ZnSe-EE-4. The thickness profile of this run was not as uniform as desired because of growths around the selenium inlet nozzle. Nodular growth was observed in the areas of the plates opposite these inlet growths. There was also a fair amount of visible scatter present in these two areas of the plates as proper mixing of the reactants did not take place. The material deposited in other areas of the plates is equivalent in quality to some of the best elemental material made under the previous contract (F33611-74-C-5145). A transmittance curve of a polished specimen from this run is shown in Figure 4.

In the next set of runs (ZnSe-EE-5 through -7) attempts were made to improve the thickness distribution of the deposit by minimizing the amount of growth around the inlet ports of the reactants. This was done by changing

TABLE 2

DEPOSITION CONDITIONS FOR ELEMENTAL ZINC SELENIDE

Run No.	Mandrel Temp (° C)	Furnace Pressure (torr)	Zn Retort Temp (° C)	Se Retort Temp (° C)	Gas Over Zn (lpm) $\frac{\text{Zn}}{\text{Ar}}$	Gas Over Se (lpm) $\frac{\text{Se}}{\text{Ar}}$	Se By Flow (lpm)	Dep Time (hrs)	Ratio Se(v) Zn(v)
ZnSe-EE-1	720	4.0	610	360	1.0	1.0	---	5	2.0
ZnSe-EE-2	720	3.0	560	340	1.0	1.0	---	10	1.8
ZnSe-EE-3	720	4.0	580	330	1.0	1.0	---	40	1.5
ZnSe-EE-4	720	4.0	580	330	1.0	1.0	---	30	~1.8
ZnSe-EE-5	720	5.0	550	330	1.0	1.0	---	30	1.7
ZnSe-EE-6	710	4.0	540	330	0.8	2.1	---	25	1.1
ZnSe-EE-7	710	5.6	530	330	0.7	3.0	---	15	2.3
ZnSe-EE-8	725	4.5	710*	265	5.0	5.0	---	31	0.97
ZnSe-EE-9	725	3.0	710*	275	5.0	5.0	---	27	1.25
ZnSe-EE-10	725	3.0	715*	270	5.0	2.0	3.0	40	0.96
ZnSe-EE-11	725	3.0	715*	285	5.0	3.0	---	55	1.58
ZnSe-EE-12	735	3.1	720*	290	5.0	3.0	2.0	40	1.80
ZnSe-EE-13	735	3.0	725*	285	5.0	3.0	2.0	60	1.56
ZnSe-EE-14	730	2.9	720*	245	5.0	4.0	2.0	20	---
ZnSe-EE-15	730	3.0	722*	288	5.0	4.0	2.0	50	1.57
ZnSe-EE-16	735	3.1	730*	335	5.0	2.4	2.0	28	1.48
ZnSe-EE-17	735	3.0	730*	315	5.0	3.0	2.0	62	1.38
ZnSe-EE-18	735	10.0	690*	324	5.0	3.0	2.0	24	1.64
ZnSe-EE-19	735	2.5	717*	315	5.0	3.0	2.0	55	1.59
ZnSe-EE-20	735	2.5	715*	310	5.0	3.0	2.0	Run Aborted	
ZnSe-EE-21	735	2.5	710*	305	5.0	3.0	2.0	24	1.45

* Zn Wire Feeder Used

Table 2 (Cont'd)

Run No.	Mandrel Temp (° C)	Furnace Pressure (torr)	Zn Retort Temp (° C)	Se Retort Temp (° C)	Gas Over Zn (lpm)	Ar	Gas Over Se (lpm)	Se By Flow (lpm)	Dep Time (hrs)	Ratio Se(v) Zn(v)
ZnSe-EE-22	745	2.4	730*	336	4.0	Ar	4.0	2.0	55	1.22
ZnSe-EE-23	800	2.1	750*	346	4.0		3.0	2.0	32	----
ZnSe-EE-24	800	2.5	735*	315	4.0		3.0	2.0	24	1.44
ZnSe-EE-25	820	1.5	570	290	1.5		1.5	---	26	0.9

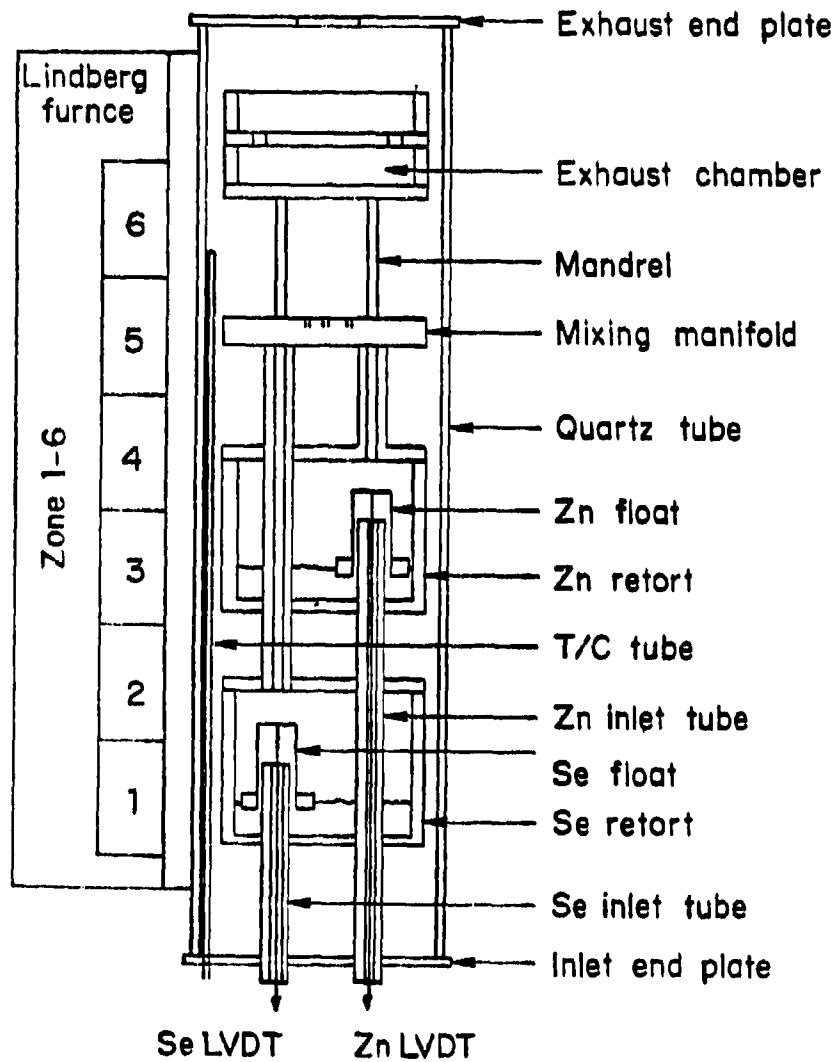


Figure 3. Internal Schematic of CVD System for Fabricating Elemental ZnSe

BEST AVAILABLE COPY

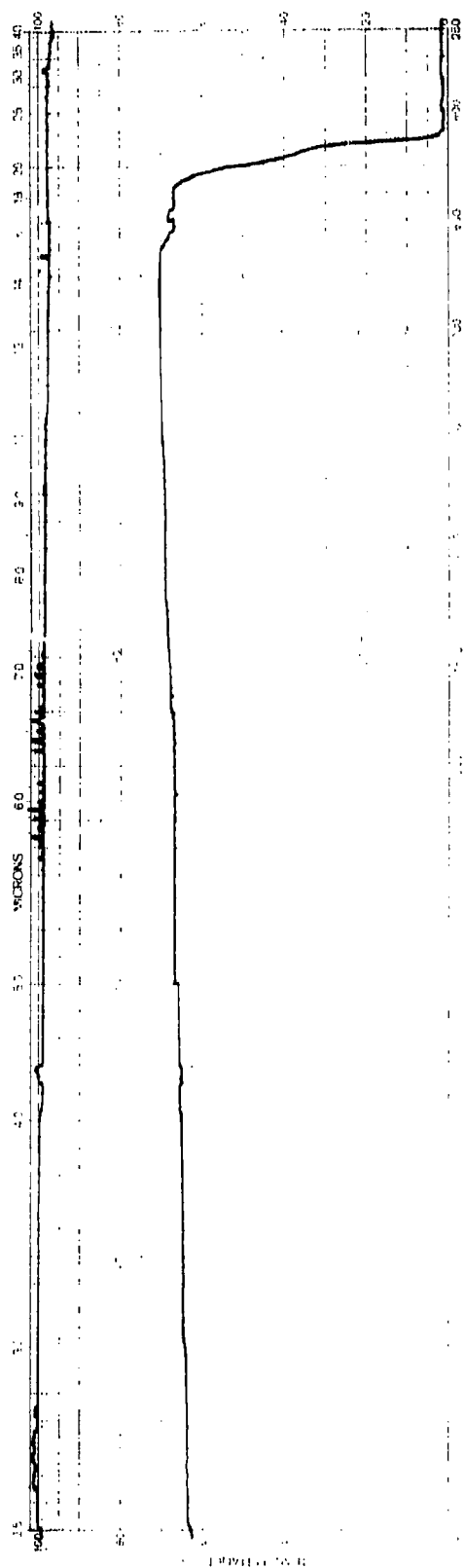


Figure 4. Spectral Transmittance, Run ZnSe-EE-4, $t = 0.059$ in.

the carrier gas flow rates and altering the geometry of the inlet ports. The best thickness profile achieved is shown in Figure 5, and a typical transmittance curve is shown in Figure 6. Although this curve appears equivalent to standard CVD material beyond 2.5 micrometers, at visible wavelengths it exhibits a greater amount of scatter.

In an attempt to obtain better control of the molar ratio of the input reactants, as well as to deposit larger size samples, the experimental deposits after run ZnSe-EE-7 were moved to a seventeen-inch diameter furnace. In this furnace a zinc feeder system, developed under F33615-74-C-5058, was used to generate the zinc vapor. To attain better control of the selenium usage rate, the retort containing the selenium was mounted external to the furnace. This setup is shown schematically in Figure 7.

Using this system seventeen (17) runs (ZnSe-EE-8 through -24) were made. The first successful run was ZnSe-EE-9. The deposition temperature was 725° C, and the Se(v)/Zn(v) molar ratio was 1.25. Even though the deposition profile was quite top-heavy (Figure 8) a polished specimen of the material indicated that it was the best elemental material made to date on the program. The infrared transmittance of the material is shown in Figure 9. The apparent (surface and bulk) absorption coefficient of 0.120 inch thick specimen was measured to be 0.0023 cm^{-1} .

In runs ZnSe-EE-10 through -14 various techniques were investigated in an attempt to improve the thickness distribution of the material. For example, in run ZnSe-EE-10 an argon byflow was used around the selenium inlet port. The purpose of the byflow was to prevent growth of material around the selenium inlet port. Growths can misdirect the gas flow pattern and cause localized turbulence which in turn results in an incorrect molar ratio in certain areas of the mandrel. The deposition profile of this run was fairly uniform, but the optical quality of the ZnSe was not as good as in previous runs since the Se(v)/Zn(v) molar ratio was 0.96. It appears that a selenium-rich atmosphere is necessary in order to deposit elemental ZnSe with minimal visible scatter. In this run the surfaces of the deposit also exhibited excessive

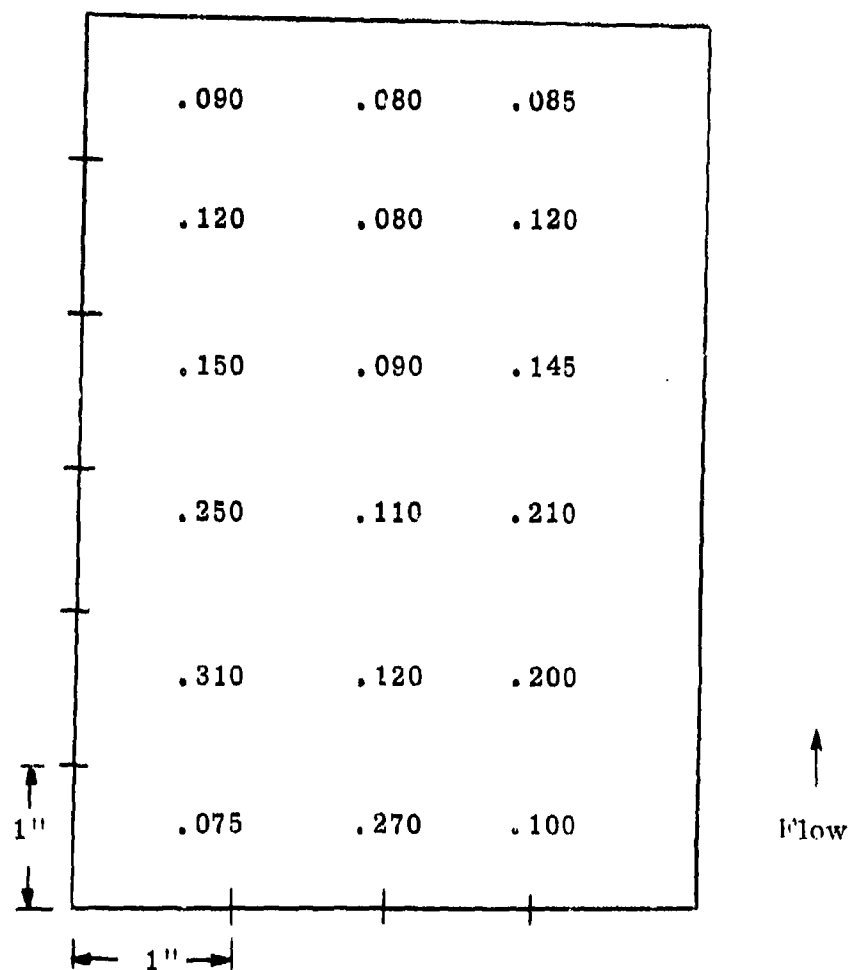


Figure 5. Deposition Profile in Inches, ZnSe-ICE-7

BEST AVAILABLE COPY

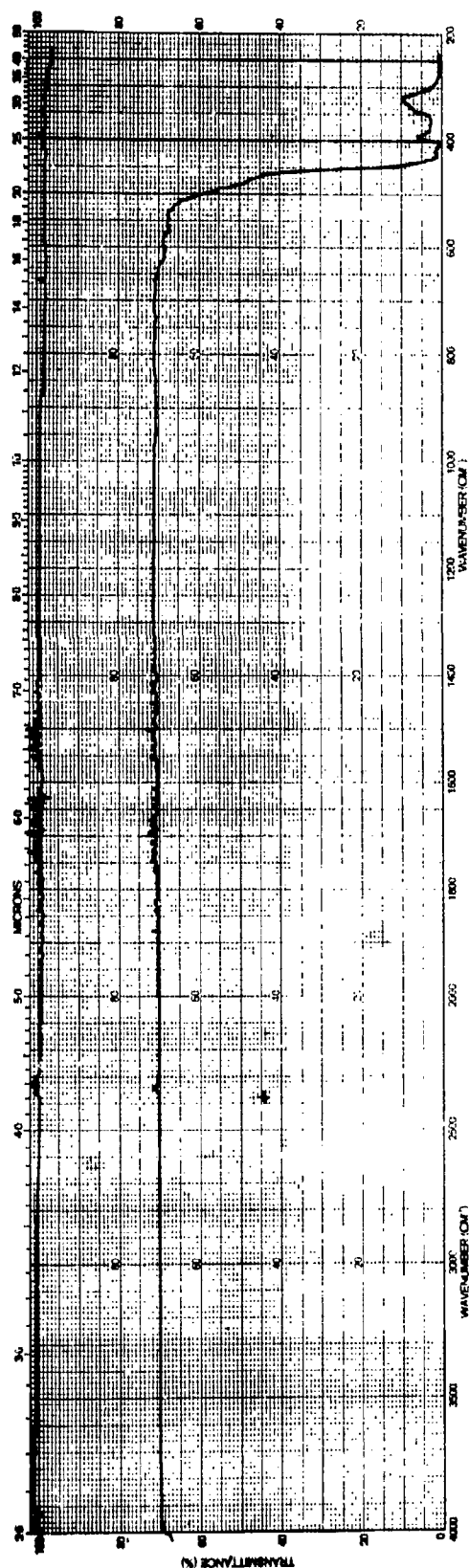


Figure 6. Spectral Transmittance of Run ZnSe-EE-7, $t = 0.065$ inch

PBN-75-686

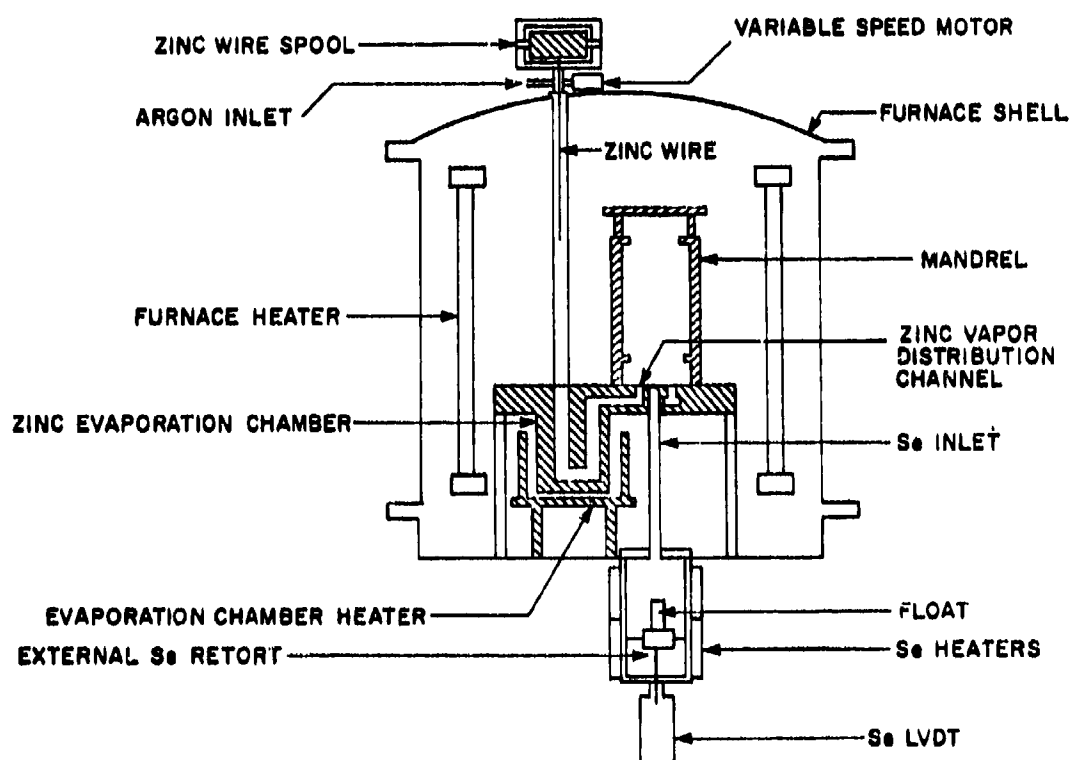


Figure 7. Schematic of CVD Zinc Selenide Apparatus

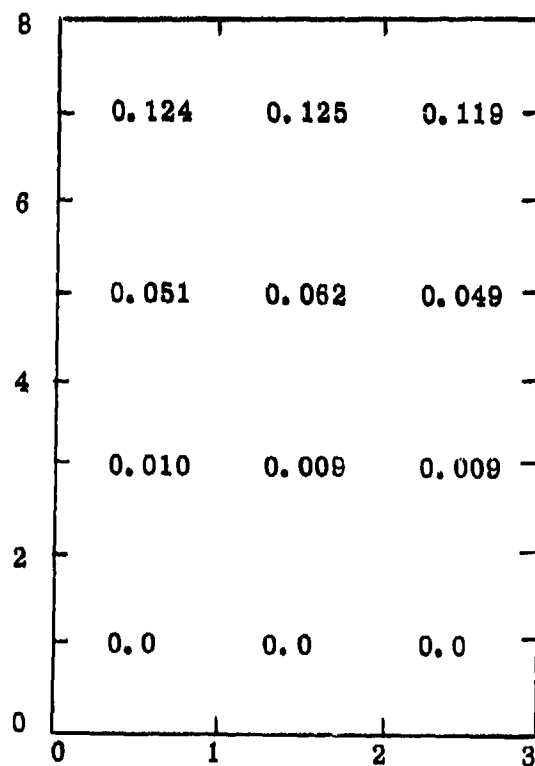


Figure 8. Deposition Profile in Inches, ZnSe-EE-9

BEST AVAILABLE COPY

PBN-75-687

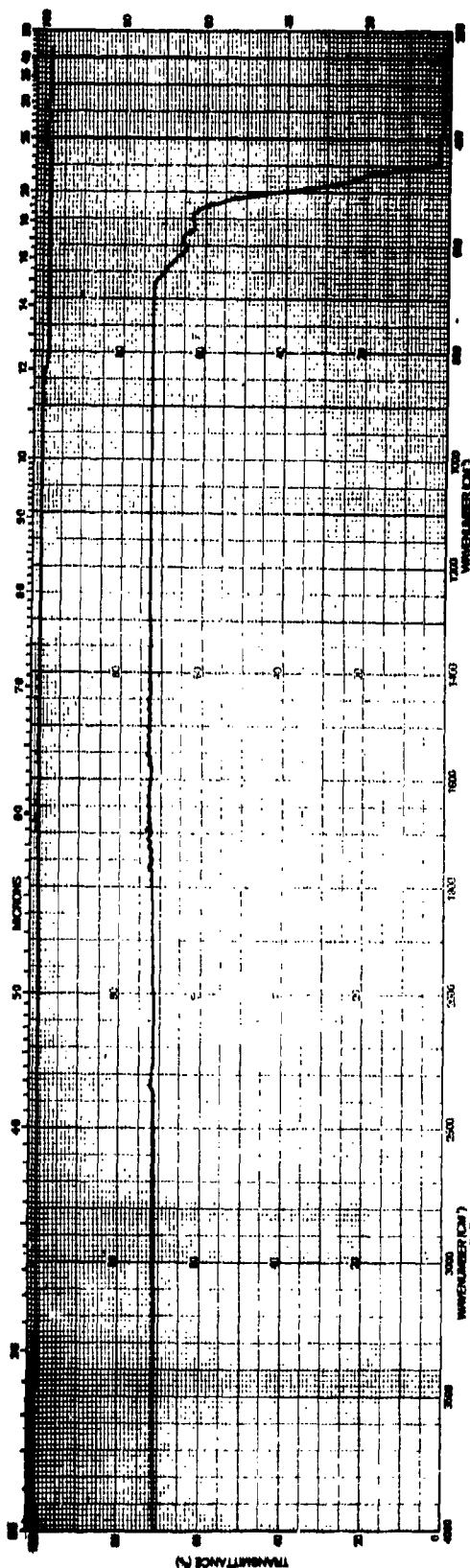


Figure 9. Spectral Transmittance, ZnSe-EE-9, thickness = 0.119 in.

nodular growth. In run ZnSe-EE-11 the selenium inlet port size was reduced from a diameter of 0.625 in. to 0.125 in. in an attempt to obtain a better deposition profile. As a result of growth around the selenium inlet port, however, poor material with an uneven deposition profile resulted. The material deposited on the selenium-rich side of a ridge formed on the plates contained fewer visible scatter sites than the material deposited on the zinc-rich side of the plate.

From the results of the two previous runs it became evident that the size of the inlet port, the gas flow through the port, as well as the amount of byflow used around the port, were all interrelated and governed whether growths would occur around the inlet port. In run ZnSe-EE-12 an argon byflow was used around a 0.250 in. selenium inlet. The byflow concept worked well in that the selenium inlet port was not obstructed by ZnSe growths. However, the thickness profile was quite uneven; material was deposited in the top section of the mandrel only. Visual examination of the material indicated that it was of good quality. A transmittance curve for this material from the visible to the far infrared is shown in Figure 10.

In run ZnSe-EE-14 the diameter of the selenium inlet port was $3/16$ in., and the argon flow over the selenium was increased from 3 to 4 lpm (Table 2). This change caused the selenium vapor core to spread more rapidly and resulted in deposition at a lower point in the mandrel.

In runs ZnSe-EE-15 through -17 the inlet size of the selenium port was progressively decreased and the amount of carrier gas used with selenium vapor was increased in an attempt to improve the thickness profile. For ZnSe-EE-15 where the size was 0.187 in. the deposition profile was still uneven. In some areas of the mandrel the material was free of visible scatter sites, while in other areas the material contained scatter sites. A core of selenium and argon gas had evidently passed through the mandrel and hit the exhaust plate above the deposition area. Any deposition which took place in the mandrel was apparently due to a back-diffusion of the reactants.

NOT AVAILABLE COPY

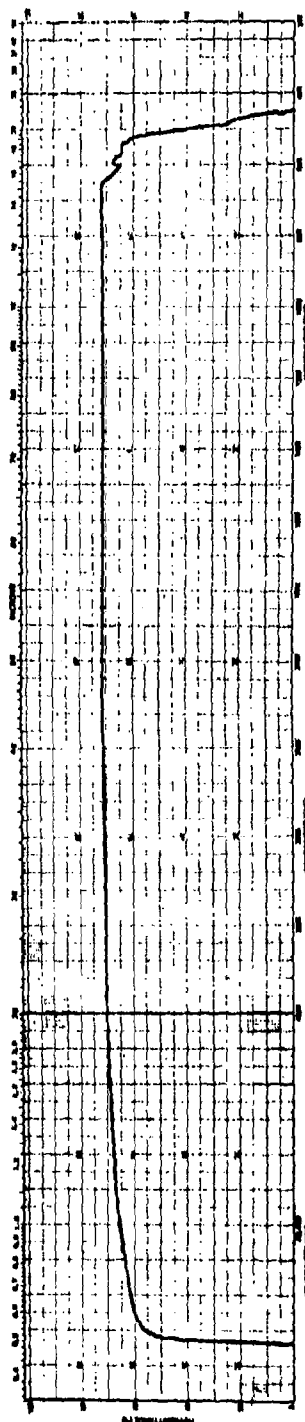


Figure 10. Infrared Transmittance, ZnSe-EE-12, $t = 0.120$ in.

In run ZnSe-EE-16 the selenium inlet port size was reduced to 0.086 inch in an attempt to destroy the core of selenium vapor. While this change improved the deposition profile, it was still top-heavy. Adequate mixing of the vapors was still a problem. Areas of the deposit receiving enough selenium were of good optical quality, while areas that were apparently selenium-poor exhibited visible scatter.

Conditions for run ZnSe-EE-17 were similar to those for the previous run with one exception --- the amount of argon flowing over the selenium retort was increased to further promote mixing of the reactants. The material deposited in the mandrel was of poor optical quality indicating that the Se/Zn molar ratio was < 1.0 . All of the material deposited in the exhaust zone of the setup, however, was of excellent optical quality.

Run ZnSe-EE-18 was made to determine if the thickness profile could be improved by depositing material at a higher system pressure. The furnace pressure was held at 10 torr and the molar ratio of the reactants (Se(v)/Zn(v)) was maintained at 1.64. Gas phase nucleation took place under these conditions and only zinc selenide powder was produced. To produce zinc selenide by the elemental process it appears that the deposition pressure must be less than 5 torr; preferably around 2.5 torr.

Even though the thickness profile of the deposits were troublesome, of greater concern was the optical quality of the material. It became evident that unless adequate mixing of the reactants could be achieved before deposition occurred that the material would have scatter sites. In an attempt to improve the mixing of the reactants the nozzle tube shown schematically in Figure 11 was designed and built. This nozzle was first used successfully in ZnSe-EE-19. The deposition profile was quite uniform and $3 \times 12 \times 0.2$ inch plates were produced. The material still scattered at visible wavelengths. Microstructural analysis of this material indicated that the majority of the scatter sites occurred along the grain boundaries of the columnar grains.

In runs ZnSe-EE-20 and EE-21 the reactant concentrations were

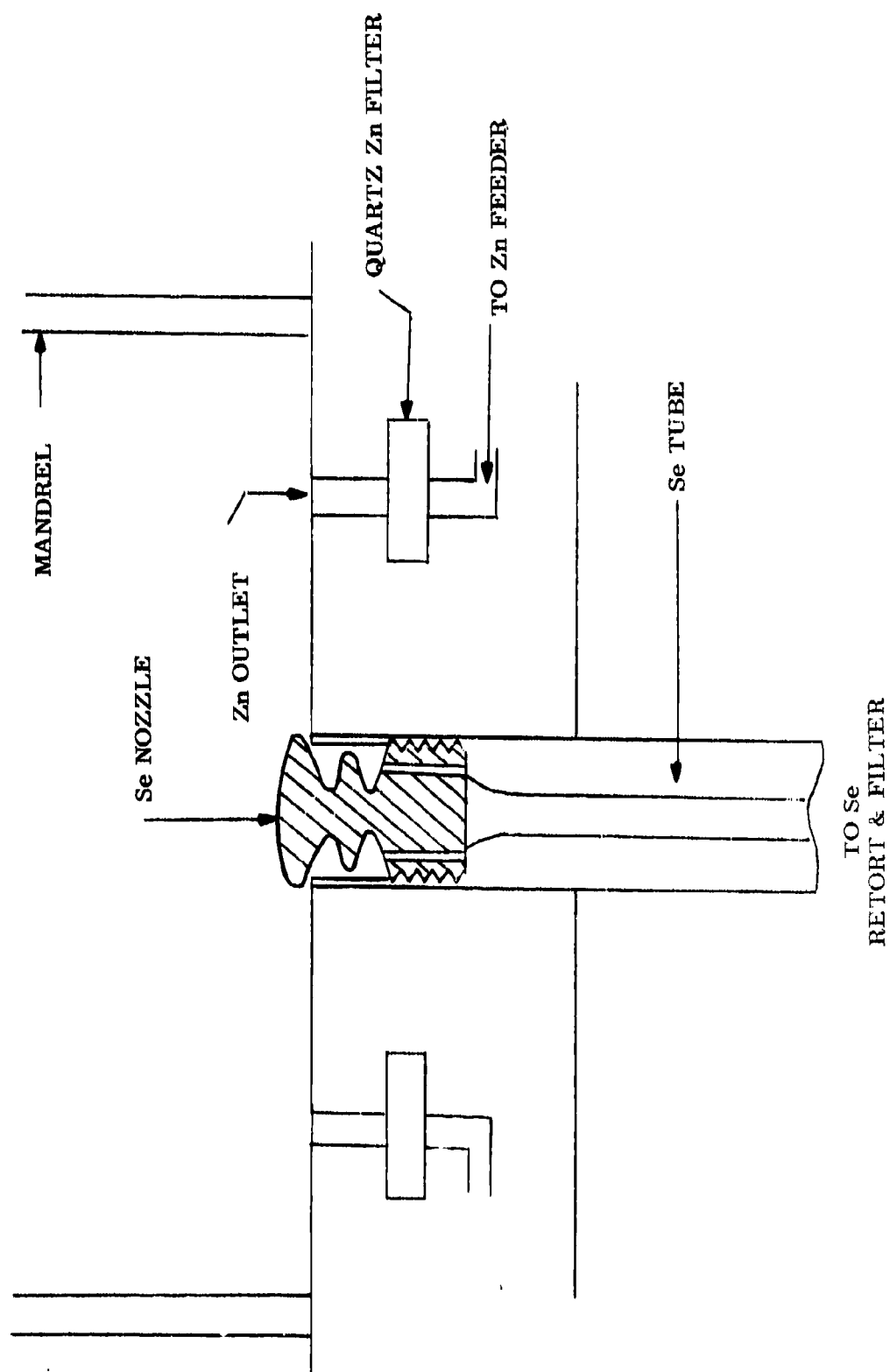


Figure 11. Details of Se Nozzle in Assembly

increased in an attempt to minimize columnar growth. The former run was aborted after two hours due to a malfunction of the zinc feeder system. The latter run went for the scheduled time of 24 hours. Columnar grain growth and scatter was again prevalent.

It was felt that if the deposition temperature were increased the individual grains would become larger, the total grain boundary area would decrease, and visible scatter in the material would be minimized. In runs ZnSe-EE-22 through -24 the deposition temperature was increased from 730° C to 745° C, and subsequently to 800° C (Table 2). The material produced in the above three runs did not show an appreciable decrease in visible scatter sites even though the grain size of the material was significantly larger.

One final run, ZnSe-EE-25 was carried out in the vertical 6-zone Lindberg furnace in order to determine if at a high deposition temperature (820° C) and low furnace pressure (1.5 torr) visible scatter could be decreased. Even though the material produced from this run was thin (~40 mils), it did not appear to scatter as much as previous elemental material when examined visually. Under polarized light, scattering at grain boundaries was also minimal. It appears that the higher temperature and lower pressure resulted in elemental zinc selenide of better optical quality than that produced under other process conditions. The strength of this material was determined to be quite low, however, and it was anticipated that problems would occur when we attempted to overcoat it with zinc sulfide. In addition, the process conditions for its fabrication were so stringent that it did not appear that the process could be easily scaled to produce large-size hardware.

The properties of elemental zinc selenide deposited at 750° C are summarized in Table 3 and are compared to the standard material deposited by the CVD process. As noted, in most cases they are quite similar. The absorption coefficient given for the elemental material may be somewhat higher than the true value since it was measured on a thin sample (0.120 in.) and has not been corrected for surface absorptions. As previously noted, significant

TABLE 3

PROPERTIES OF ZINC SELENIDE DEPOSITED AT 750° C

	<u>Elemental</u>	<u>C V D</u>
Density (gm/ cc)	5.27	5.27
Grain Size (μm)	70-100	70
Flexural strength (psi) 3-point loading	7630 ± 1500	8600 ± 1300
Young's modulus (psi)	-----	9.75×10^6
Hardness (Knoop, 50 gm)	110	100
Thermal expansion ($^{\circ}\text{C}$) (range, 20-170° C)	7.65×10^{-6}	7.57×10^{-6}
Transmission limits (μm)	0.5-22	0.5-22
Uncoated transmission (3-14 μm)	> 70%	> 70%
Bulk absorption coefficient (cm^{-1})	2×10^{-3}	4×10^{-4}

differences were found in the grain structure of the two materials. Figure 12 shows the microstructure of a polished elemental sample which has been etched with a 0.5% Br in methanol solution. In the growth direction the grains are columnar in structure and propagate throughout the thickness of the sample. This columnar structure is not evident in the standard CVD material as shown in the microstructure of Figure 13. This difference in microstructure is probably the result of the relatively low system pressure and reactant concentrations under which the elemental material is deposited. Under these conditions new nucleation sites are harder to form, and the reacting species apparently prefer to deposit on previously formed sites. Thus a columnar grain can propagate through the thickness of the deposit. This type of structure contributes to the somewhat lower flexural strength of the elemental ZnSe as compared to the regular CVD material (Table 3).

c. Physical Vapor Deposition

The physical vapor deposition (PVD) method of fabricating a material is, as noted earlier, a vaporization-condensation process that occurs at high temperatures and relatively low pressures. Based on experimental work prior to beginning this task of the program, it had been determined that most of the properties of the material, although not equivalent to CVD material, were adequate for FLIR window applications. Figure 14 represents the visible transparency achievable with this material, while Figure 15 shows its transmittance beyond 2.5 micrometers. The goal of this task was to determine whether the visible imaging properties could be improved and whether the process could be scaled to fabricate large-size hardware economically.

The experimental setup used in this process is schematically shown in Figure 16. Zinc selenide power is vaporized in a high temperature retort and the vaporized molecules are transported to the lower temperature mandrel. A porous filter is used to eliminate particulate matter that is sometimes generated during the evaporation process. The material quality is apparently

PBN-75-382

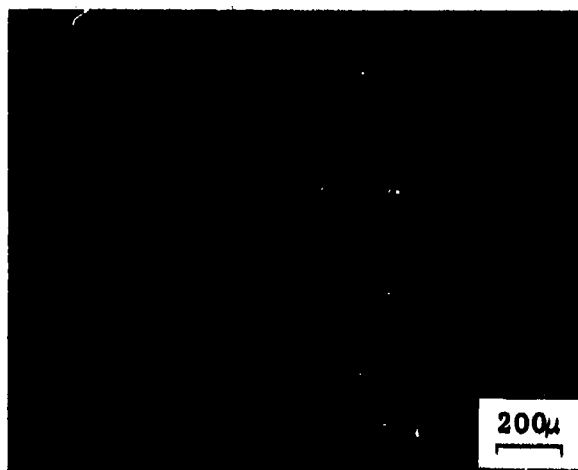


Figure 12. Microstructure of Elemental ZnSe,
Edge View, Se/ Zn Molar ratio = 1.34

PBN-75-381



Figure 13. Microstructure of CVD ZnSe, Edge View,
 H_2Se / Zn Molar ratio = 1.25

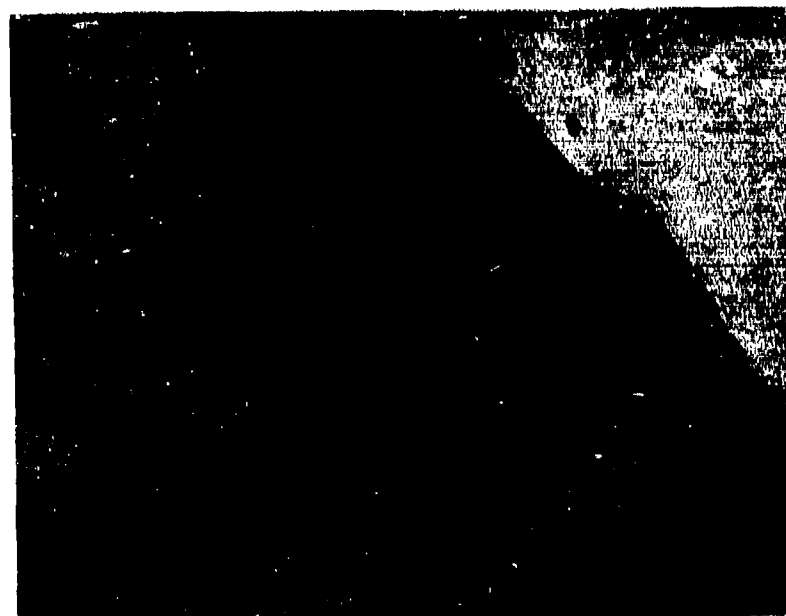
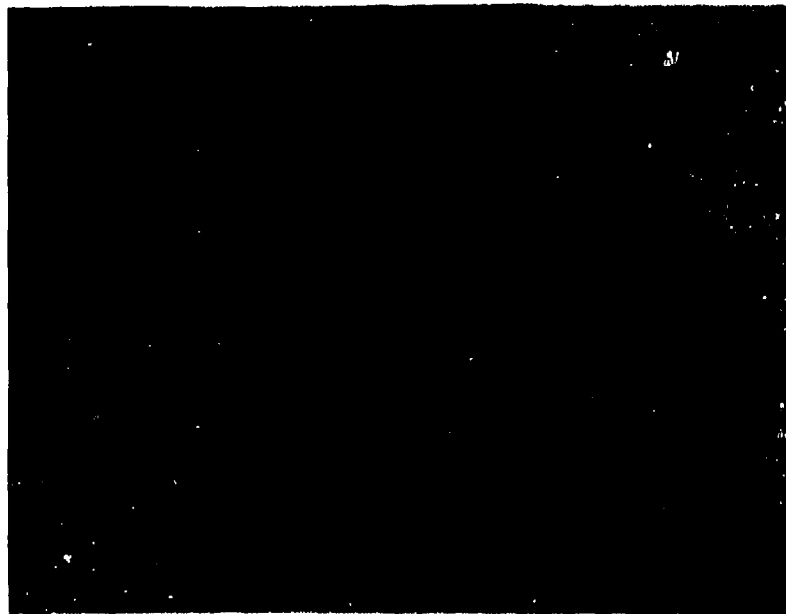


Figure 14. Visible Transparency of Physical Vapor Deposited Zinc Selenide

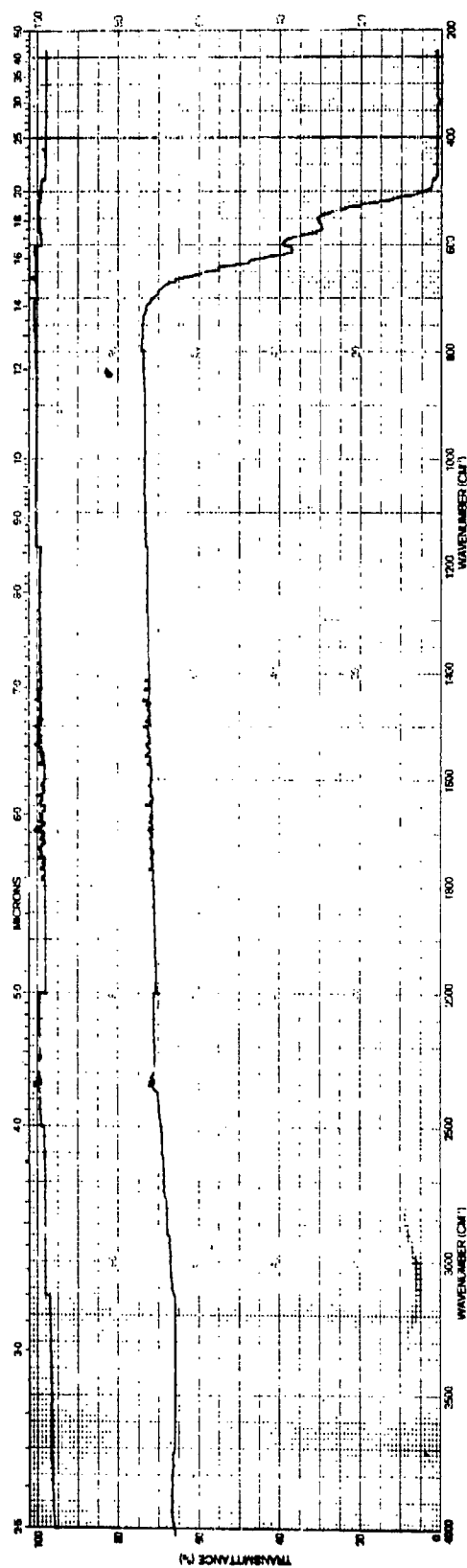


Figure 15. Typical Infrared Transmittance of 1.5 cm thick PVD Zinc Selenide

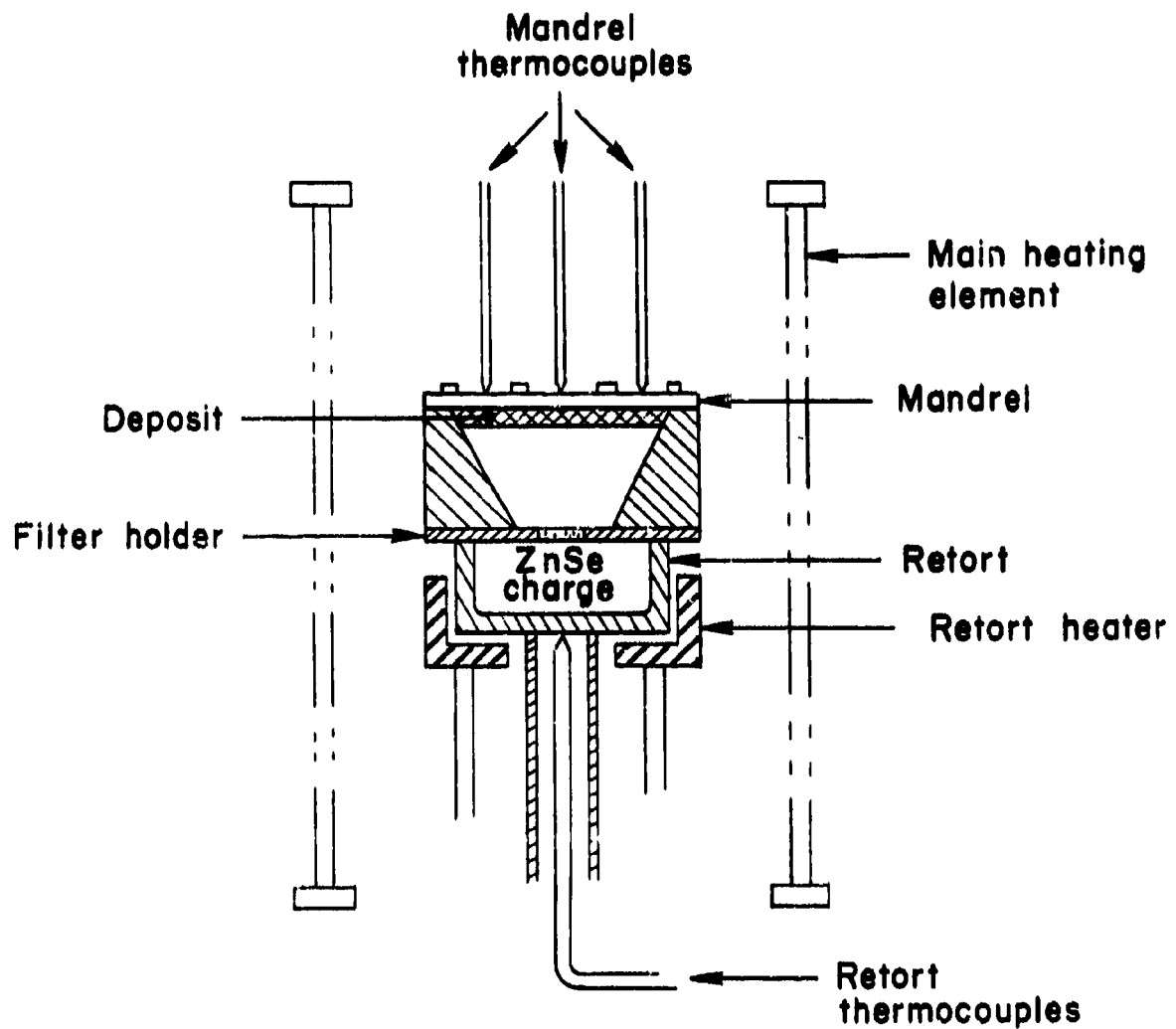


Figure 16. Schematic of Physical Vapor Deposition Apparatus.

determined by the retort temperature, the mandrel temperature, the temperature distribution on the mandrel, and the system pressure.

During this phase of the program, seventeen (17) depositions were made. The process conditions used are summarized in Table 4.

The first deposit made under this program was run PVD-39. It was made primarily to yield substrate material for the zinc sulfide overcoat process work. The run was successful and a 9-inch diameter by 5/8 inch thick disc was deposited and cut into $3 \times 3 \times 5/8$ inch samples. The optical quality of the material was considered to be good even though inclusions on the order of 0.5 mm in size were observed. The apparent absorption coefficient, as measured calorimetrically at 10.6 micrometers, was 0.05 cm^{-1} for a 1.27 cm sample. This value is an order of magnitude greater than material produced earlier, but it is felt that the higher value was primarily caused by the inclusions. Figures 17 and 18 present the visible and infrared transmittance of a 1 cm sample taken from this deposit. Also shown on Figure 18 is the transmittance of standard CVD and, as noted, the PVD material transmits to a lower wavelength. The band gap of the PVD material appears to occur at a slightly higher energy, probably because the material is more nearly stoichiometric. The microhardness of this deposit was measured with a 50-gram Knoop indenter. The measured value of 100 compares favorably with chemical vapor deposited material.

A closer examination of the transmittance curve in Figure 18 shows the presence of a broad absorption band centered around 3 micrometers. This band had been observed in previous deposits and is apparently associated with oxide impurities that are introduced into the deposit by use of the porous silica filters that are used to eliminate particulate matter from the deposit. Run PVD-40 was made with an alumina filter in order to determine if the absorption could be minimized. As evidenced by the infrared transmittance of this

TABLE 4

DEPOSITION CONDITIONS FOR PVD ZINC SELENIDE

<u>Run No.</u>	<u>Retort Temp (° C)</u>	<u>Mandrel Temp (° C)</u>	<u>Furnace Pressure (torr)</u>	<u>Mandrel Size (in.)</u>	<u>Deposition Time (hrs)</u>
PVD-39	1115	985	0.4	9	151
PVD-40	1130	950	0.6	9	52
PVD-41	1120	950	0.4	9	97
PVD-42	1140	950	0.4	15	34
PVD-43	1150	950	0.5	15	93
PVD-44	1210	935	0.5	15	77
PVD-45	1175	900	0.6	15	No Charge
PVD-46	1170	890	0.6	15	5
PVD-47	1220	910	300	15	No Deposit
PVD-48	1215	925	100	15	3
PVD-49	1190	915	0.7	15	28
PVD-50	1200	905	0.9	15	82
PVD-51	1160	899	0.3	15	79
PVD-52	1148	909	0.85	15	73
PVD-53	1120	930	0.8	15	90
PVD-54	1100	950	0.8	15	90
PVD-55	1150	950	0.8	15	100

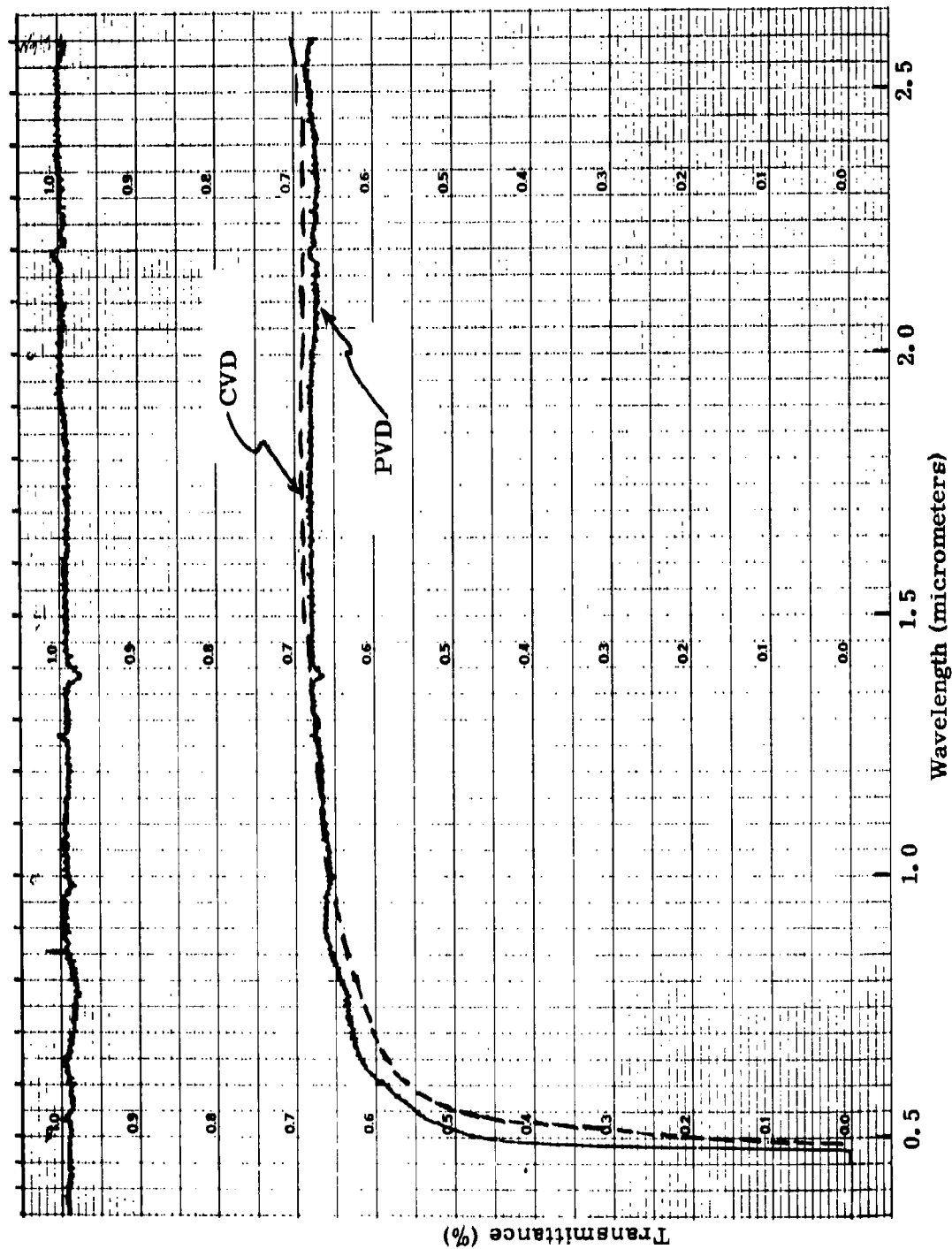


Figure 17. Visible Transmittances of 1.27 cm Thick PVD-39 ZnSe and Standard CVD ZnSe

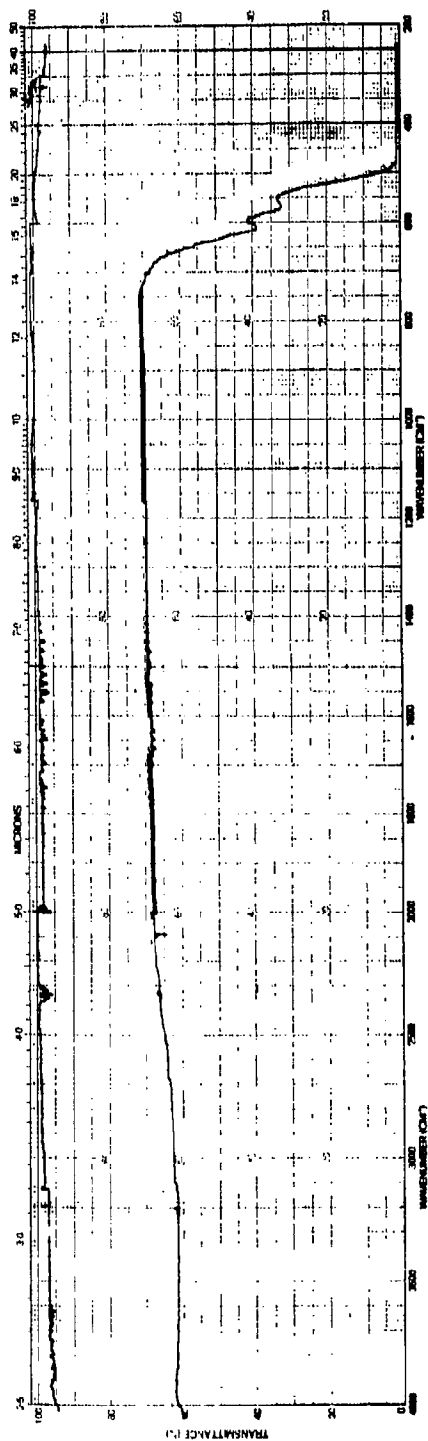


Figure 18. Infrared Transmittance of Run PVD-39, 1.27 cm thick.

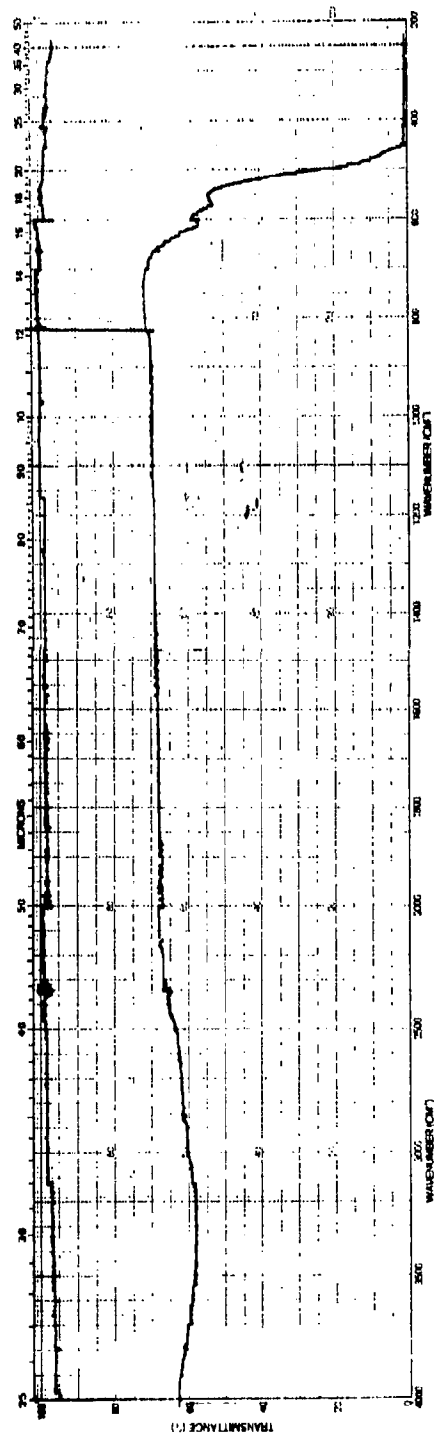


Figure 19. Infrared Transmittance of Run PVD-40, 0.49 cm thick.

deposit (Figure 19) the absorption increased in magnitude. The material also showed some scatter as indicated from the visible transmittance shown in Figure 20.

In run PVD-41 a fritted quartz filter was again used. Although heat sensor problems limited the amount of information obtained from this deposit with respect to the impurity problem, it can be seen from the infrared transmittance curve in Figure 21 that the 3 micrometer absorption band is still present although not as pronounced as in the previous run. Since visually the optical quality of this material appeared to be quite good its imaging characteristics in the 8 to 12 micrometer range were determined. The techniques used for this measurement are described in the Appendix. Table 5 presents the results of these measurements and, as indicated, there is an increase in the image width (at 15% intensity). Even though the magnitude of the increase is higher than desired it was felt that the material could be improved and it was decided to scale the process to fabricate 15-inch diameter samples.

Run PVD-42 was the first attempt at a 15-inch diameter deposit. The deposit was intentionally terminated after 34 hours of deposition to determine the deposition rate. The resultant disc was of good optical quality with very few inclusions. Comparison with other PVD runs indicated that the material was equivalent and that the 3 micrometer absorption band is somewhat reduced in magnitude. It is possible that with the repeated use of the same silica filter that its impurity content is progressively reduced. The apparent absorption coefficient of this material at 10.6 micrometers was determined to be 0.03 cm^{-1} .

Runs PVD-43 through -55 were concerned with depositing a $10 \times 10 \times 3/4$ in. specimen (to be cut from a 15 in. diameter disc). In run PVD-44 it was determined from three thermocouples located at 0 and $\pm 3-1/2$ in. radially from the center of the 15-inch disc that the temperature distribution measured would result in high residual stresses. Therefore in the next four runs (PVD-45 through -49) additional thermocouples were used to determine

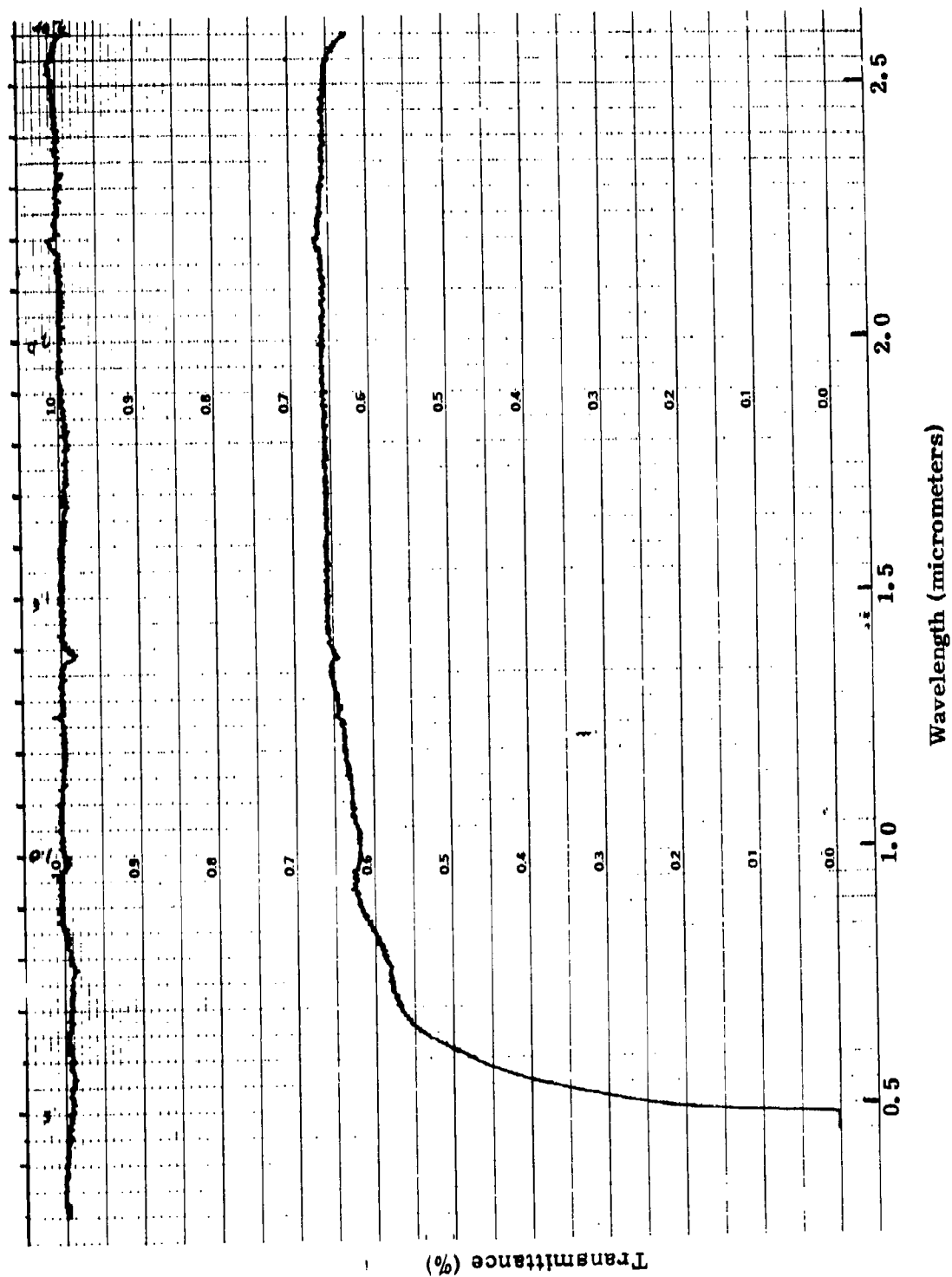


Figure 20. Visible Transmittance of Run PVD-40, 1.43 cm thick.

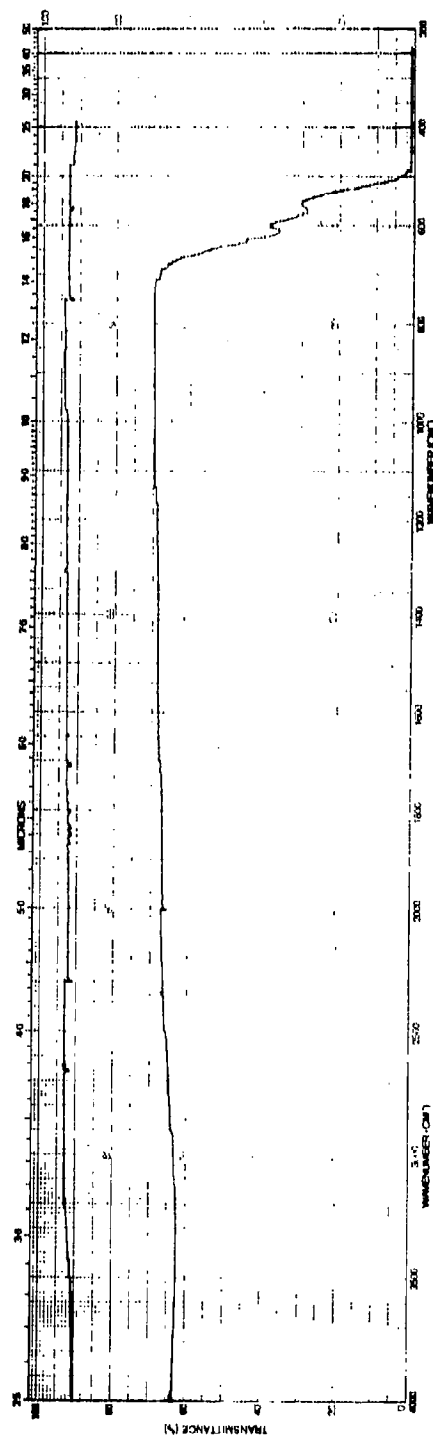


Figure 21. Infrared Transmittance of Run PVD-41, 1.43 cm thick.

TABLE 5

IMAGE SPOILING CHARACTERISTICS OF INFRARED MATERIALS

<u>Sample</u>	<u>Aperture (in.)</u>	<u>Incident Angle (deg)</u>	<u>$\Delta 15\%$ (μrad)</u>	<u>Image Growth (μrad)</u>
PVD-41	7	0	96.3	
None	7	---	87.5	8.8
PVD-41	4-1/2	45	144.2	
None	4-1/2	---	133.7	10.5
CVD-ZnS*	5	0	127.2	
None	5	---	123.6	3.6
CVD-ZnSe (I-23)	7	0	98.8	
None	7	0	97.5	1.3

* Run ZS-157P

the mandrel temperature before and during deposition. Based on the temperature gradients observed in each of these runs, the thermal insulation around the mandrel was altered to reduce the radial temperature difference. In run PVD-49 the temperature difference between the middle and edge of the mandrel was approximately 50° C. The thickness and thickness distribution of this run was excellent. Because of the high retort temperature used, however, an abnormally high deposition rate was attained that caused the deposited material to scatter more than normal. The infrared transmittances of three sections of this deposit are presented in Figures 22, 23, and 24.

Run PVD-51 yielded a 15-inch diameter \times 0.75 inch thick blank. Evaluation of the blank, however, indicated that approximately the first third of the deposit was rather porous. Porous material had been observed previously but never to this great an extent. It is apparently caused by non-equilibrium conditions that exist early in the deposition process. The infrared transmittance of this deposit with the porous layer removed is presented in Figure 25. The lower-than-normal transmittance is attributed to particulate matter that evidently bypassed the filters.

Run PVD-52 was deposited in order to determine if the start-up procedures caused the formation of the porous layer. In this run a slow evacuation period (\sim 2 hrs) was used prior to depositing at full vacuum. The resulting material showed only a 0.010 to 0.020 in. porous layer. The infrared transmittance of the remaining material is shown in Figure 26.

Run PVD-53 yielded a 15-inch disc in excess of one inch in thickness with an excellent thickness distribution (Figure 27). The thickness and optical clarity, at visible wavelengths, can be seen in the edge polished specimen shown in Figure 28, and its infrared transmittance in Figure 29. The apparent absorption coefficient at 10.6 micrometers was 0.012 cm^{-1} .

Further investigation of this disc under transmitted light, revealed unfortunately the presence of major cracks that were not discernible with normal lighting (Figure 30). The cracks observed are tensile in nature

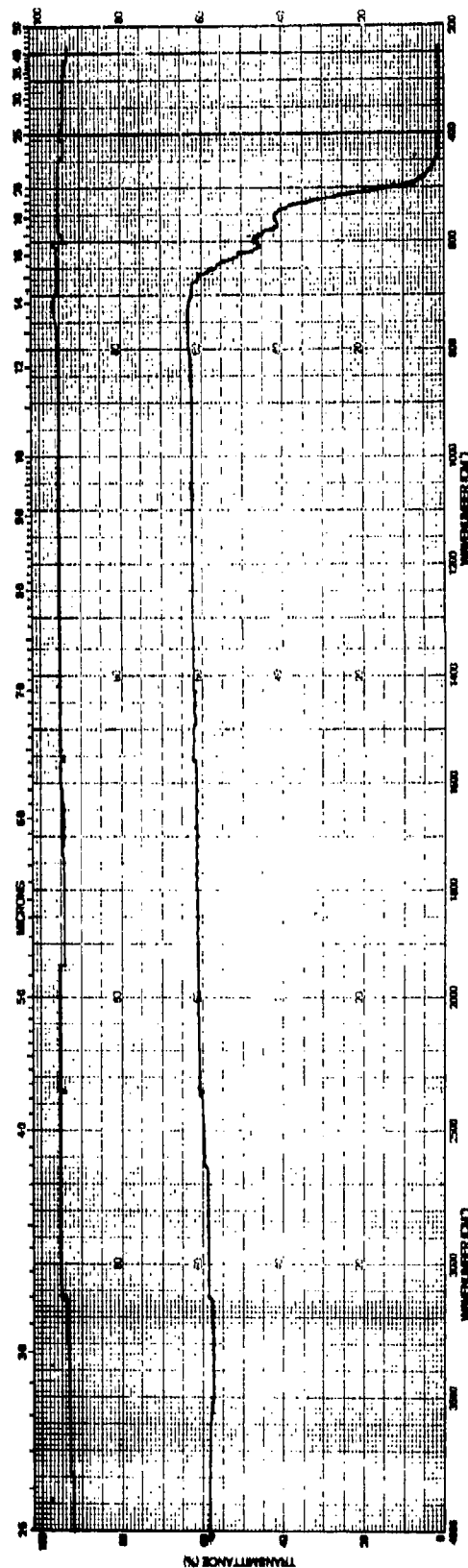


Figure 22. Infrared Transmittance of Area Near Center of 15 Inch Dia. Disc, PVD-49, 0.50 cm thick.

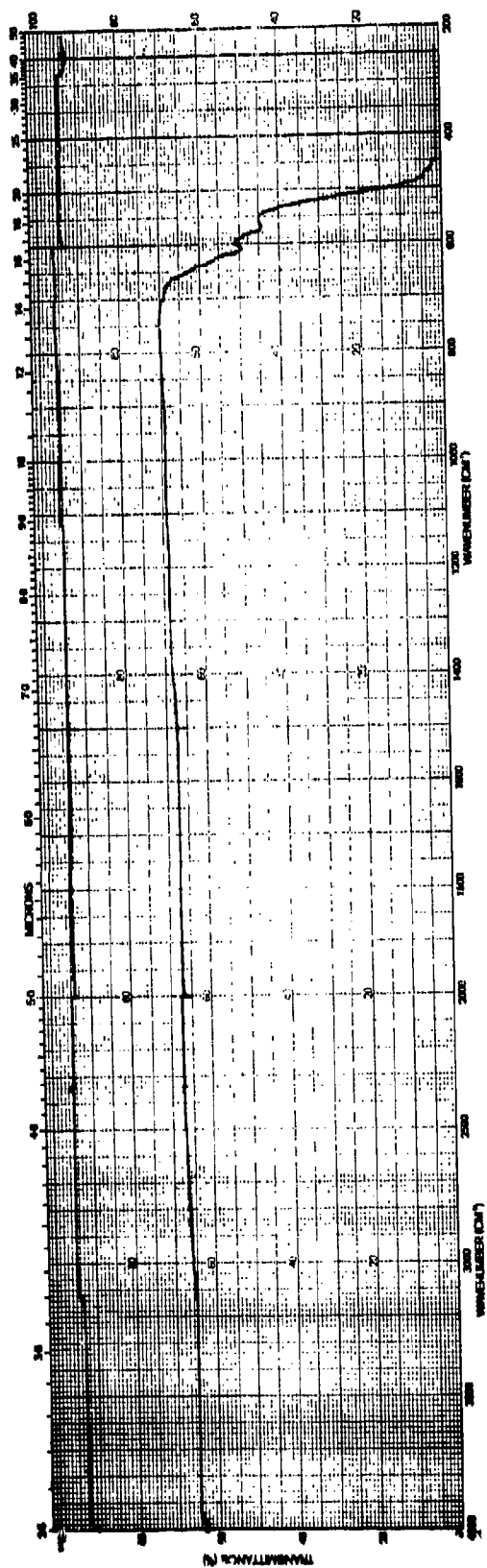


Figure 23. Infrared Transmittance of Area Located ~ 7 in. From Center of 15 in. Dia. Disc.
PVD-49, 0.73 cm thick.

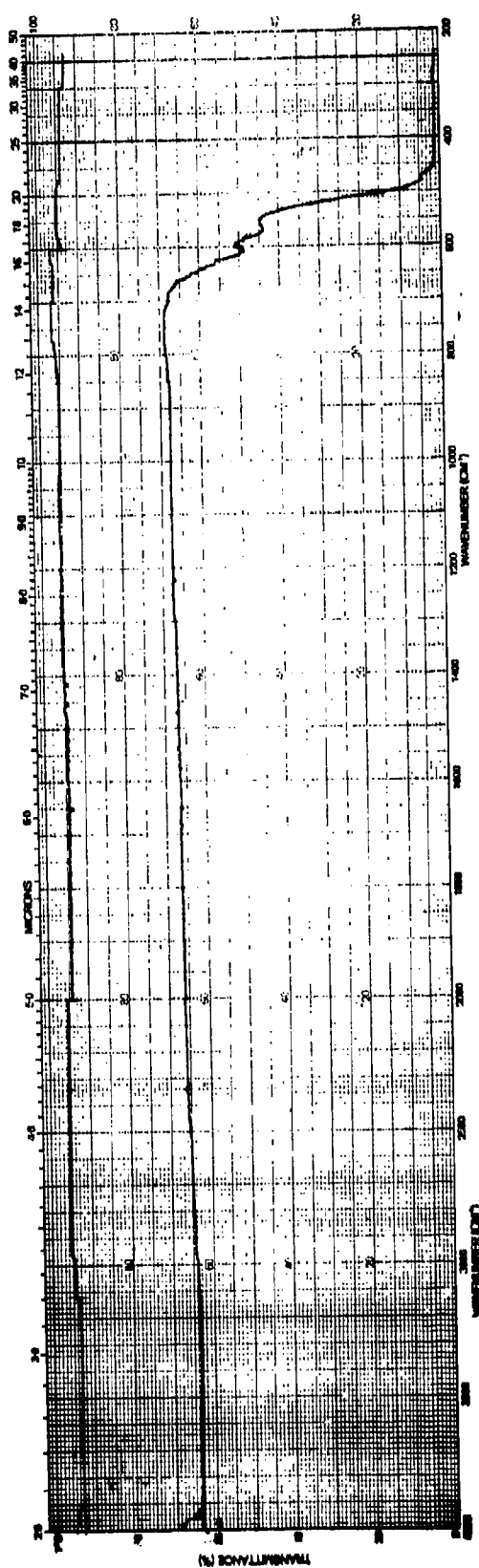


Figure 24. Infrared Transmittance of Area Located ~14 in. From Center of 15 in. Dia. Disc.
PVD-49, 0.73 cm Thick.

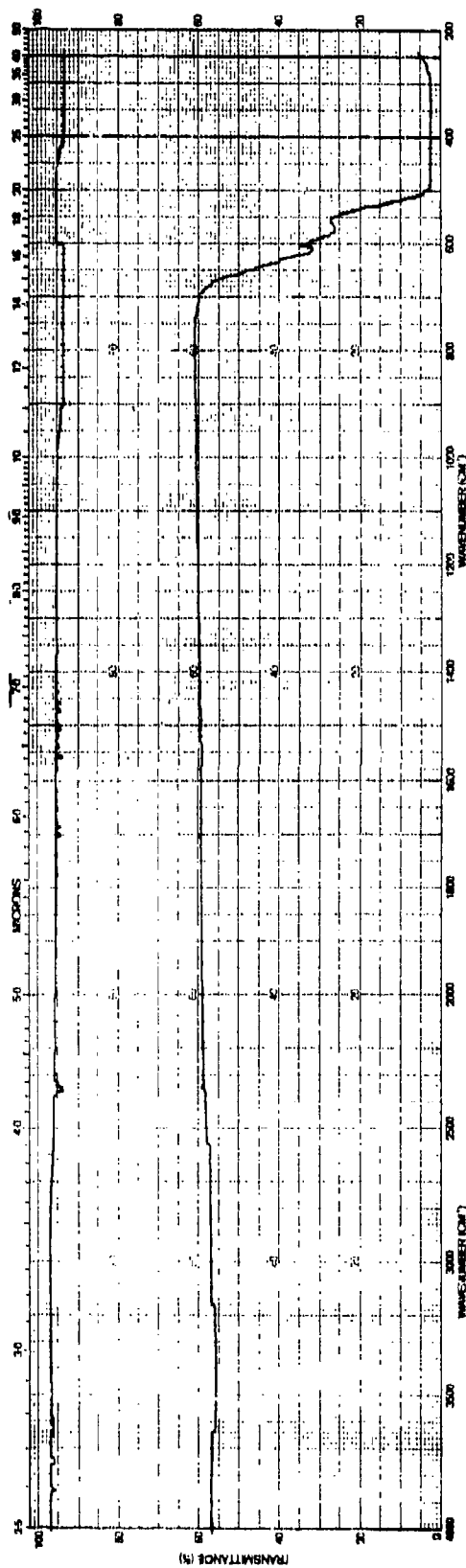


Figure 25. In-line Transmittance, PVD -51, Thickness 1.5 cm

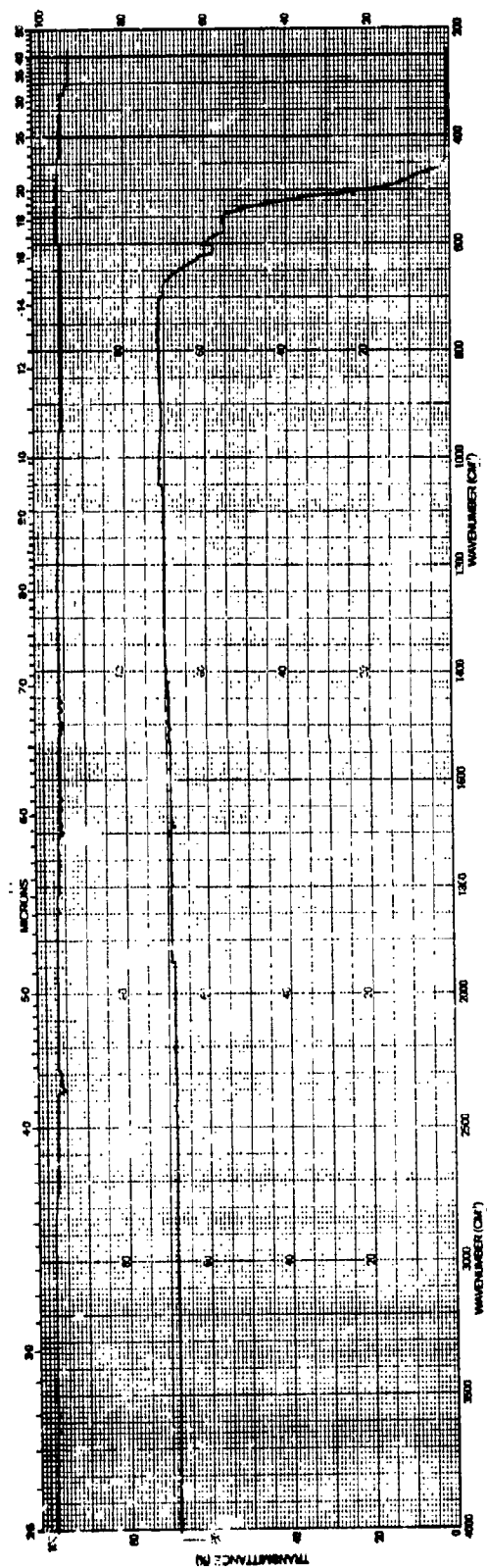


Figure 26. Infrared Transmittance, PVD-52, Thickness 0.5 cm

PBN-76-449

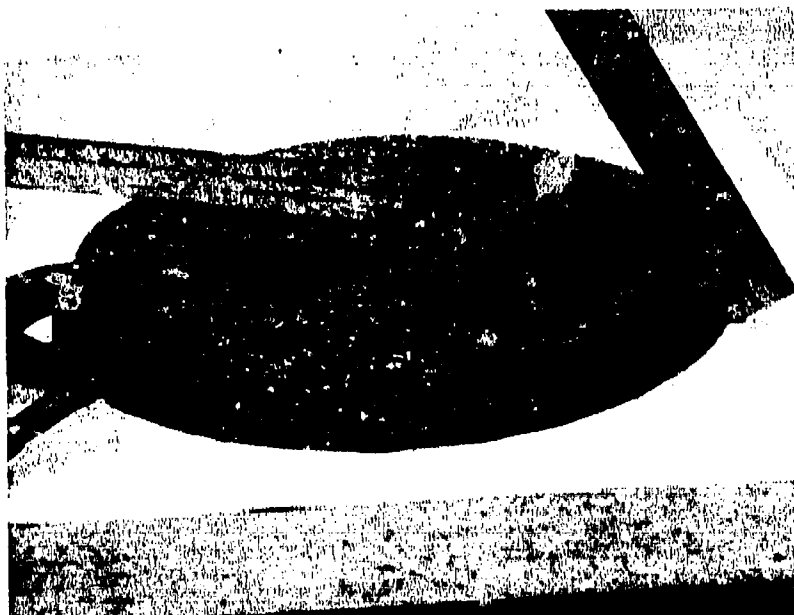


Figure 27. Run PVD-53 "As Deposited" Disc

PBN-76-450

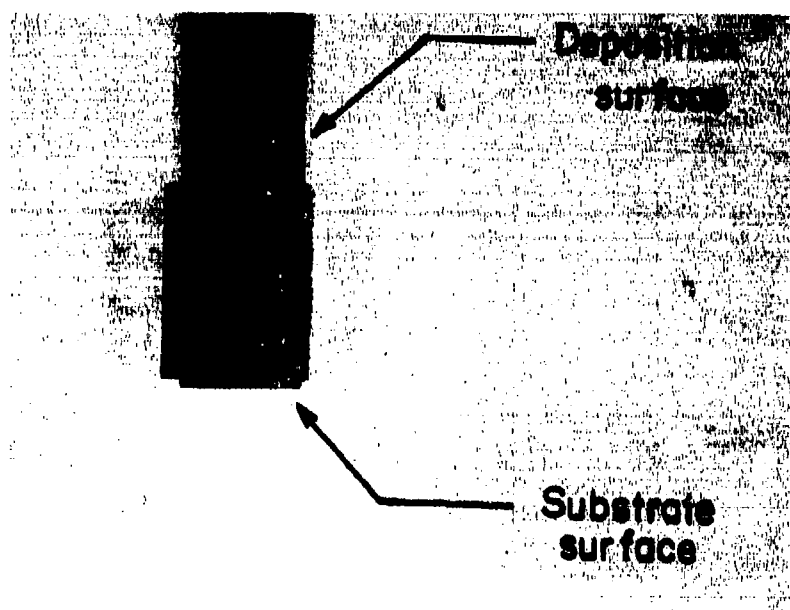


Figure 28. PVD-53 Edge Polished Specimen Showing Thickness, and Optical Clarity at Visible Wavelengths

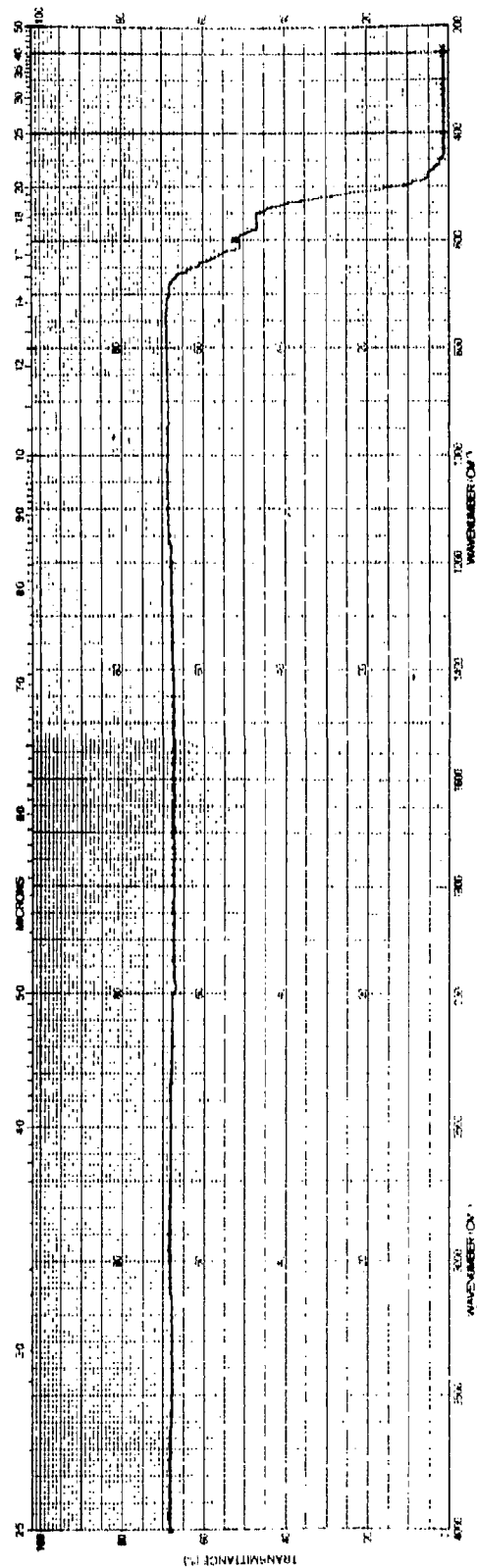


Figure 29. Infrared Transmittance, PVD-53, $t = 0.265$ inch, Edge View

PBN-76-451

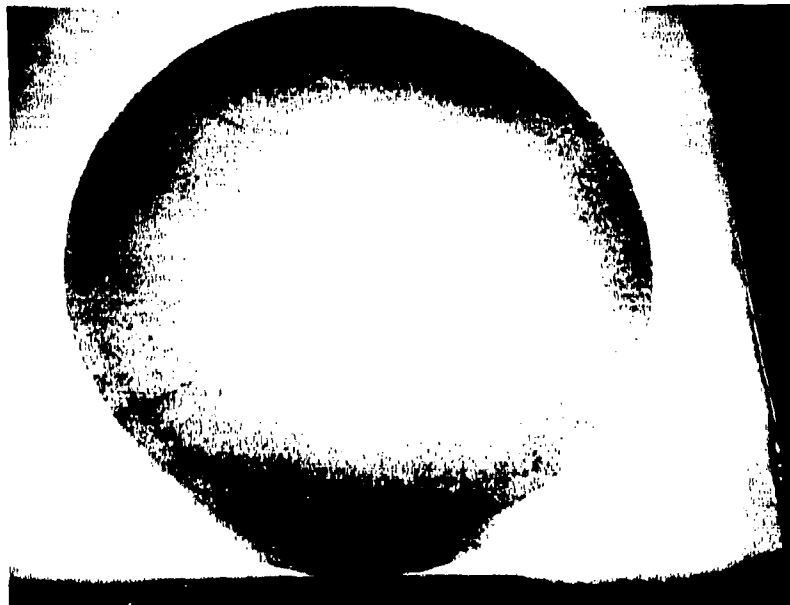


Figure 30. PVD-53 Under Transmitted Light

and propagate radially in from the outer diameter. They do not propagate through the thickness, hence the disc remained intact. The cracks are apparently caused by either an excessively rapid cooldown from deposition temperature or a radial temperature gradient that is initially set-up during deposition. The latter reason is, in our opinion, the most probable cause of the failure.

As previously mentioned, several attempts were made during this series of runs to decrease the radial temperature gradients on the 15-inch diameter mandrel by the use of carbon felt insulation. The diametrical temperature differences with respect to the center of this deposit were + 50° C, 0° C, and + 100° C. The stresses corresponding to these temperature variations can cause failure.

Since the use of insulation did not satisfactorily solve the temperature gradient problem it was decided that the only other viable method available was with the use of an external heating source at the center of the mandrel. A flat graphite heater, 5 inches in diameter, was designed and fabricated for this purpose and used in runs PVD-54 and -55. The results achieved with this heater, however, were not significantly different than those achieved without the heater. Because of this problem, the marginal imaging quality of the material, as well as the problems that were being encountered with this material in the zinc sulfide overcoat experiments, it was decided that a modified CVD process should be evaluated before the final choice on a fabrication process was made.

d. Low-Cost Chemical Vapor Deposition for Zinc Selenide

As discussed in an earlier section, the major drawbacks to the use of zinc selenide as a FLIR window are its durability in a rain environment and its cost. Techniques for improving durability are discussed in the following section. In this section techniques used to decrease cost are discussed.

The two major factors that govern the cost of CVD material are the yield achieved from a furnace run and the cost of one of the reactants, hydrogen selenide gas.

Yield can be maximized (and thus cost reduced) by utilizing as much of the deposition area as possible. That is, by using a mandrel size that is compatible with the size of the components desired and attaining a uniform thickness distribution over that area, the majority of the deposit can be utilized. During this task of the program a production size mandrel was designed and a thickness distribution attained in a similar size mandrel was used to determine the number of units ($13 \times 19 \times 0.6$ in.) that could be yielded per run. It was found that because of an increase in yield the cost of an unpolished unit in production quantities (100 to 200 units) could be reduced by approximately 37 percent over the standard costs of the material.

To further reduce the cost of zinc selenide window blanks the use of lower purity H_2Se gas was evaluated. The purity of the H_2Se gas used to deposit laser quality material is normally greater than 99.95 percent. The major impurities that are removed to attain this purity level are sulfur, water vapor, carbon dioxide and oxygen. A less expensive ($\sim 20\%$) 98 percent pure gas whose major impurity is sulfur (as H_2S), however, was available and was purchased for evaluation.

A process run was made using this gas and it was found to be equivalent in all respects to laser quality material, except that it had an apparent absorption coefficient at $10.6 \mu m$ of 0.006 cm^{-1} . The magnitude of absorption, although higher than laser quality material, is more than sufficient for FLIR window applications. Figure 31 shows the infrared transmittance of this material and, as noted, there are no obvious extrinsic absorptions over the entire spectrum.

Based on the results of this run a production run was made in the apparatus, shown schematically in Figure 32, to deposit a large zinc selenide plate. The material from this run was uniform in both thickness and optical quality. The as-deposited thickness profile of this blank is shown in Figure 33, and the spectral transmittance in Figure 34. The apparent absorption coefficient of this material at 10.6 micrometers was measured to be 0.0015 cm^{-1} . Laser quality material has an absorption coefficient at 10.6 micrometers that lies between 0.0004 and 0.0009 cm^{-1} .

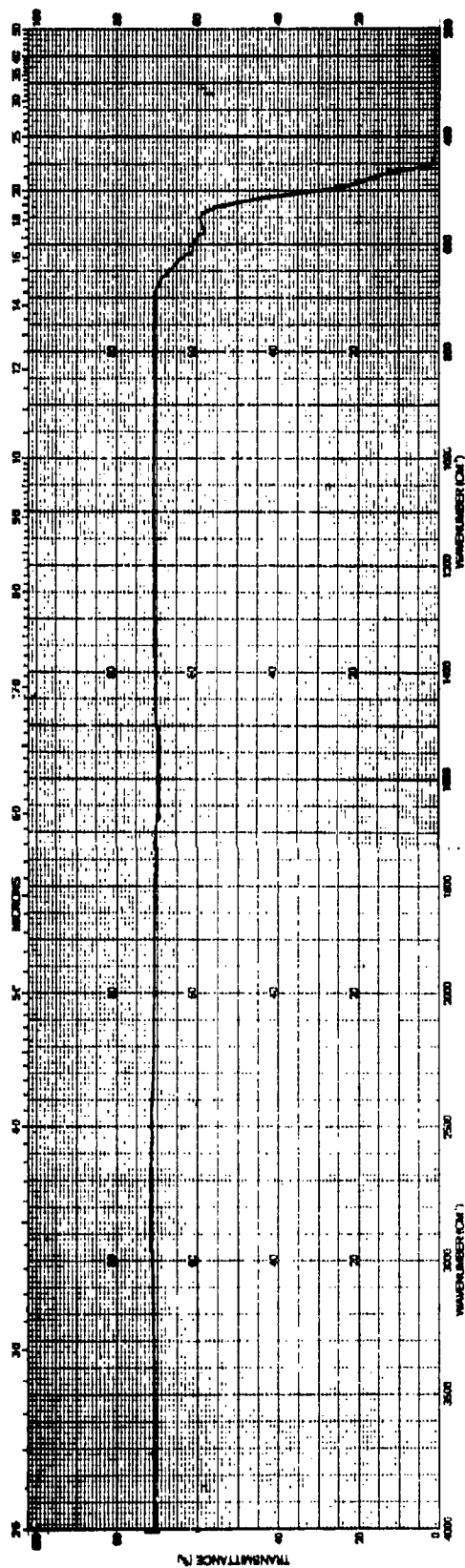


Figure 31. Infrared Transmittance of CVD ZnSe Produced With Low-Cost Materials

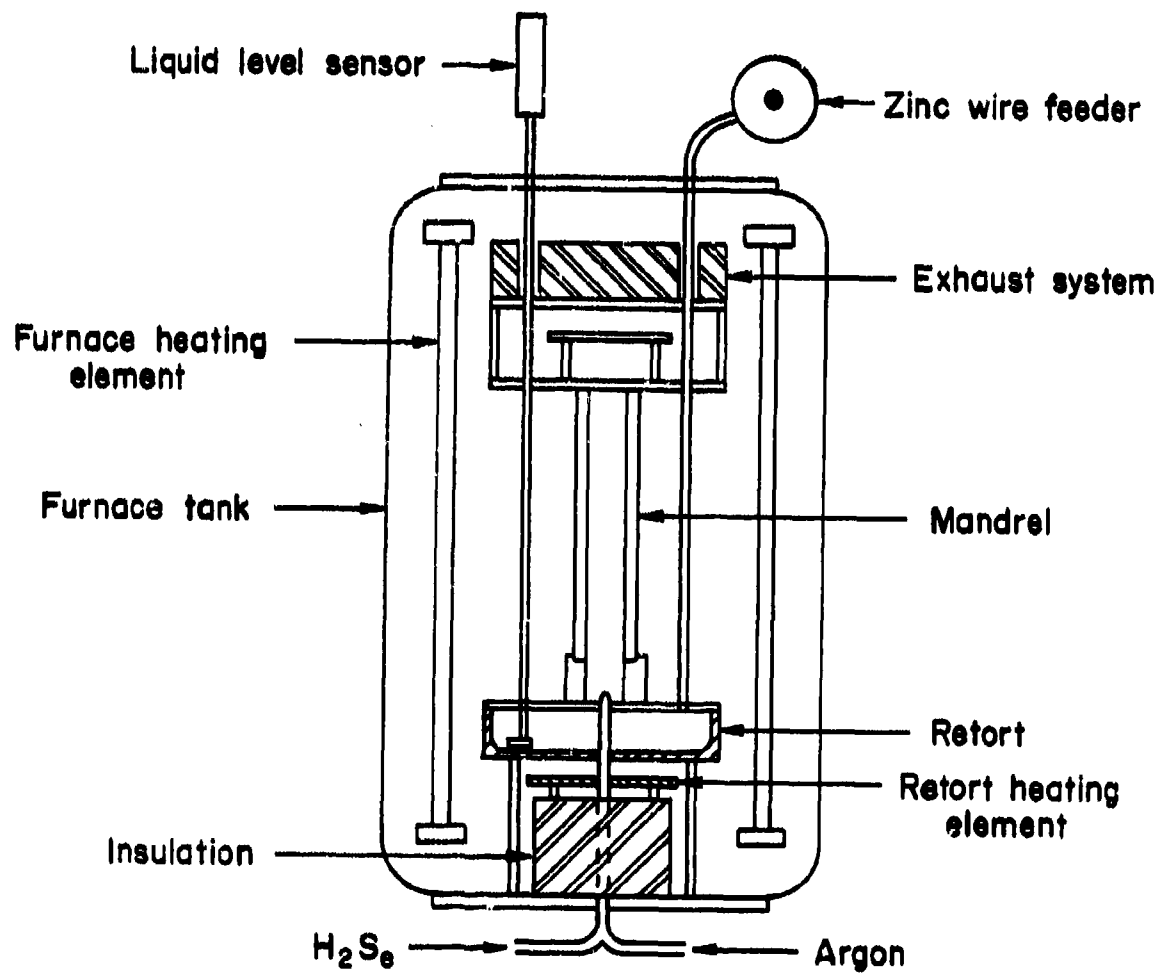


Figure 32. Schematic of Apparatus Used for Depositing CVD Zinc Selenide.

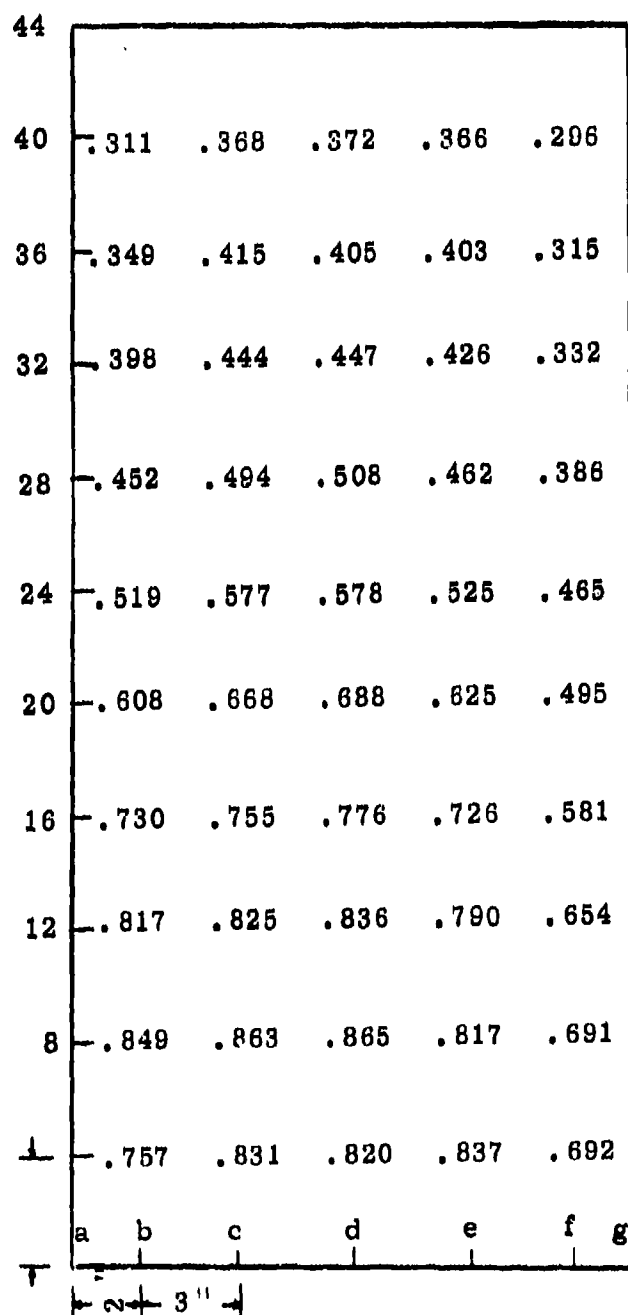


Figure 33. Low Cost ZnSe "As Deposited" Thickness Profile

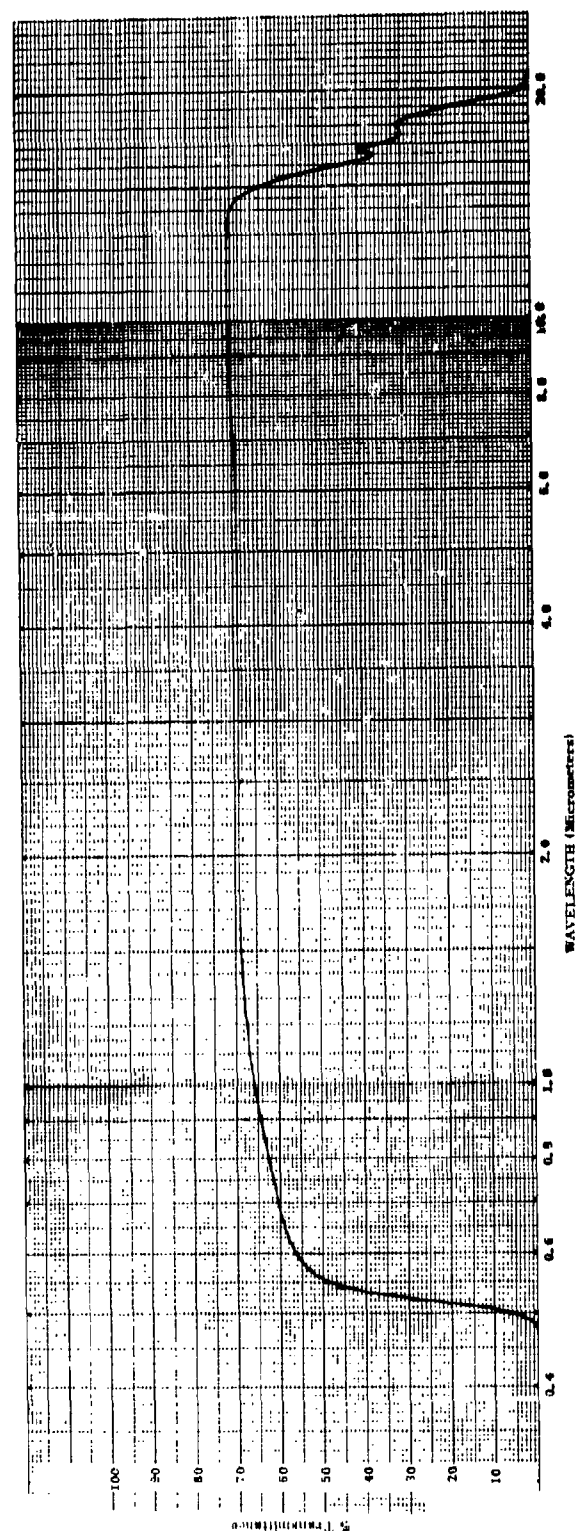


Figure 34. Spectral Transmittance of Low-Cost ZnSe, $t = 1.27$ cm

The results of this run allow a further reduction (~12 percent) in the cost of zinc selenide for multispectral FLIR windows. It is estimated that a $13 \times 19 \times 0.60$ inch blank of this material in production quantities will cost ~\$11,000. This cost is consistent with the goals established for this program.

Following the evaluation of the run two window blanks of 10×10 and a $13\text{-}1/4 \times 20$ inch size were cut and plate-glass polished. The 10×10 inch plate was submitted to the Air Force Materials Laboratory for further evaluation. One of the surfaces of the $13\text{-}1/4 \times 20$ inch blanks was optically polished and then overcoated with a thin layer (~0.050 in.) of CVD zinc sulfide. The blank was then polished and submitted to the Air Force Materials Laboratory for evaluation.

e. Composite Window Fabrication

In this task of the program the chemical vapor deposition process for coating zinc selenide with a thin overcoat layer (< 0.1 in.) of zinc sulfide was developed. Earlier efforts under other programs had established the basic feasibility of this method of attachment. The purpose of the thin layer is to allow the use of zinc selenide in a rain environment. The use of CVD zinc sulfide for protection from raindrop impingement is based on test results from the rotating arm apparatus at the Air Force Materials Laboratory. As mentioned in an earlier section of the report, there should be no appreciable optical degradation caused by the presence of this layer on the surface of zinc selenide.

To develop a reliable process for coating zinc selenide with zinc sulfide fifteen (15) deposits were made during this phase of the program. Table 6 presents the operating conditions used for these deposits.

The first three zinc sulfide coating deposits were made to determine the optimum process conditions. These deposits were made on graphite substrates. The remaining deposits were made on zinc selenide substrates fabricated by the CVD and PVD processes.

TABLE 6

DEPOSITION CONDITIONS FOR ZINC SULFIDE OVERCOAT EXPERIMENTS

<u>Run No.</u>	<u>Dep Temp (° C)</u>	<u>Dep Pressure (torr)</u>	<u>Molar Ratio (S/ Zn)</u>	<u>H₂S Flow (lpm)</u>	<u>Deposition Time (hrs)</u>
ZnSC-1	650	30	0.5	0.5	10
ZnSC-1A	650	30	1.0	1.0	10
ZnSC-2	725	15	0.5	0.5	9
ZnSC-2A	725	60	0.5	0.5	9
ZnSC-3	650	60	0.25	0.25	15
ZnSC-3A	650	60	0.5	0.5	8
ZnSC-4	725	60	0.4	0.4	10
ZnSC-5	750	60	0.5	0.5	10
ZnSC-6	725	60	0.5	0.5	10
ZnSC-7	725	60	0.5	0.5	10
ZnSC-8	725	50	0.5	0.5	10
ZnSC-8A	725	50	1.0	1.0	5
ZnSC-9	725	50	0.5	0.5	15
ZnSC-10	700	50	0.5	0.5	15
ZnSC-11	700	50	~0.5	0.6	24
ZnSC-12	700	50	~0.5	0.6	17
ZnSC-13	600	30	~1.0	0.6	14
ZnSC-14	700	50	0.5	0.6	8
ZnSC-15	700	50	0.5	0.6	15
ZnSC-16	690				

Runs ZnSC-1, -2, and -3 were deposited at various temperatures, system pressures, and hydrogen sulfide-to-zinc molar ratios. Run ZnSC-1 was deposited at 650° C and molar ratios of 0.5 and 1. As expected, the infrared properties of the higher-molar-ratio material are slightly better than the lower-molar-ratio material, although the visible imaging quality of the lower-molar-ratio material is considerably better. Figure 35 presents the infrared transmittance of both materials from this deposit. Note the presence of the 6-micrometer absorption band that is indicative of a low temperature deposit. This band is reduced in magnitude when deposition occurs at higher temperatures.

A higher deposition temperature (725° C) was used for run ZnSC-2. The run was divided into two parts. For the first half of the run the material was deposited at 15 torr, while for the second half of the run the material was deposited at 60 torr. Both materials exhibit good infrared transmissions as can be seen in Figure 36. Run ZnSC-3 was an attempt to achieve low-molar-ratio material at a high pressure and low temperature. The deposit was too thin to properly analyze. Based on the results of these three runs it was decided that the thin overcoats of zinc sulfide should be made with conditions similar to ZnSC-2.

The substrate used for coating in ZnSC-4 was $3 \times 3 \times 1/4$ inch sample of CVD zinc selenide. The deposition was made at 725° C for 10 hours at a H_2S/Zn molar ratio of 0.4. Some difficulty was experienced in the operation of this run and it was later determined that it was due to growths around the H_2S gas inlet port. Although the coating showed good adherence to the substrate, the optical quality of the composite was poor. The composite zinc sulfide/zinc selenide material scattered badly as indicated by the infrared transmittance shown in Figure 37. The scatter was caused by improper mixing of the reactants.

Similar operational problems occurred during run ZnSC-5. This deposit was completed successfully in spite of the pressurized gas inlet by operating the flowmeters at higher than atmospheric pressure. The

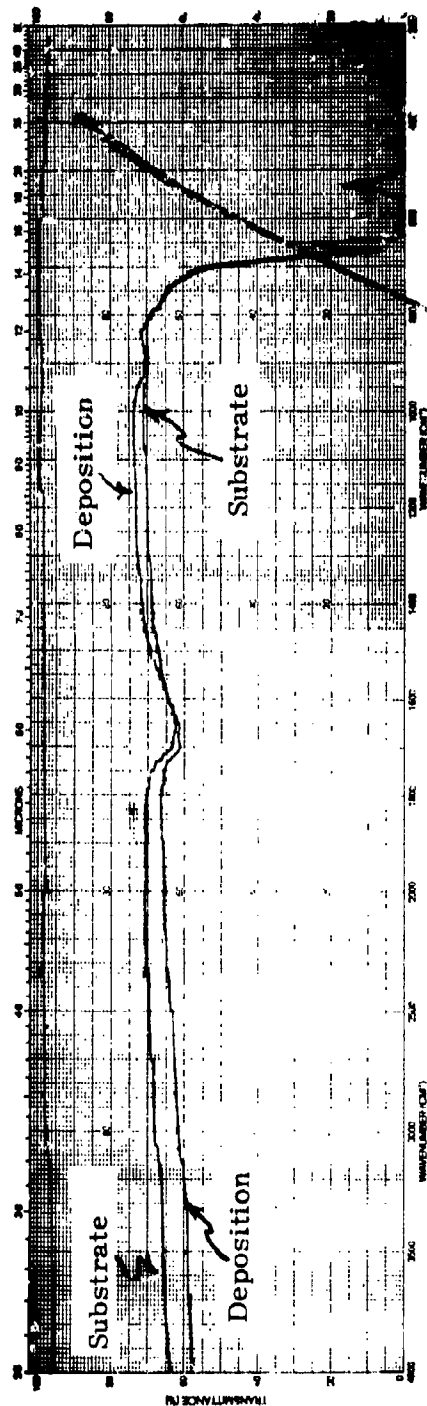


Figure 35. Infrared Transmittance of Zinc Sulfide Coating Run, ZnSC-1; 0.1 cm Substrate and 0.12 cm Deposition Thickness.

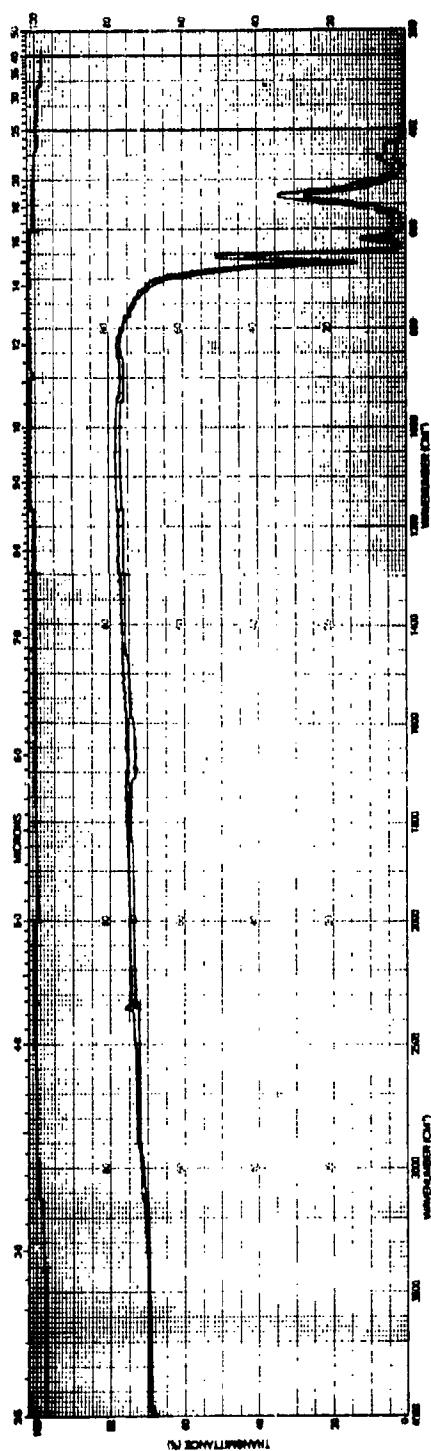


Figure 36. Infrared Transmittance of Zinc Sulfide Coating Run, ZnSC-2; 0.07 cm Substrate and 0.05 cm Deposition Thickness

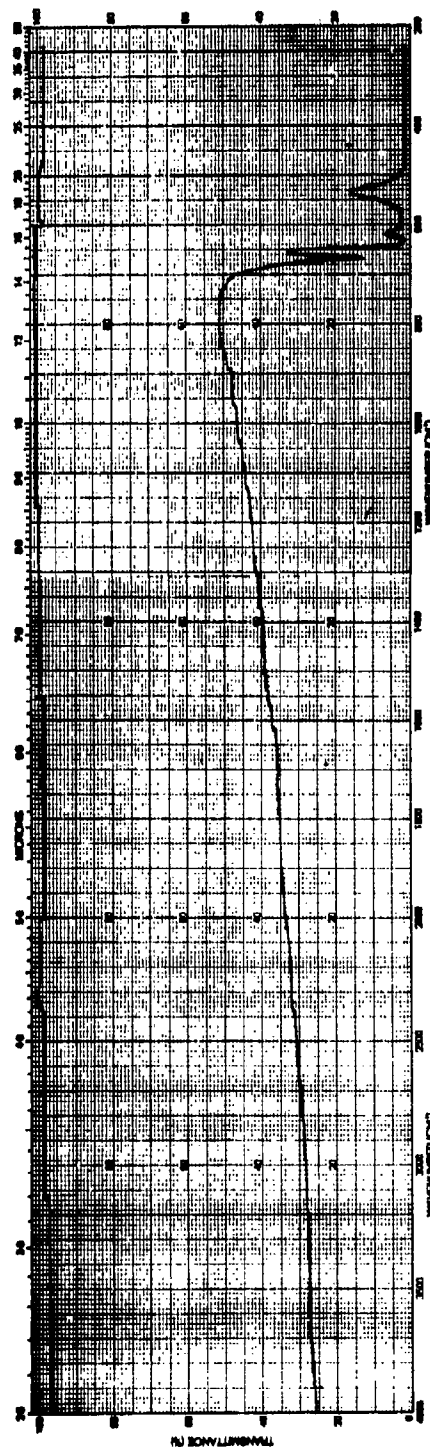


Figure 37. Infrared Transmittance of Zinc Sulfide Coating Run, ZnSC-4; 0.07 cm Thick ZnS Deposition on 0.5 cm Thick CVD ZnSe.

resulting material again showed good adherence and less scatter as indicated in the infrared transmittance shown in Figure 38. The magnitude of the transmittance in the 8 to 12 micrometer range was also better than had been previously achieved.

Run ZnSC-6 was deposited under conditions similar to ZnSC-5 after setup adjustments were made to prevent adverse inlet growth. The resulting material showed less scatter and an improved infrared transmittance as indicated by the curve in Figure 39.

In Run ZnSC-7 a thin zinc sulfide layer was deposited on a PVD zinc selenide substrate. Although the adhesion was good, the optical properties were poor. Optical examination of the zinc sulfide/ zinc selenide interface revealed the presence of many micro-fissures in the PVD material. These micro-fissures act as scattering sites as evidenced by the infrared transmittance of the composite shown in Figure 40. The transmittance of the zinc sulfide after removal from the substrate is shown in Figure 41 and, as observed, it has good optical properties.

Run ZnSC-9 was deposited with two PVD zinc selenide substrates to yield sufficient material for rain erosion samples. However, both substrates apparently crazed (cracks in the zinc selenide at the zinc sulfide-zinc selenide interface) on cooling from the deposition temperature. The type of failure observed is shown in Figure 42. Since these cracks are in the PVD material only, and do not propagate to the free surface of the substrate, it appears that they are caused by a thermal expansion mismatch between the zinc sulfide and zinc selenide. Figure 43 shows the infrared transmittance of this deposit.

To determine if the observed crazing was due to thermal expansion mismatch the expansion of CVD zinc sulfide, CVD zinc selenide, and PVD zinc selenide were determined. The results which are presented in Table 7 indicate that CVD zinc sulfide and CVD zinc selenide are compatible. However, the CVD zinc sulfide and PVD zinc selenide exhibit an expansion mismatch

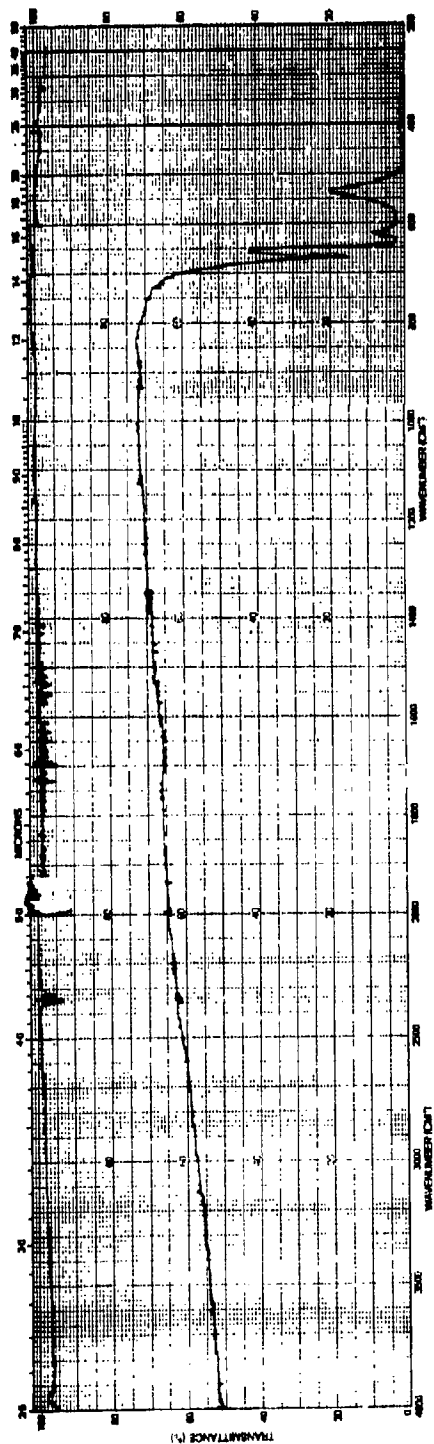


Figure 38. Infrared Transmittance of Zinc Sulfide Coating Run, ZnSC-5; 0.04 cm Thick ZnS Deposited on 0.69 cm Thick CVD ZnSe.

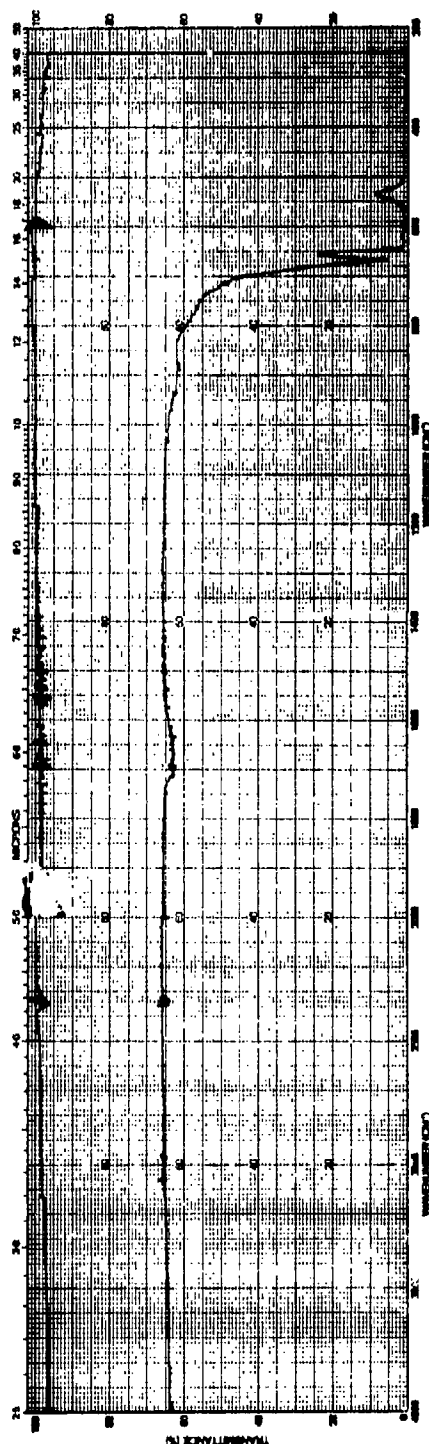


Figure 39. Infrared Transmittance of Zinc Sulfide Coating Run, ZnSC-6; 0.1 cm Thick ZnS Deposited on 0.65 cm Thick CVD ZnSe.

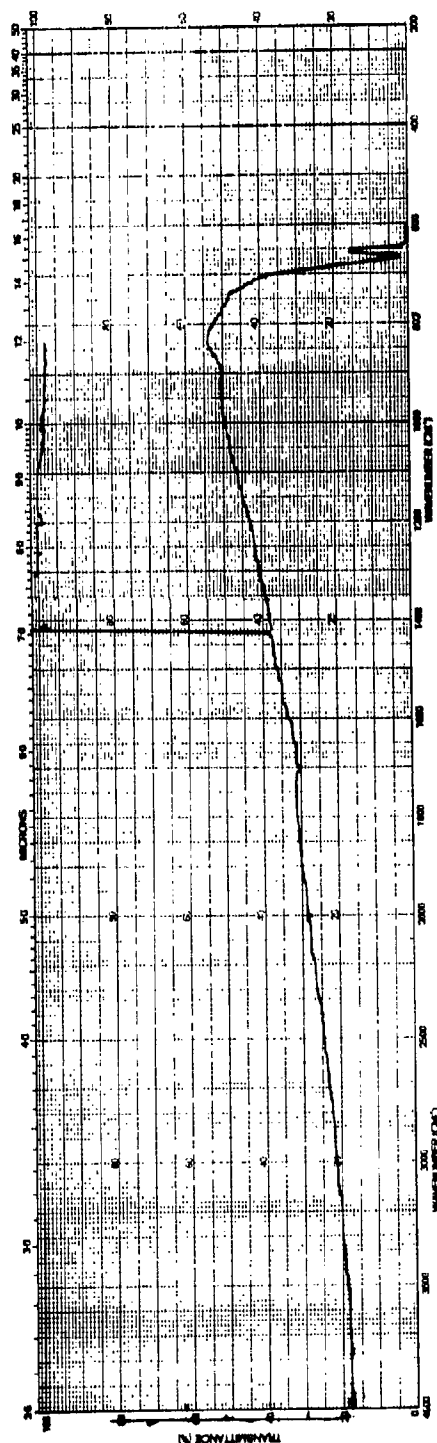


Figure 40. Infrared Transmittance of Zinc Sulfide Coating Run, ZnSC-7; 0.18 cm Thick ZnS Deposited on 0.71 cm Thick PVD ZnSe.

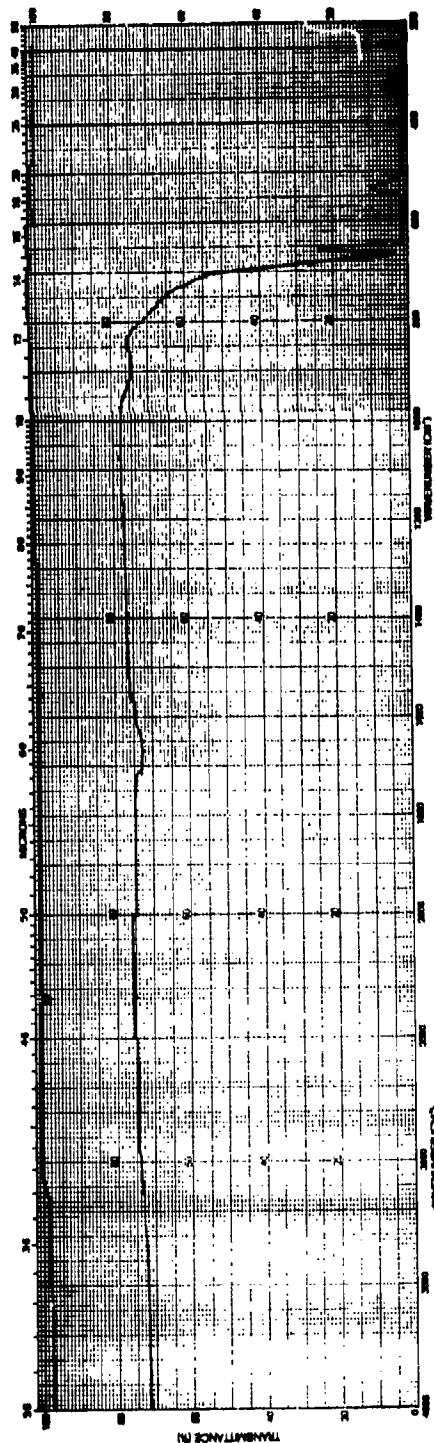


Figure 41. Infrared Transmittance of 0.16 cm Thick Zinc Sulfide Layer Deposited During Run ZnSC-7.

PBN-76-347

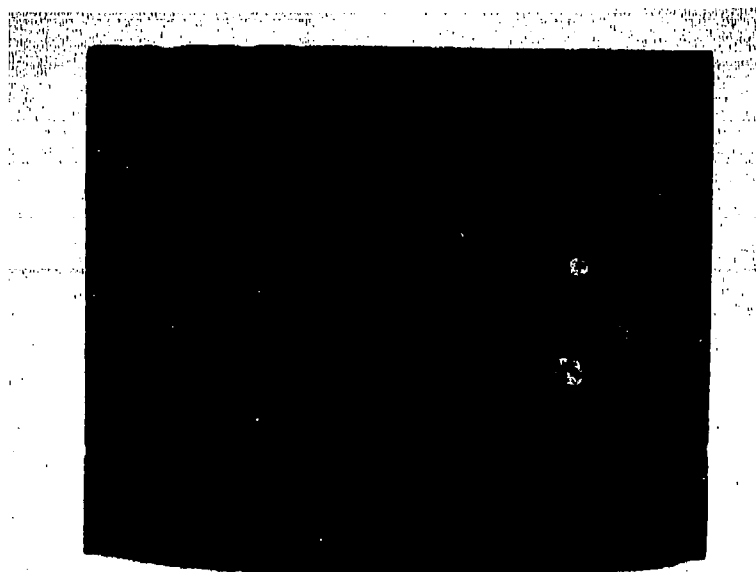


Figure 42. PVD Zinc Selenide Coated with Zinc Sulfide-Run ZnSC-9
Viewed Through Transmitted Light (Dimensions
3 in. \times 3 in.)

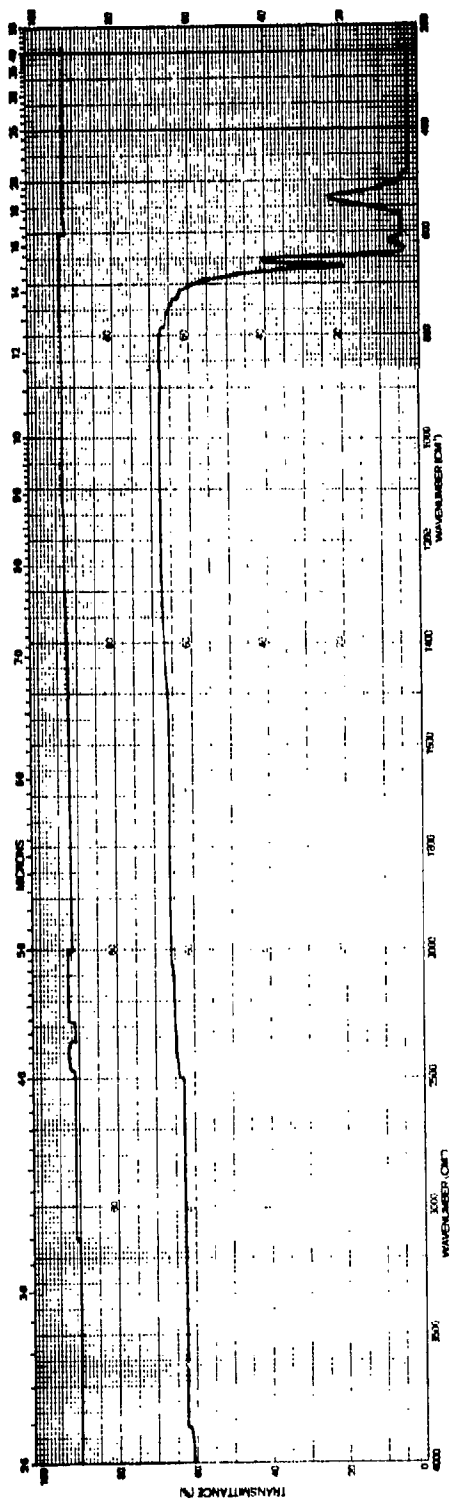


Figure 43. Infrared Transmittance of Zinc Sulfide Coating Run, ZnSC-9; 0.08 cm Thick ZnS Deposited on 0.34 cm Thick PVD ZnSe.

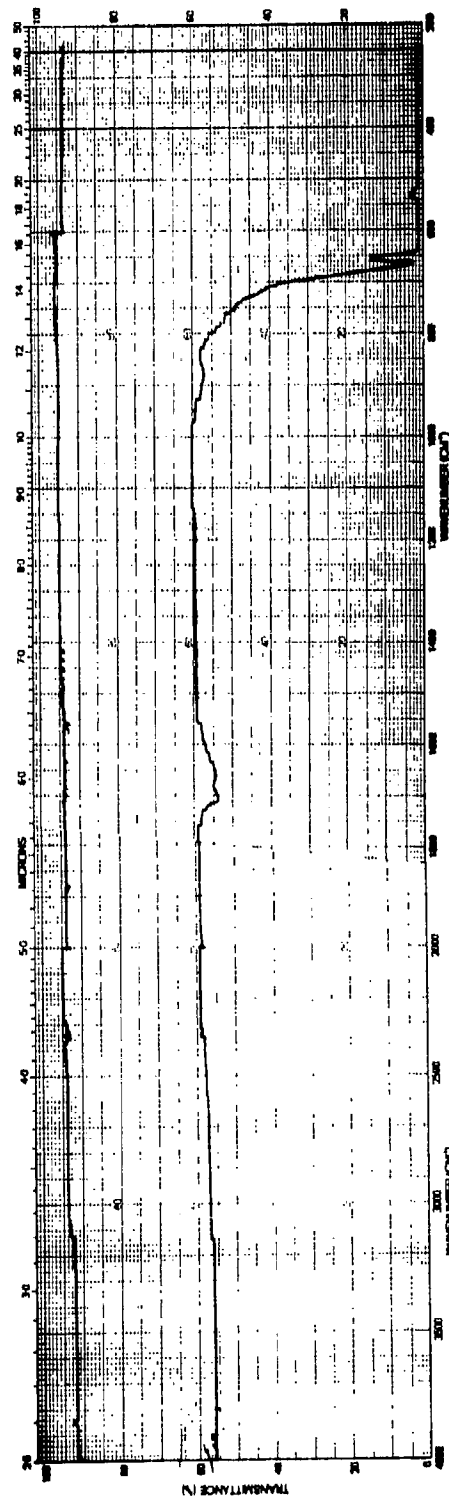


Figure 44. Infrared Transmittance of Zinc Sulfide Coating Run, ZnSC-10; 0.17 cm Thick ZnS Deposited on 0.64 cm Thick PVD ZnSe.

TABLE 7

THERMAL EXPANSION OF PVD AND CVD
ZINC SELENIDE AND CVD ZINC SULFIDE

<u>Material</u>	<u>Run No.</u>	<u>Thermal Exp Coeff.</u> <u>($\times 10^{-6}/^{\circ}\text{C}$)</u>
CVD ZnSe	ZnSe-96	7.61
PVD ZnSe	PVD-39	8.08
PVD ZnSe	PVD-40	8.05
CVD ZnS	ZnSC-10	7.60

of approximately 0.5 microinches per ° C. This thermal expansion mismatch will cause failure in tension in the PVD substrate if stress concentration factors of three are assumed. The stress in the PVD material is thickness-dependent as shown in the equation:

$$\sigma = \frac{\beta^4 + 3\beta^2 + 4\beta}{\beta^4 + 4\beta^3 + 6\beta^2 + 4\beta + 1} (\alpha_{\text{PVD}} - \alpha_{\text{ZnS}}) E_{\text{PVD}} \Delta T^*$$

where σ = Stress (psi)
 β = $\frac{\text{Thickness of ZnS}}{\text{Thickness of PVD}}$
 α = Thermal expansion coef. ($\times 10^{-6} / ^\circ \text{C}$)
 E = Modulus of elasticity (10^6 psi)
 ΔT = Temperature change ($^\circ \text{C}$)

* Assumes equal stiffness material

Using an allowable stress of approximately 1500 psi, it can be seen from this equation that thickness ratios of 0.1 or greater will fail the PVD material, whereas thickness ratios of less than 0.1 may survive. This accounts for the frequent but not total failures observed in the PVD substrates after coating. It is also obvious from this equation that lower deposition temperatures linearly reduce the residual stress.

In run ZnSC-10 both CVD and PVD zinc selenide substrates were coated at a lower temperature (700°C) to reduce the aforementioned thermal stress. Cracking occurred in the PVD substrate material, while the CVD substrate remained intact. The infrared transmittances of both coated substrates are shown in Figures 44 and 45.

Run ZnSC-11 was made on CVD material to yield sufficient material for rain erosion specimens. The deposit was successful and rain

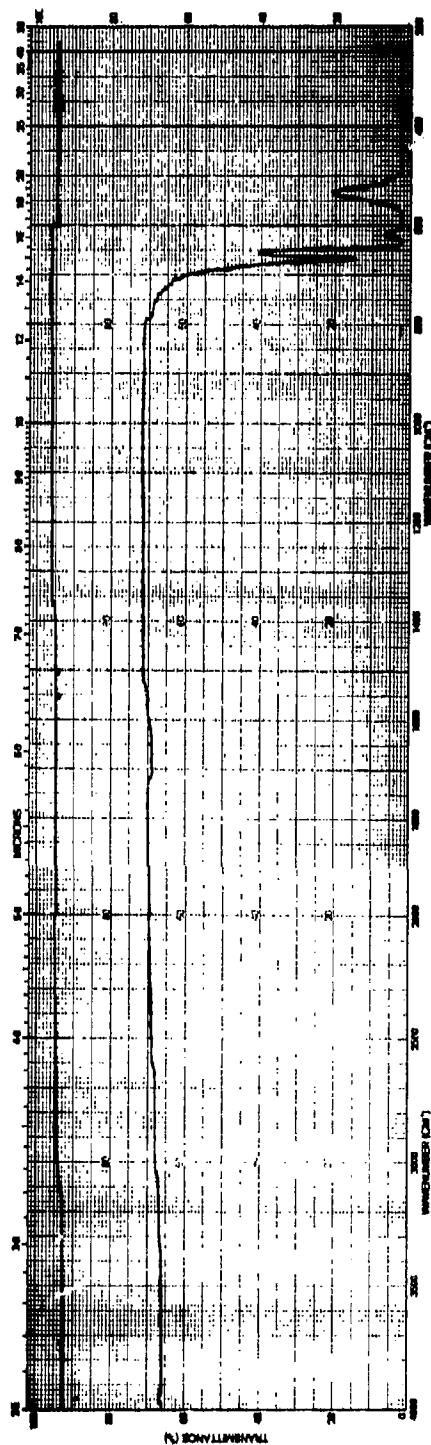


Figure 45. Infrared Transmittance of Zinc Sulfide Coating Run, ZnSC-10; 0.06 cm Thick ZnS Deposited on 0.37 cm Thick CVD ZnSe.

erosion specimens from this and an earlier deposit (ZnSC-6) were fabricated and submitted to the Air Force Materials Laboratory for evaluation. Typical infrared transmittances for these specimens are shown in Figures 48 through 49. The material from ZnSC-6 was chosen to evaluate the effect of coating thickness on rain erosion behavior with no concern for optical quality. It should be noted that the transmittance in the 8-12 μm range for the composite fabricated in run ZnSC-11 is similar to pure zinc selenide, indicating that the thin overcoat does not alter transmittance to any appreciable degree.

Run ZnSC-12 was deposited on CVD material. The infrared transmittance of the composite and the zinc sulfide is presented in Figures 50 and 51. The composite was of good optical quality, and a 2 X 2 in. evaluation specimen was prepared and forwarded to the Air Force Materials Laboratory for further evaluation.

One additional attempt was made to fabricate rain erosion samples using a PVD zinc selenide substrate. In this run (ZnSC-13) a 600° C deposition temperature for the zinc sulfide was used. Since the deposition temperature was 600° C a lower system pressure and higher molar ratio of input reactant was needed to insure that a sufficient supply of zinc vapor was available. In spite of these measures, zinc liquid condensed in the zinc sulfide deposit and the optical quality of the deposit was poor. However, no cracking occurred in the PVD substrate and the interface showed no signs of crazing. Figure 52 shows the transmittance of this composite sample.

Runs ZnSC-14 and -15 were made to supply additional rain erosion specimens. Sixteen (16) samples were fabricated from these runs. The zinc sulfide coating thickness in the finished samples was varied from 0.020 in. to 0.130 in.

Run ZnSC-16 was made to deposit a thin (~ 0.050 in.) overcoat of zinc sulfide on the large optically polished zinc selenide plate (13-1/4 X 20 X 0.590 in.). The deposit was carried out at 690° C; unfortunately the coating layer did not adhere uniformly to the substrate and cracking of the plate occurred.

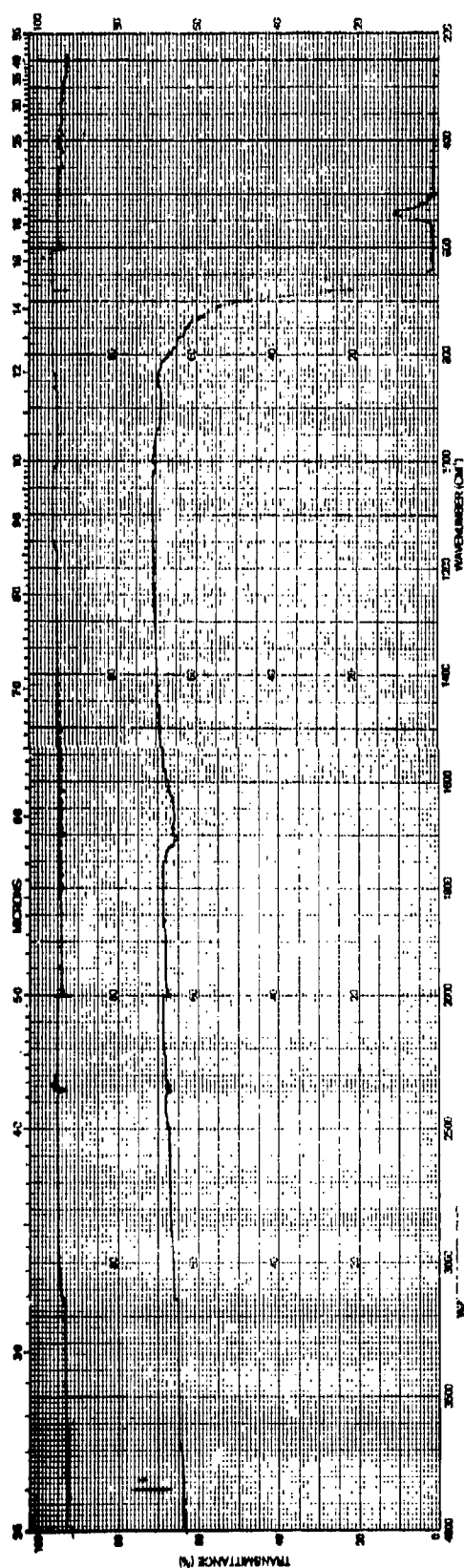


Figure 46. Infrared Transmittance of Zinc Sulfide Coating Run ZnSC-11 (Sample B); 0.11 cm ZnS and 0.40 cm CVD ZnSe Thickness.

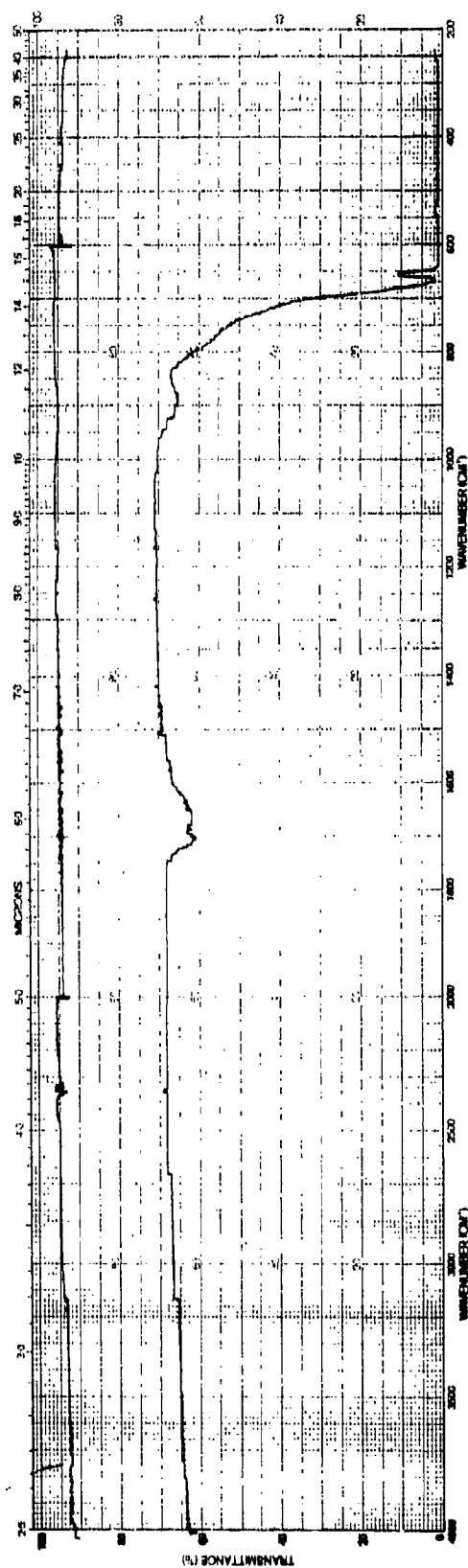


Figure 47. Infrared Transmittance of Zinc Sulfide Coating Run ZnSC-11 (Sample C); 0.25 cm ZnS and 0.26 cm CVD ZnSe Thickness.

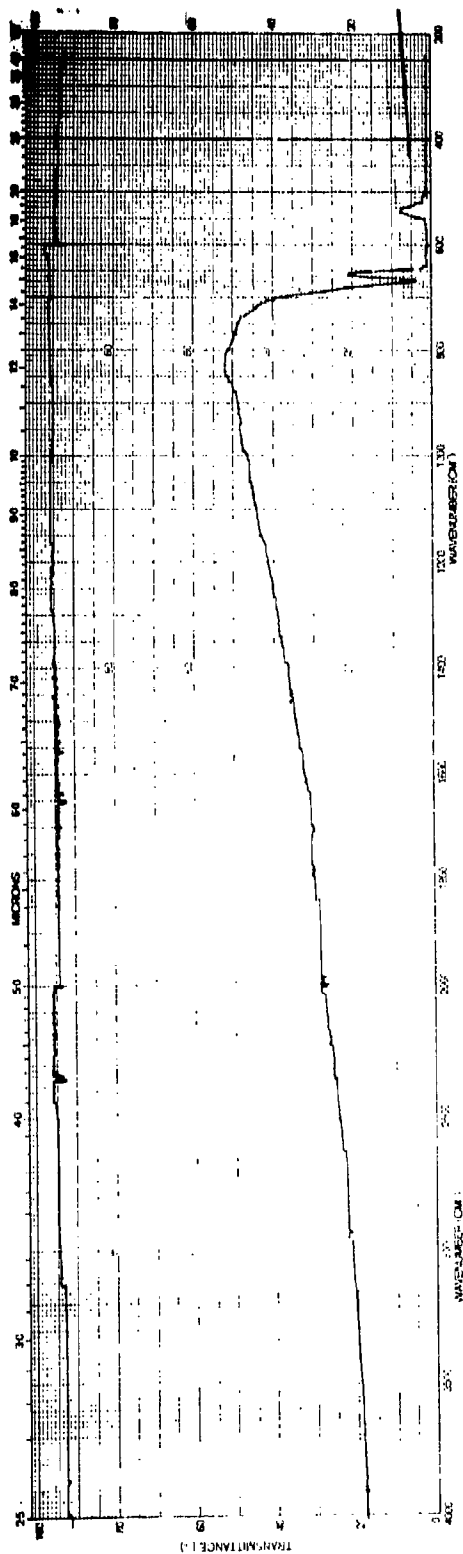


Figure 48. Infrared Transmittance of Zinc Sulfide Coating Run ZnSC-6 (Sample A); 0.1 cm ZnS and 0.4 cm CVD ZnSe Thickness.

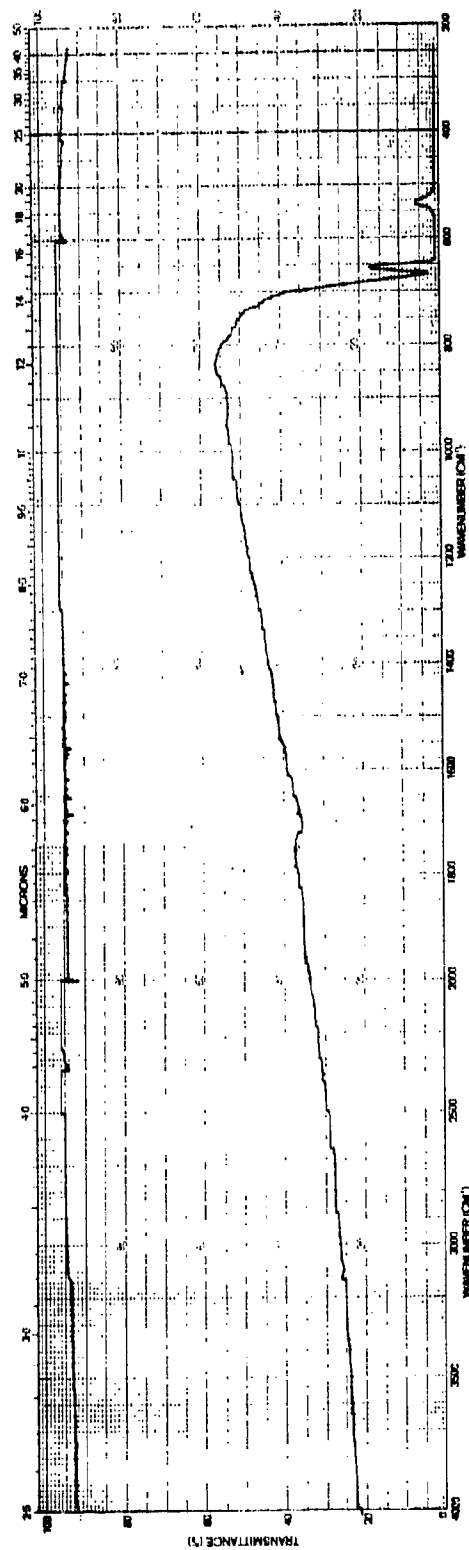


Figure 49. Infrared Transmittance of Zinc Sulfide Coating Run ZnSC-6 (Sample B); 0.16 cm ZnS and 0.38 cm CVD ZnSe Thickness.

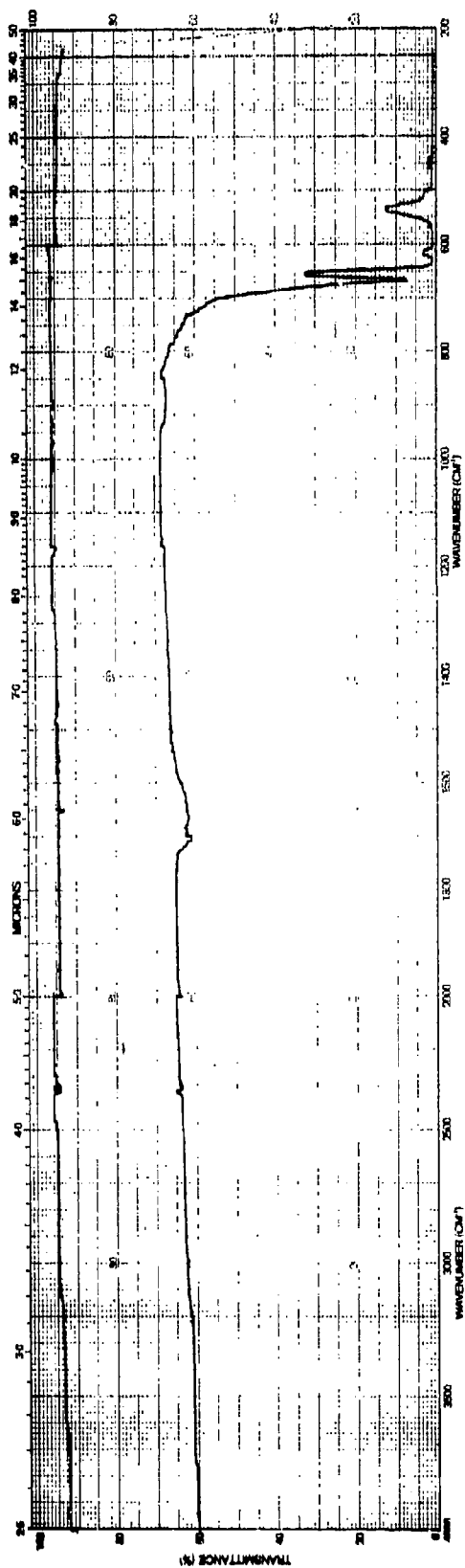


Figure 50. Infrared Transmittance of Zinc Sulfide Coating Run, ZnSC-12, 0.04 cm ZnS and 0.72 cm CVD ZnSe Thickness.

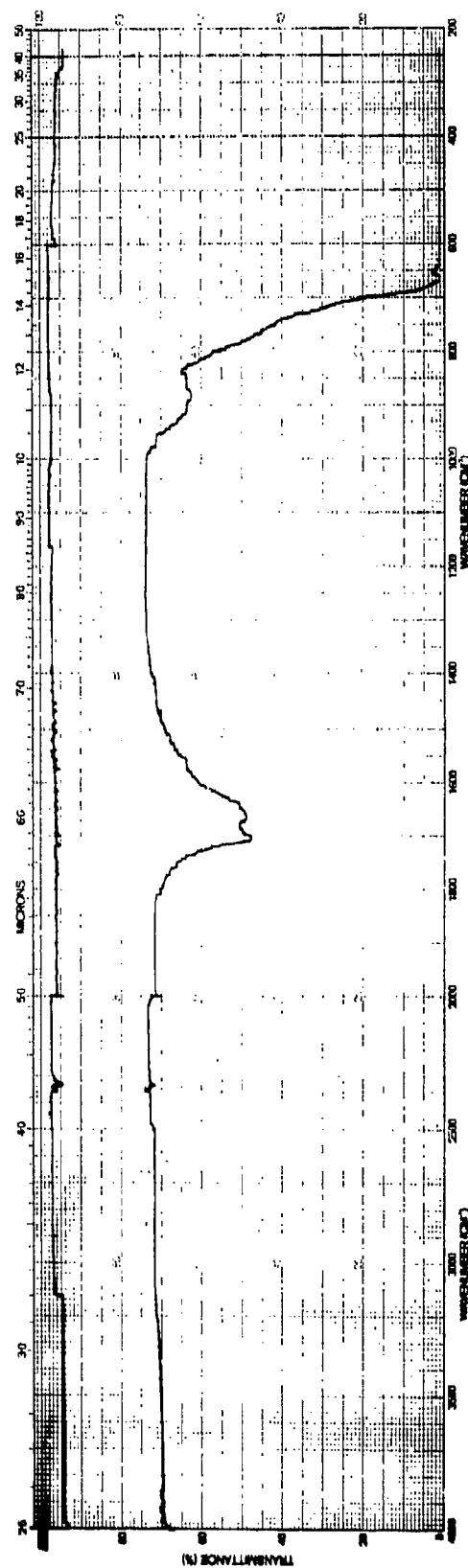


Figure 51. Infrared Transmittance of 0.4 cm Thick Zinc Sulfide Layer Deposited During Run ZnSC-12.

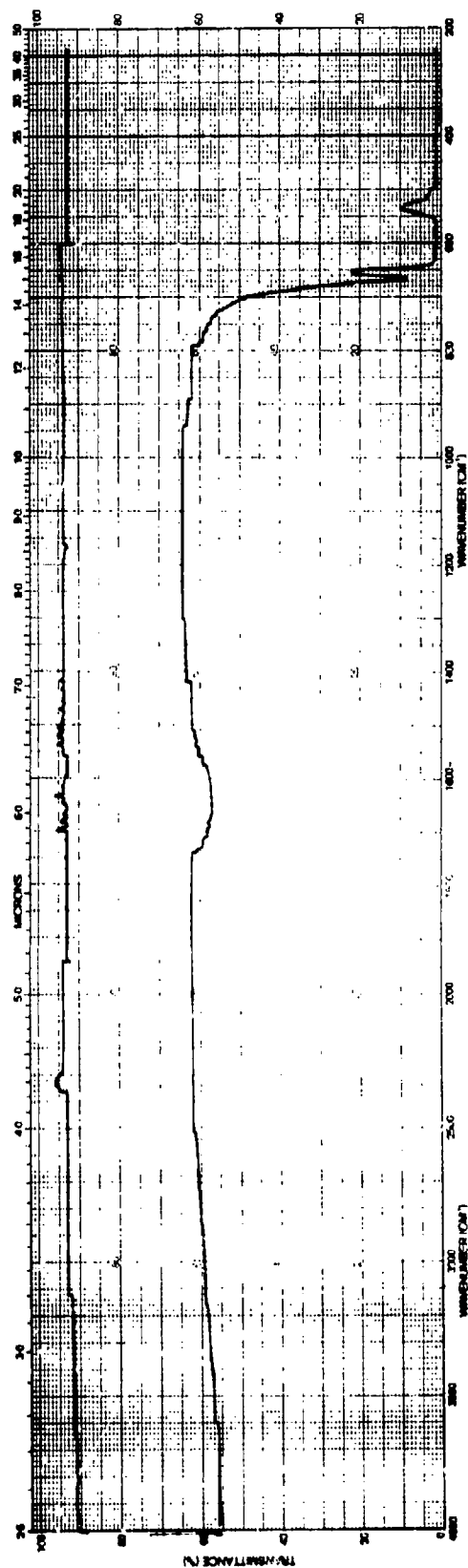


Figure 52. Infrared Transmittance of Zinc Sulfide Coating Run ZnSC-13, 0.11 cm ZnS and 0.65 cm CVD ZnSe Thickness.

The transmittance of a witness sample obtained from this run is shown in Figure 53, and as indicated, in the 8 to 12 micrometer region, the transmittance is within 2 percent of that predicted from theory. At other wavelengths, and particularly in the visible range, the transmittance is lower than anticipated because of scatter from the interface. The absorptivity of this composite that consists of 0.089 cm of ZnS and 1.22 cm of ZnSe was determined to be ~3 percent at 9.27 micrometers. This value is higher than anticipated (by ~2 percent) and is probably due to the presence of impurities at the interface.

f. Rain Erosion Testing

To evaluate the resistance to rain erosion of the composite ZnS/ZnSe materials produced during this program over fifty samples were fabricated and sent to the Air Force Materials Laboratory for testing in their rotating arm apparatus. All the samples were $1.5 \times 0.5 \times 0.2$ in. in size. The thickness of the CVD ZnS layer deposited on the ZnSe substrates varied from ~0.100 in. to ~0.020 in. The majority of the samples submitted had only the large faces (0.5×1.5) polished, although late in the program a series of samples were submitted in which all six surfaces were optically polished.

Testing was performed at two speeds, 470 and 575 mph, in a one-inch per hr simulated rainfall where the average drop size is 1.8 mm. The flat face of the specimens were at an impingement angle of 78 degrees to the rain drops. Exposure times were 20 minutes at 470 mph and 1 minute at 575 mph.

In general, most of the samples tested survived without fracturing completely. In all cases ring-type failures were observed in the zinc sulfide overcoat layers. When the overcoat layer thickness was greater than ~0.050 in. the amount of damage was similar to that observed for monolithic zinc sulfide. The loss in transmittance at 2.5 and 5.3 μm was usually between 3 and 5 percent while at 10 μm it was less than 3 percent.

It can tentatively be concluded from these tests that approximately 0.050 in. of zinc sulfide is needed to protect the zinc selenide. At this thickness the amount of damage observed in the zinc sulfide layer is similar to that observed in monolithic samples of this material.

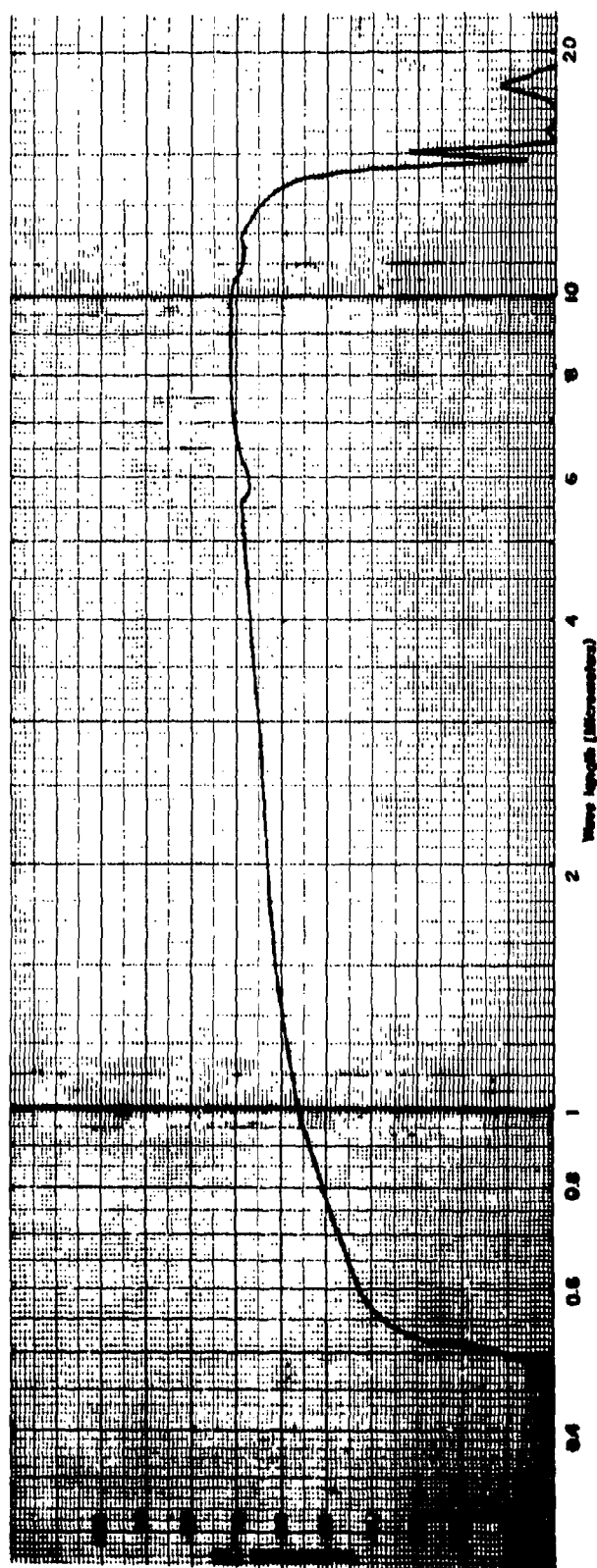


Figure 53. Spectral Transmittance of Composite ZnS/ ZnSe Window
(ZnSe 1.22 cm, ZnS 0.089 cm)

IV. SUMMARY AND CONCLUSIONS

This program has established the feasibility of fabricating large size (13×20 in.) durable multispectral windows by a chemical vapor deposition process at a cost consistent with the program goals. The window is a composite that consists of two layers; a relatively thick (~ 0.600 in.) zinc selenide substrate and a thin (0.050 in.) zinc sulfide overcoat. The zinc selenide is thick enough to resist both mechanical fracture and deflection under the expected aerodynamic and mechanical loads. This material, after optical polishing of one surface, is covered with a thin layer of zinc sulfide to provide protection from rain erosion and dust abrasion. The zinc sulfide grown onto the selenide surface by chemical vapor deposition. The composite structure can then be optically polished to its final specifications. This technique eliminates the use of antireflection coatings at the interface and the need to figure the final surfaces because of optical path differences due to a nonuniform thickness of the interface adhesive. Even though we were not successful in coating a full size window, several samples of 3×5 in. size were successfully overcoated and optically polished. The transmittance of the samples indicated that the ZnS overcoat layer does not significantly alter the transmittance of the ZnSe substrate.

To achieve the results summarized above and to reduce the cost of zinc selenide to an acceptable level, three vapor deposition processes were evaluated. The first two of these processes, an elemental process that uses only zinc and selenium vapors, and the physical vapor deposition process produced material that was satisfactory for use in the 8 to 12 micrometer range. However, it was not satisfactory for use at visible wavelengths and at 1.06 micrometers because of scatter. Furthermore, difficulties were encountered in fabricating large-size samples with both processes and it was not possible to successfully overcoat the material produced by the PVD process with zinc sulfide because of a thermal expansion mismatch.

The cost to produce excellent optical quality zinc selenide window blanks by a modified chemical vapor deposition process, the third process evaluated, was lowered by improving yield and using less expensive reactants. In addition, chemical vapor deposition techniques were developed for growing a thin layer of zinc sulfide directly onto a polished zinc selenide substrate. Using these techniques it is estimated that in production window blanks can be procured for approximately \$11,000 each. These costs are consistent with the goals established for this program.

APPENDIX

IMAGE SPOILING MEASUREMENTS

1. INTRODUCTION

If a sample of transparent material is used as an element in an imaging system, one is obviously concerned with such properties as the transmittance, the surface figure and polish, etc. Even if these commonly measured properties are satisfactory, however, the material may cause an unacceptable degradation of the image quality by causing random angular deviations of the radiation passing through. Such deviations may result from bubbles or inclusions, crystal interfaces, inhomogeneity of refractive index, etc.

Thus, for example, one may design a system to image a point at infinity, i. e., to focus a parallel beam of light to a point. If the parallel beam first passes through a plane parallel plate of material which introduces a small angular spreading of the light, the image will be enlarged to some extent. The properties whereby the material introduces the angular deviations may be called image spoiling properties, and the extent to which the image is enlarged may be used as a measure of the image spoiling properties.¹

We have developed an image spoiling test apparatus for the immediate purpose of evaluating the usefulness of varying qualities of CVD materials produced for 8 to 12 μm range FLIR systems. This test equipment is also available to conduct quality control tests on the window blanks that are fabricated in exploratory or production phases of other programs. By suitable change in the detector and filters the measurements could be carried out at wavelengths other than 8-12 μm .

2. APPARATUS

Our image spoiling measurement apparatus (Figure 1) utilizes the radiation from a black body source (Barnes Engineering Co.) operating at

875 K. A blocking filter (Grubb-Parsons & Co.) is used to cut off the radiation below $8\text{ }\mu\text{m}$ (see Figure 2). The radiation is passed through an adjustable slit, typically set at $30\text{ }\mu\text{m}$, which serves as an object for an off-axis paraboloidal mirror (Space Optics Research Labs) of 8 inch diameter and 64 inch focal length, which renders the radiation parallel. A second off-axis paraboloid is used to refocus the collimated beam to an image of the slit. By means of a scanning mirror system (General Scanning, Inc.), the image is swept across the detector at a rate of approximately 60 Hz. The detector (Arthur D. Little, Inc.) utilizes a mercury cadmium telluride element 0.001 inch wide and 0.020 inch high. The spectral response of this detector with a 1000 K black body source is shown in Figure 3. This characteristic, combined with that of the blocking filter, results in an effective wavelength band for the measurement of approximately $8\text{-}12\text{ }\mu\text{m}$. The amplified detector output is applied to a computer of average transients or CAT (Technical Measurement Corp.) which builds up an acceptably noise-free record of the intensity distribution across the image in a minute or so.

3. MEASUREMENT PROCEDURE

The stored up record of intensity versus position may be displayed on an x-y recorder. By examining this distribution, a suitable measure of the image width may be obtained. This is illustrated in Figure 4, which shows, with some smoothing, a typical output curve obtained from the CAT. The baseline is the level observed far off the peak of the image; the versatility of the CAT allows this to be displayed below the peak as shown. The width of the image is indicated at 50% and at 15% of peak.

To test the image spoiling property of a plate of material, measurements are made with and without the plate placed in the collimated beam between the two paraboloids, and the extent to which the width of the image is changed by the presence of the plate is observed. An actual record of outputs from the CAT is shown in Figure 5 reduced in size. The two curves near the center are the image curves for a clear aperture of 7 inches (determined by the iris

diaphragm; see Figure 1) and for a sample of zinc sulfide, with their respective baselines recorded below the curves. (The original curves may be recorded in four different colors, which facilitates separating out the curves obtained under various conditions.) The two curves near the outer edges of the figure are used to calibrate the abscissa scale. These two curves are segments of the image obtained from a double slit of known separation ($404\text{ }\mu\text{m}$). Since the source is placed at the focal point of a 64 inch focal length reflector, the separation of the two peaks on the image corresponds to an angular subtense of the source of $249\text{ }\mu\text{rad}$. From the linear separation of the image peaks of 28.2 cm , we thus conclude that 1 cm on the abscissa corresponds to $8.83\text{ }\mu\text{radians}$.

4. RESULTS

A typical set of results are shown in Table 1. The samples listed are three CVD zinc sulfides of two different input reactant molar ratios, one zinc sulfide of unknown identity but poor quality, and zinc selenide prepared by the physical vapor deposition process. The aperture was determined by the iris diaphragm which was normal to the test beam except as noted. The incident angle is the angle between the test beam and normal to the surface; this is further clarified in the notes. The width of the image is characterized by $\Delta_{15\%}$, the width in microradians of the curve at 15% of peak intensity. (We have used this 15% specification because it is the practice currently being followed in image spilling measurements at WPAFB.²

In the case of the first three zinc sulfides, it will be noted that insertion of the sample at normal incidence resulted in a decrease of the width at 15% peak of about $5\text{ }\mu\text{rad}$. This effect was reproduced a number of times and is not the result of a simple blunder or noise. One possible explanation for this effect is that it arises from the decreasing transmissivity of the sample at the longer wavelengths ($> 10.5\text{ }\mu\text{m}$) which contribute a greater diffraction width than the shorter wavelengths. When the sample was rotated by 45 degrees about a vertical axis (i. e., an axis parallel to the slit) the image width observed

was about equal to that for the clear aperture. This is also true when the sample was tilted 45 deg about a horizontal axis which itself is perpendicular to the test beam. It would appear that for these three materials the image spoiling is minimal. This is clearly not true for the unknown ZnS nor the PVD ZnSe.

5. MODULATION TRANSFER FUNCTION

It may be recognized that the curves generated by the image spoiling measurement apparatus contain more information than merely the width at some arbitrary fraction of peak intensity. These curves are an approximation of the line spread function (LSF) for the system under test. (Some distortion of the LSF arises from the non-zero widths of source and detector.) The modulus of the Fourier transform of the LSF is the Modulation Transfer Function (MTF), which is frequently used to characterize the image qualities of optical components. If the image is formed of an object consisting of alternating light and dark bars, the MTF describes the way in which the contrast in the image depends on the spatial frequency. We are in the process of setting up the appropriate hardware and software to obtain the MTF from the output of the CAT.

REFERENCES

1. L. H. Reynolds, Infrared Physics 8, 233 (1968).
2. N. Krut, Private Communication.

TABLE A1

Sample	Aperture (in.)	Incident Angle (deg)	$\Delta_{15\%}$ (μ rad)	Note
None	5-1/2	--	114.4	A
ZS-207	"	0	108.9	
(0.4 H ₂ S/ Zn)	"	45	114.5	
None	8	--	86.5	B
ZS-207	"	45	87.0	
None	5-1/2	--	116.5	A
ZS-213	"	0	112.3	
(0.7 H ₂ S/ Zn)	"	45	118.0	
None	8	--	86.3	B
ZS-213	"	45	87.0	
None	5	--	123.6	A
ZS-157P (0.4 H ₂ S/ ZnS)	"	0	127.2	
None	5-1/2	--	114.8	A
Unknown ZnS	"	0	162.4	
None	7	--	87.5	A
ZnSe-PVD-41	"	0	96.3	
None	4-1/2	--	133.7	A
ZnSe-PVD-41	"	45	144.2	

Notes:

- A. The iris diaphragm was perpendicular to the test beam. For the 45 deg measurement, the sample only was rotated about a vertical axis (see Fig. 1).
- B. The iris diaphragm was always tilted at an angle of 45° with respect to the vertical, so that the effective height of the test beam was $8/\sqrt{2}$ inch. The sample was placed parallel to the diaphragm.

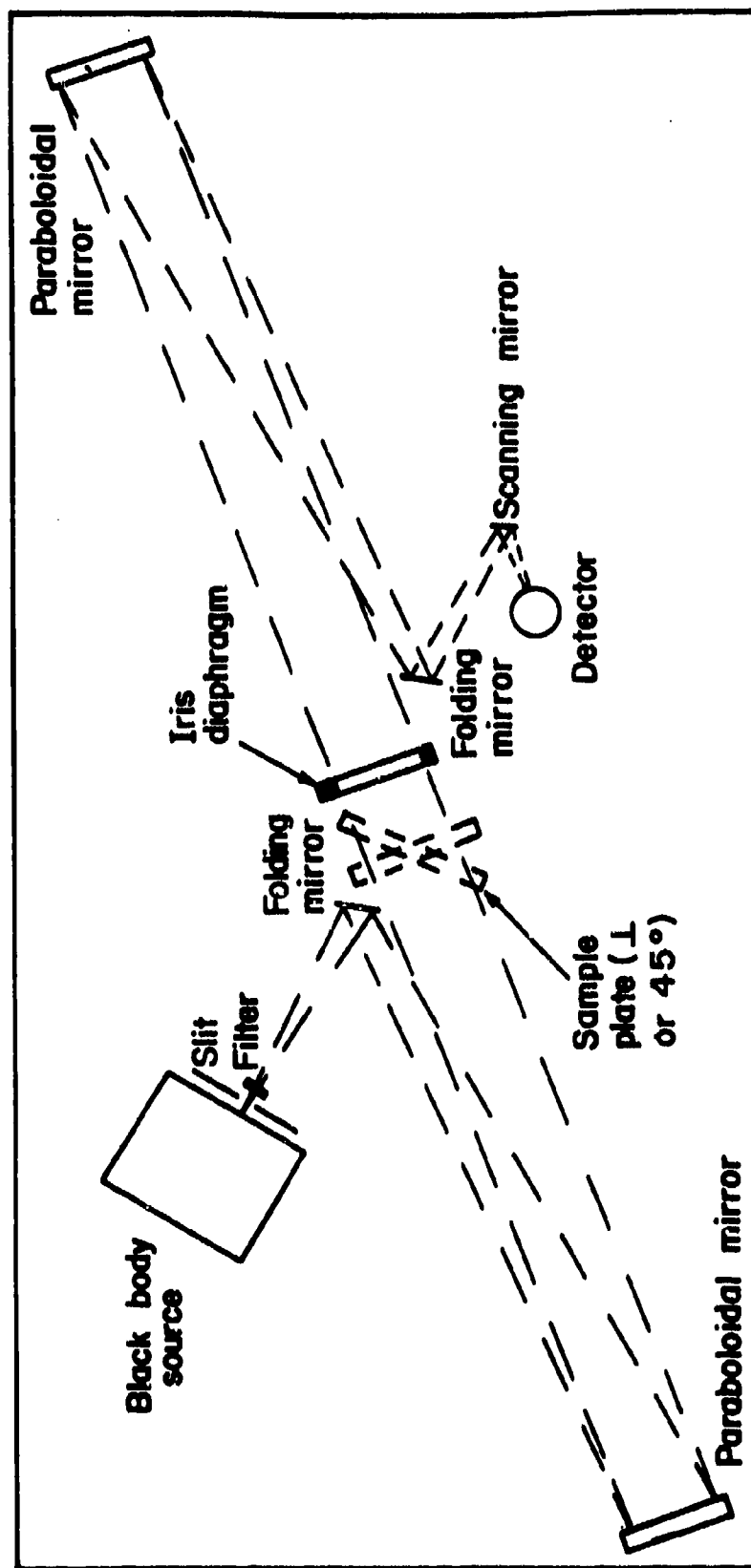


Figure A. 1. Image Spoiling Apparatus.

Grubb Parsons

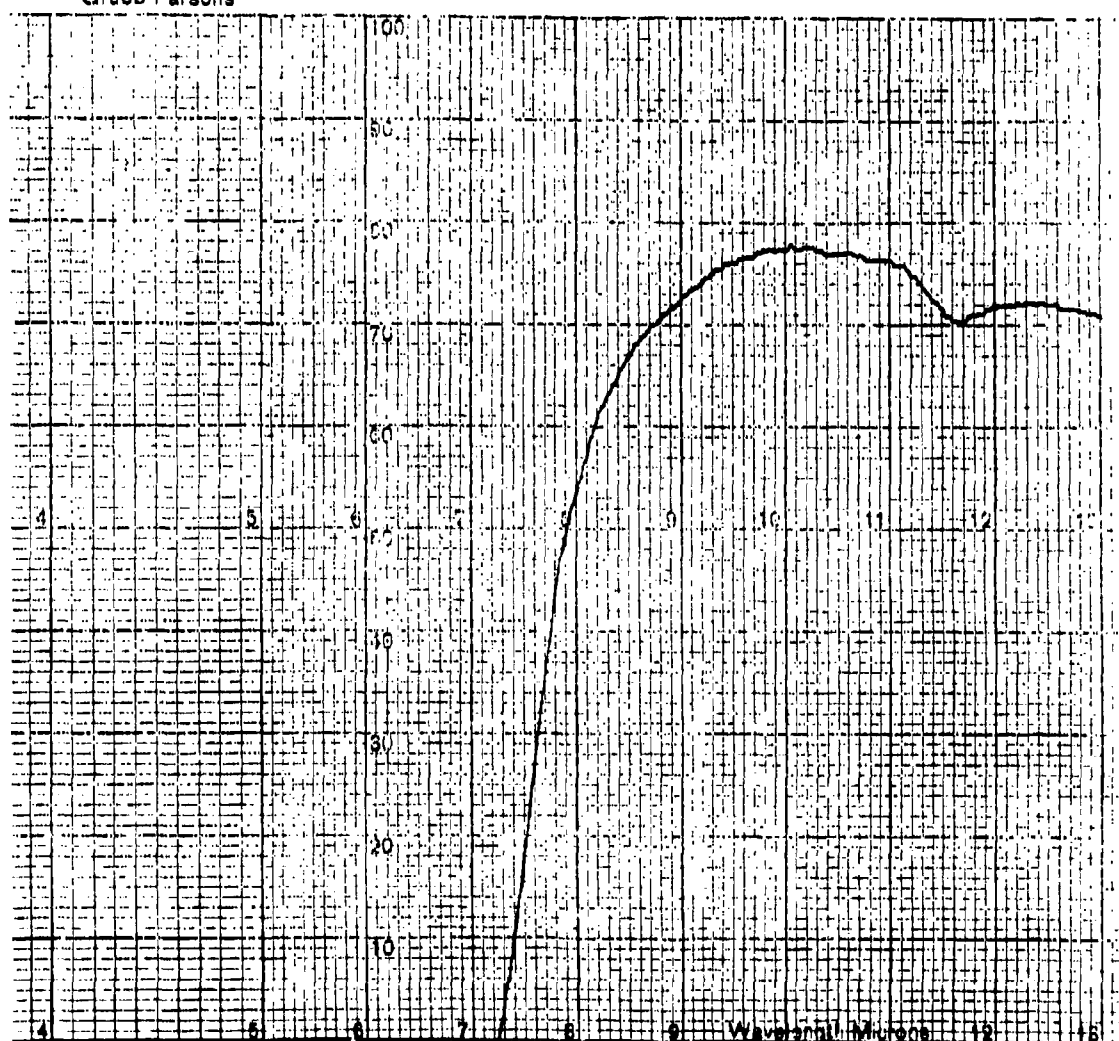


Figure A.2. Long Wave Pass Filter Characteristic.

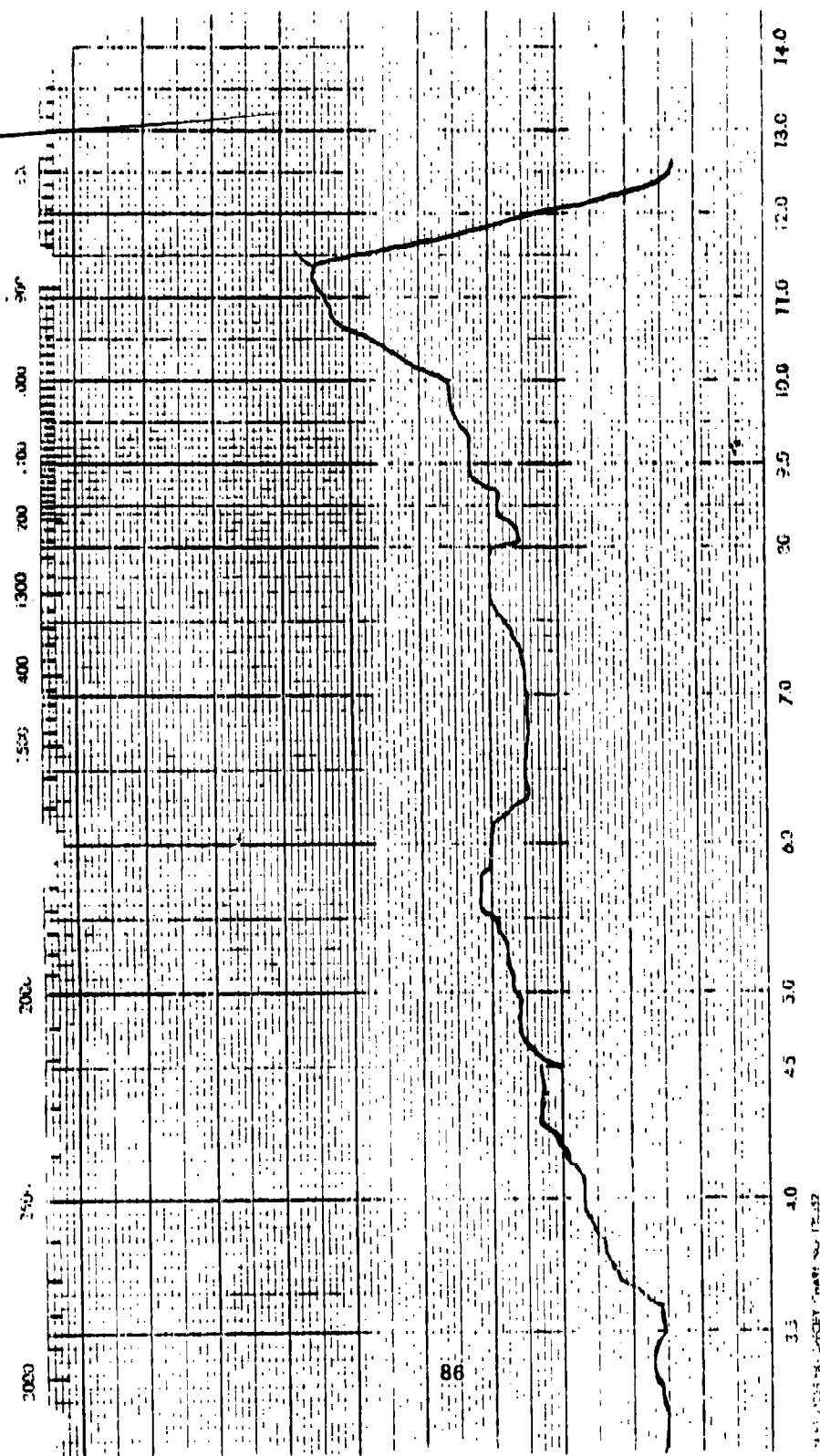


Figure A. 3. Detector Response With 1000 K Black Body Source.

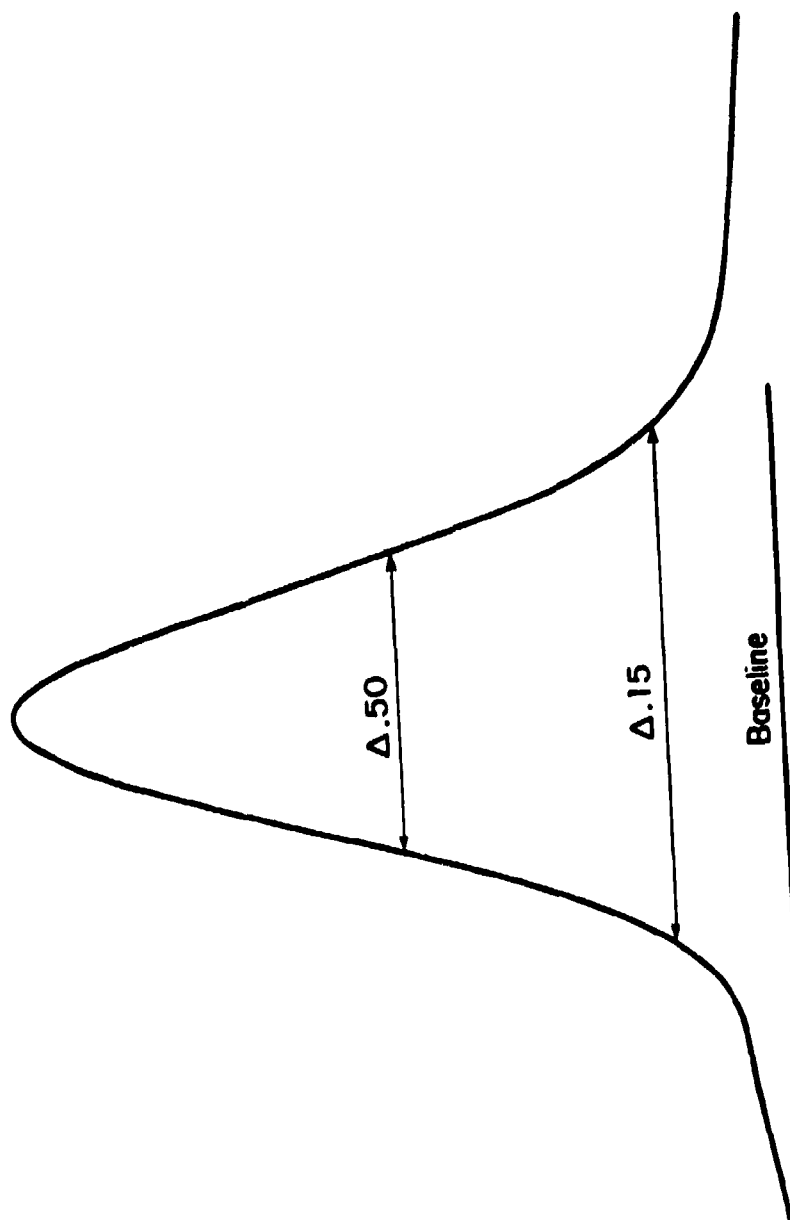


Figure A. 4. Typical Image Spoiling Scan.

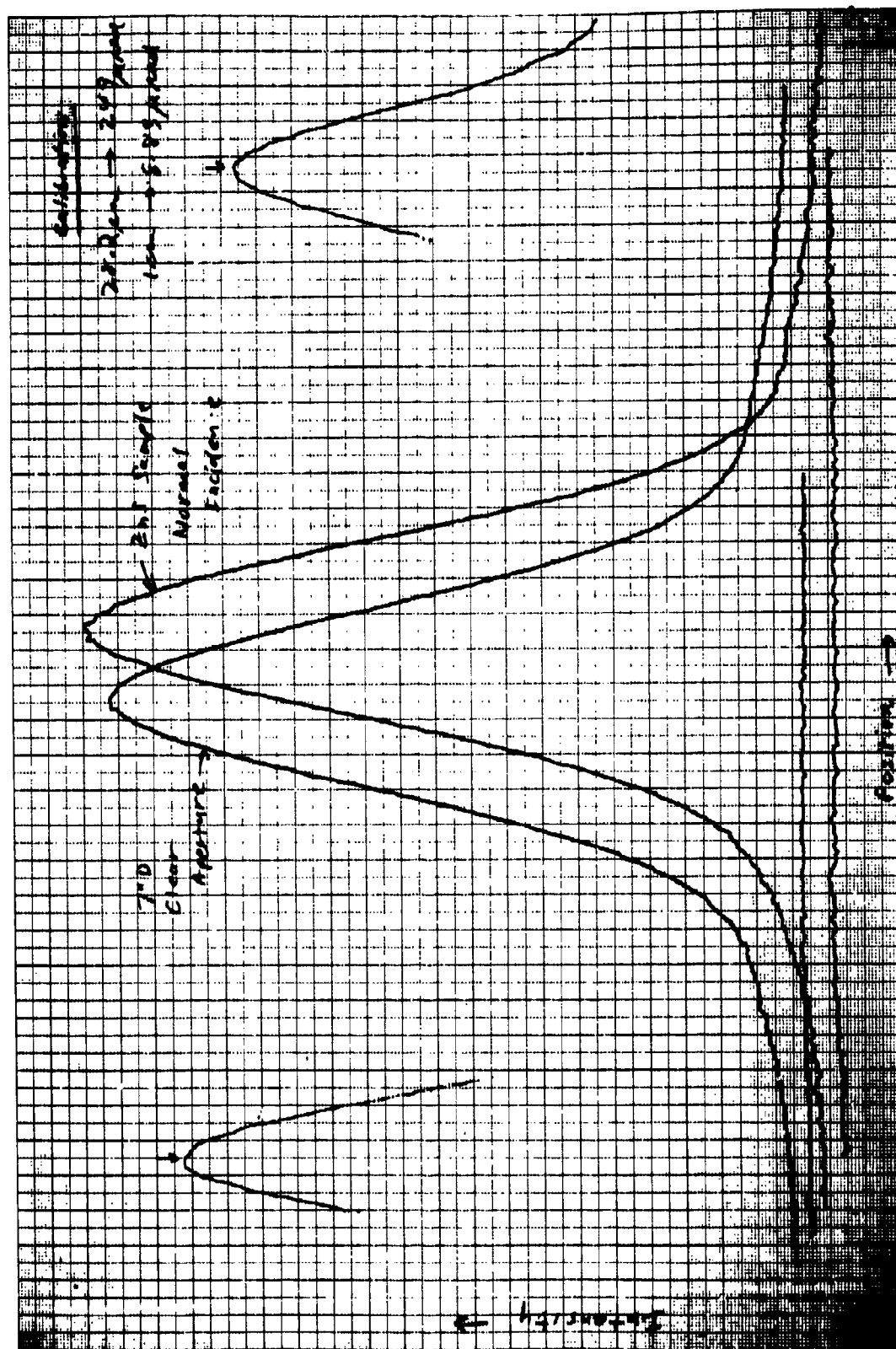


Figure A.5. CAT Output Curves.